

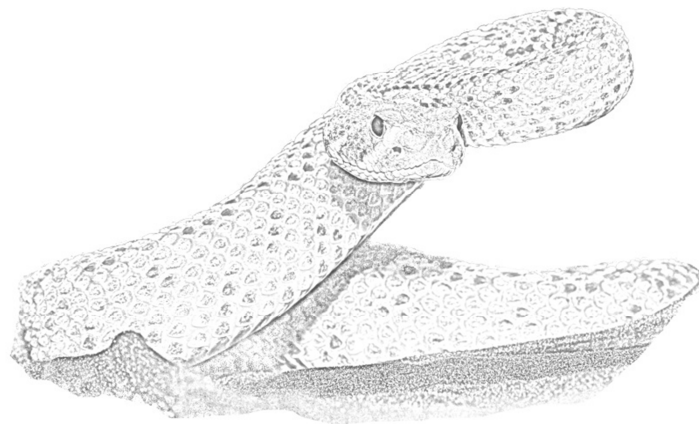
Graduate School of  
Systemic Neurosciences

LMU Munich



Technische Universität München

Dissertation der Graduate School of Systemic Neurosciences der  
Ludwig-Maximilians-Universität München



**Sensory processing in the infrared pathway of the western  
diamondback rattlesnake, *Crotalus atrox***

**Maximilian Sebastian Bothe**

June 28<sup>th</sup> 2018

*Picture of C. atrox on title page is the author's own work.*

Supervisor: Prof. Dr. Harald Luksch

Chair of Zoology  
TUM School of Life Sciences Weihenstephan  
Technical University of Munich  
Liesel-Beckmann-Straße 4  
85354 Freising-Weihenstephan, Germany

2<sup>nd</sup> Reviewer: Prof. Dr. Hans Straka

Division of Neurobiology  
Department Biology II  
Ludwig-Maximilian-Universität München  
Großhaderner Straße 2  
82152 Planegg-Martinsried, Germany

3<sup>rd</sup> Reviewer: Prof. Dr. Gerhard von der Emde

Neuroethology/Sensory Ecology  
University of Bonn  
Meckenheimer Allee 169  
Poppelsdorfer Schloss (Raum 2.030)  
53115 Bonn, Germany

Date of defense: November 15<sup>th</sup> 2018

## Table of contents

|  |     |
|--|-----|
| List of abbreviations.....   | 4   |
| List of figures.....   | 6   |
| Introduction .....   | 9   |
| Chapter 1.....   | 20  |
| Organotopic organization of the primary Infrared Sensitive Nucleus (LTTD) in the western diamondback rattlesnake ( <i>Crotalus atrox</i> ) |     |
| Chapter 2.....   | 38  |
| Physiological basis for infrared motion detection in the brainstem of the western diamondback-rattlesnake ( <i>Crotalus atrox</i> )        |     |
| Chapter 3.....   | 74  |
| Infrared object motion-processing in the rattlesnake hindbrain depends on rate- as well as spike time encoding mechanisms                  |     |
| Discussion.....  | 94  |
| Appendix 1 .....   | 111 |
| Published manuscripts included in this thesis .....  | 112 |
| Copyrights .....   | 113 |
| Eidesstattliche Versicherung/Affidavit .....   | 115 |
| Declaration of author contributions .....  | 116 |

## List of abbreviations

|            |  |
|------------|--|
| ADVR       | anterior dorsal ventricular ridge                  |
| BO         | olfactory bulb                                     |
| C          | celcius  |
| CB         | cerebellum   |
| CH         | optic chiasm                                       |
| cm         | centimeter   |
| e.g.       | example given                                      |
| ET         | electrode track                                    |
| HYP        | hypophysis   |
| Hz         | hertz  |
| i.e.       | <i>id est</i>                                      |
| <i>IF</i>  | instantaneous frequency                            |
| IR         | infrared   |
| kHz        | kilohertz  |
| ltd        | lateral descending trigeminal tract                |
| LTTD       | nucleus of the lateral descending trigeminal tract |
| $\mu$ A    | microampere  |
| $\mu$ m    | micrometer   |
| max        | maximum  |
| min        | minimum  |
| min.       | minute   |
| mm         | millimeter   |
| MMG        | maxillo-mandibular trigeminal ganglion             |
| M $\Omega$ | megaohm  |
| ms         | millisecond  |
| mV         | millivolt  |
| mW         | milliwatt  |

|       |  |
|-------|--|
| nl    | nanoliter  |
| nm    | nanometer  |
| n-t   | naso-temporal  |
| N.V1  | ophthalmic trigeminal nerve                          |
| N.V2d | deep branch of the maxillary trigeminal nerve        |
| N.V2s | superficial branch of the maxillary trigeminal nerve |
| OG    | ophthalmic ganglion                                  |
| OT    | optic tectum   |
| Psf   | point spread function                                |
| RC    | nucleus reticularis caloris                          |
| Rt    | nucleus rotundus                                     |
| s     | second   |
| SC    | spinal cord  |
| SC    | spike count  |
| SDI   | signed directionality index                          |
| SEM   | standrad error of the mean                           |
| STD   | standard deviation                                   |
| TE    | telencephalon  |
| t-n   | temporo-nasal  |
| TNM   | terminal nerve mass                                  |
| ttd   | descending trigeminal tract                          |
| TTD   | nucleus of the descending trigeminal tract           |
| UV    | ultraviolet  |
| VIS   | visual electromagnetic spectrum                      |
| W     | watt   |

## List of figures

### Introduction

Figure 1: Phylogeny of snakes and loreal pit organ anatomy. 11

Figure 2: Anatomy and circuitry of the rattlesnake IR system. 14

### Chapter 1

Figure 1: Schematic of the brain of the western diamondback rattlesnake and location of tracer application to different trigeminal nerve branches 24

Figure 2: Anterograde tracing of TNMs in the pit membrane and retrograde labeling of corresponding cell bodies in the trigeminal ganglion 25

Figure 3: Anatomical organization of the trigeminal nuclear complex 27

Figure 4: Anatomical delineation of the infrared (LTTD) and common trigeminal nuclei (TTD) on transverse sections through the hindbrain. 28

Figure 5: Sagittal view of primary infrared afferent projections within the LTTD 29

Figure 6: Transversal view of primary infrared afferent projections within LTTD 30

Figure 7: Diagram summarizing the corresponding peripheral and central topographic organization of infrared afferent projections 31

## Chapter 2

|  |    |
|--|----|
| Figure 1: Isolated rattlesnake whole brain and pit organ for probing IR signal processing in the LTTD.                         | 48 |
| Figure 2: Topography of trigeminal nerve branch-evoked field potentials in the LTTD  | 50 |
| Figure 3: Spectrum of trigeminal afferent-evoked input patterns in LTTD-neurons  | 52 |
| Figure 4: Convergence pattern of synaptic responses from adjacent N.V2s sub-branches in LTTD neurons                           | 54 |
| Figure 5: Differential response dynamics in LTTD neurons following sequence-specific activation of adjacent N.V2s sub-branches | 55 |
| Figure 6: Quantification of response dynamics following sequence-specific activation of adjacent N.V2s sub-branches            | 56 |
| Figure 7: Discharge dynamics of LTTD and RC neurons during IR object motion  | 59 |

## Chapter 3

|   |    |
|---|----|
| Figure 1: Experimental setup and spontaneous activity of RC neurons   | 80 |
| Figure 2: RC neuron response differences with respect to spike count and instantaneous frequency towards increasing velocities of a moving IR emitter | 82 |
| Figure 3: Directional tuning of RC neurons' rate- and temporal code towards horizontal IR emitter motion  | 86 |
| Figure 4: Summarized directional tuning of RC neurons towards horizontal IR-emitter motion  | 87 |

## Discussion

Figure 1: Axon termination patterns in the LTTD

97

## Introduction

To cope with and adapt to changes in their environment, living organisms from all three domains of life have developed a great variety of sensory structures (Smith, 2008a; Taiz et al., 2014). Especially in higher taxa of the eukaryote animal kingdom, these sensory structures have evolved into complex sensory organs that enable animals to perceive and interpret many different physical modalities. Depending on the ecological requirements and evolutionary pressure animals cope with, many sensory organs have developed into highly specialized systems that are optimized to perceive particular qualities of these general modalities. However, in order to make maximal use of information gathered by different sensory organs, multimodal input needs to be properly integrated and aligned. In vertebrates, such integration takes place, for example, in the optic tectum (OT, superior colliculus in mammals), where sensory maps built from different modality inputs are topographically aligned (Dräger & Hubel, 1975, 1976; Knudsen, 1982; Newman & Hartline, 1981). The origin of the midbrain circuitry that comprises such multisensory alignment is based on a mixture of early developmental processes and forebrain guided conjunction between multimodal synaptic inputs. In mice, the alignment of somatotopic maps with respective areas of visuotopic representations in the superior colliculus seems to take place at very early developmental stages, probably through chemical gradient guidance and way before sensory visual inputs can impact map formation (Triplett et al., 2012). However, for orientation in space the visual modality is often most important in many higher vertebrates. Accordingly, sensory input from the second common space-mapping system, the auditory system, was found to be actively aligned to the visual coordinate system in the OT and superior colliculus (Feldman & Knudsen, 1997; King et al., 1988; Knudsen & Brainard, 1991).

The electromagnetic spectra that vertebrates can perceive, reach from ultraviolet (UV) (Bajer et al., 2010; Bowmaker & Kunz, 1987; Losey et al., 1999; Rajchard, 2009; Whiting et al., 2006) over the “classic” primate visual spectrum (VIS) (Jacobs, 1996) up to infrared (IR) radiation (Kürten & Schmidt, 1982; Noble & Schmidt, 1937). However, other than for UV or VIS radiation, so far no photochemical transduction mechanism has been described for the perception of IR radiation. Rather, radiation in the IR spectrum gets absorbed by biological tissue, thereby heating it up. IR electromagnetic waves are therefore generally not providing input to the visual, but to the somatosensory system. Absorbed heat energy spreads by conduction and convection until it eventually triggers the transduction process in heat sensitive free nerve endings formed by primary afferents of the somatosensory system. It is known that ion channels from the TRP-family play an

important role in this mechanism in vertebrates (Lumpkin & Caterina, 2007; Smith, 2008b). When it comes to the detection of IR radiation, all known somatosensory heat sensors rely on such “indirect” reception through tissue heating that causes signal transduction in primary afferents. However, while this “bolometer-like” mechanism seems universal, some organisms evolved specialized sensory organs in which the thermal mass of the tissue that supports primary somatosensory afferents is minimized to a point that allows for short latency detection of low energy electromagnetic radiation from the IR spectrum.

Three groups of animals have evolved sensory organs that allow such direct detection of thermal radiation. Within insects, different families possess specialized structures to detect IR radiation. Among them are certain beetles (e.g. Buprestidae, Acanthocnemidae) (H. Schmitz et al., 2000, 2002; H. Schmitz & Bleckmann, 1998) and flat bugs (e.g. Aradidae) (A. Schmitz et al., 2008) which possess the ability to detect infrared radiation with specialized organs. Although there are differences in the anatomy and transduction mechanisms of the IR organs of these insects, they all function according to a same basic principle: The tissue within the IR organ absorbs heat energy which leads to morphological or physiological changes that eventually trigger activity in a primary afferent neuron. It has long been assumed that these animals might use their highly sensitive IR organs to detect and approach forest fires, to lay their eggs into the freshly burned woods. However, this idea has recently become a matter of discussion again (Hinz et al., 2018). Among mammals, vampire bats (*Desmodus rotundus*) have evolved a specialized IR detection system to spot blood vessels under their hosts’ skin (Gracheva et al., 2011; Kishida et al., 1984; Kürten & Schmidt, 1982). Heat- and cold-sensing nerve endings are densely packed within the thin nose pad of the bats. This pad forms the thermal mass reduced supporting tissue for the primary afferents. It allows the bats to detect thermal radiation from blood vessels in up to 16 cm distance (Kürten & Schmidt, 1982).

### **Snake IR Organs**

The snakes (Serpentes) are a third group in which specialized IR sensory organs have evolved. According to the phylogeny described in Lee et al., 2007, species from three alethinopidian families have evolved such organs – the Pythonidae (Pythoninae), Boidae (Boinae) and Viperidae (Crotalinae). While there are species from all of these families that are able to detect IR, the layout of their IR-organs differs between pythons and boas and the crotaline snakes. Many pythons and boas possess labial IR organs which form arrays of IR sensitive units on or between the scales of their upper and lower jaws (Lynn, 1931; Noble & Schmidt, 1937; von Düring, 1974) (Fig. 1b,c). In some

species, the labial scales further specialized and form shallow depressions which are then referred to as labial pits (Lynn, 1931; Molenaar, 1992; Warren & Proske, 1968). Labial pits are innervated by the trigeminal nerve, with the mandibular branch (N.V3) innervating the lower and the maxillary (N.V2) and ophthalmic (N.V1) branches innervating the upper jaw pits (Lynn, 1931; Molenaar, 1992; Warren & Proske, 1968). Primary trigeminal afferents from these nerves form heat sensitive free nerve endings within the labial scales (Molenaar, 1992; Warren & Proske, 1968). Via the lateral descending trigeminal tract (ltd), they relay primary input to the hindbrain nucleus of the lateral descending trigeminal tract (LTTD). In boas and pythons the LTTD is the only hindbrain nucleus involved in IR processing and secondary LTTD-neurons directly project to the contralateral lobe of the OT (Meszler, 1983; Molenaar, 1992).

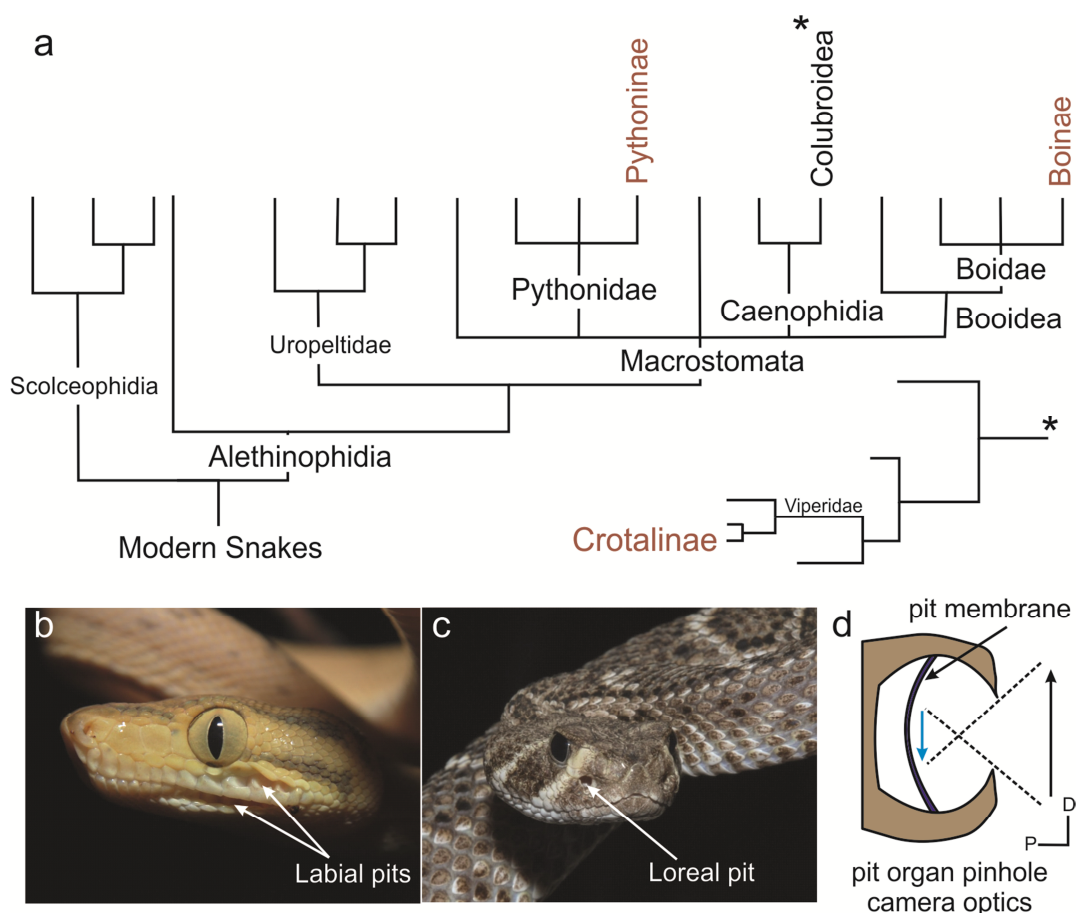


**Fig. 1:** (a) Phylogeny of snakes and position of IR sensitive species (highlighted in brown). Note that only one subfamily within the superfamily of Colubroidea (\* in a), i.e. pit-vipers (Crotalinae), which belong to the family of vipers (Viperidae), is specialized in IR reception. (b,c) Pictures of a boid (*Corallus hortulanus*, b) and a crotaline (*Crotalus atrox*, c) snake. Both species possess different types of IR organs. (d) Schematic of the crotaline loreal pit organ and its pinhole camera optics. Images on the pit membrane are inverted by the pit opening (i.e. “aperture”). D: dorsal; P: proximal. Phylogenetic tree in a reproduced from Fig. 10, Lee et al., 2007 (Permission for reuse kindly granted by Taylor & Francis Group, <http://www.tandfonline.com>, Permission Reference: JB/TSAB/P18/1050); Phylogenetic tree in inset (\*) drawn after Pyron et al., 2011. Pictures in (b,c) are own work.

## **Anatomy of the crotaline IR system**

Other than boids and pythons, pit-vipers (Crotalinae) possess loreal pit organs which are situated bilaterally on their upper jaws (Lynn, 1931)(Fig. 1c). Through each of these pits spans a thin sensory epithelium, the pit membrane (Fig. 1c,d), which divides the pit cavity into an inner and outer chamber (Bullock & Diecke, 1956; Bullock & Fox, 1957; Goris, 2011). The membrane is innervated and supplied with blood through a thin connection to the surrounding tissue at its outer margins (Amemiya et al., 1999; Goris, 2011; Lynn, 1931). With a thickness of only about 15  $\mu\text{m}$  and the insulation from body heat by the surrounding air (Goris & Nomoto, 1967; Krochmal et al., 2004), the pit membrane's thermal mass is greatly reduced. Its structure is therefore optimized for heat detection after the bolometer-principle described above. Another striking feature of the loreal pit organ is the existence of an aperture in form of the pit opening. Although the opening is rather big it still implements pinhole-camera optics to the pit organ (Bakken & Krochmal, 2007; Otto, 1972; Sichert et al., 2006) (Fig.1d). The pit organ is therefore the only known somatosensory organ that developed a simple, yet clearly optic apparatus to receive electromagnetic waves from the IR spectrum. The pit membrane is innervated by the maxillary (N.V2) and the ophthalmic (N.V1) trigeminal nerve (Bullock & Fox, 1957; Lynn, 1931). Contrary to boids and pythons, the mandibular trigeminal nerve (N.V3), which only innervates the lower jaw (Lynn, 1931), is not involved in IR reception. Before entering the membrane, the maxillary trigeminal nerve splits into a superficial (N.V2s) and a deep (N.V2d) branch. Each trigeminal nerve innervates a distinct part of the pit membrane with N.V.1 entering the dorso-caudal, N.V2d the dorso-rostral and N.V2s the ventral part (Goris et al., 1989; Lynn, 1931)(Fig. 2a). When entering the pit membrane, the three nerves further ramify into individual sub-branches that are partly interconnected through anastomoses. Individual primary afferent fibers spread from these sub-branches to give rise to terminal nerve masses (TNMs), which are the sensory elements of the IR system. TNMs have an average diameter of about 40  $\mu\text{m}$  and occupy a particular area of the membrane with no overlap between individual TNMs (Amemiya et al., 1996; Terashima et al., 1970). Signal transduction takes place at TRPA1 channels situated on these TNMs (Gracheva et al., 2010). Interestingly, the mitochondrial density within the TNMs is extremely high with mitochondria occupying about 90 % of the intracellular volume (Amemiya et al., 1996; Meszler & Webster, 1968; Zischka et al., 2003). The TNMs are embedded in a dense capillary network that spans through the pit membrane. Capillaries form loops, each of which encloses between two to four TNMs (Amemiya et al., 1999). The capillary network is assumed to play an important role in both, the oxygen and glucose supply of mitochondria as well as the quick dissipation of arriving heat radiation to keep the heat receptors in their optimal, dynamic working range (Amemiya et al., 1999; Goris et al., 2007). Primary afferent somata lie in the trigeminal ganglia

and, via the lateral descending trigeminal tract (ltd), send axons to the trigeminal nucleus of the lateral descending trigeminal tract (LTTD, Fig. 2a,c,d). The LTTD is a specialized part of the trigeminal hindbrain nuclei and can be clearly differentiated from the common descending trigeminal tract (ttd) and its nuclei (TTD), even with simple light microscopy (Newman et al., 1980). Its anatomical position as well as its cellular and synaptic structure have raised assumptions of a possible homology to the mammalian nucleus caudalis (Newman et al., 1980). However, this homology is debated and other authors rather support a development of the IR processing trigeminal nuclei independent from the nucleus caudalis (Molenaar, 1992). The LTTD seems to be only present in vertebrates that are specialized in IR reception. A similar, presumably IR receptive nucleus has been found in the trigeminal hindbrain of vampire bats (*Desmodus rotundus*) (Kishida et al., 1984). The crocotine LTTD is exclusively innervated by IR sensitive trigeminal fibers (Meszler et al., 1981). Terminating primary afferents form a dense neuropil that tightly embeds the soma and dendrites of secondary neurons in the LTTD. However, detailed studies on the termination patterns of primary afferents from distinct membrane innervating trigeminal sub-branches are yet missing. Histological studies in different crocotine species revealed that the population of LTTD neurons can be subdivided into two distinct groups of smaller and larger cell size (Meszler et al., 1981). The larger, multipolar cells are found in the main neuropil of the LTTD, while smaller cells are predominantly found in the marginal region. The immunoarchitecture of the main and the marginal neuropil also differs, which might correlate with different functional roles in IR processing (Molenaar, 1992). About 30 % of the synapses in the LTTD have been found to be axo-axonic (Meszler et al., 1981). This indicates heavy presynaptic modulation of primary LTTD input (Meszler et al., 1981). However, there is so far no definitive proof of the origin of these axo-axonic synapses. Secondary LTTD neurons project to the ipsilateral hindbrain nucleus reticularis caloris (RC, Fig. 2b,c,d) (Gruberg et al., 1979; Meszler, 1983). Retrograde tracing of ascending LTTD neurons from the RC resulted in staining of only the large, multipolar cells (Newman et al., 1980). It has therefore been suggested, that axo-axonic synapses might arise from an intranuclear circuitry and originate from the smaller cells found in the LTTD (Molenaar, 1992). From the RC, IR input is finally relayed to the contralateral lobe of the OT (Fig. 2a,c,d). Here, IR recipient cells have been found in layers 7a and 7b of Cajal (Kass et al., 1978).

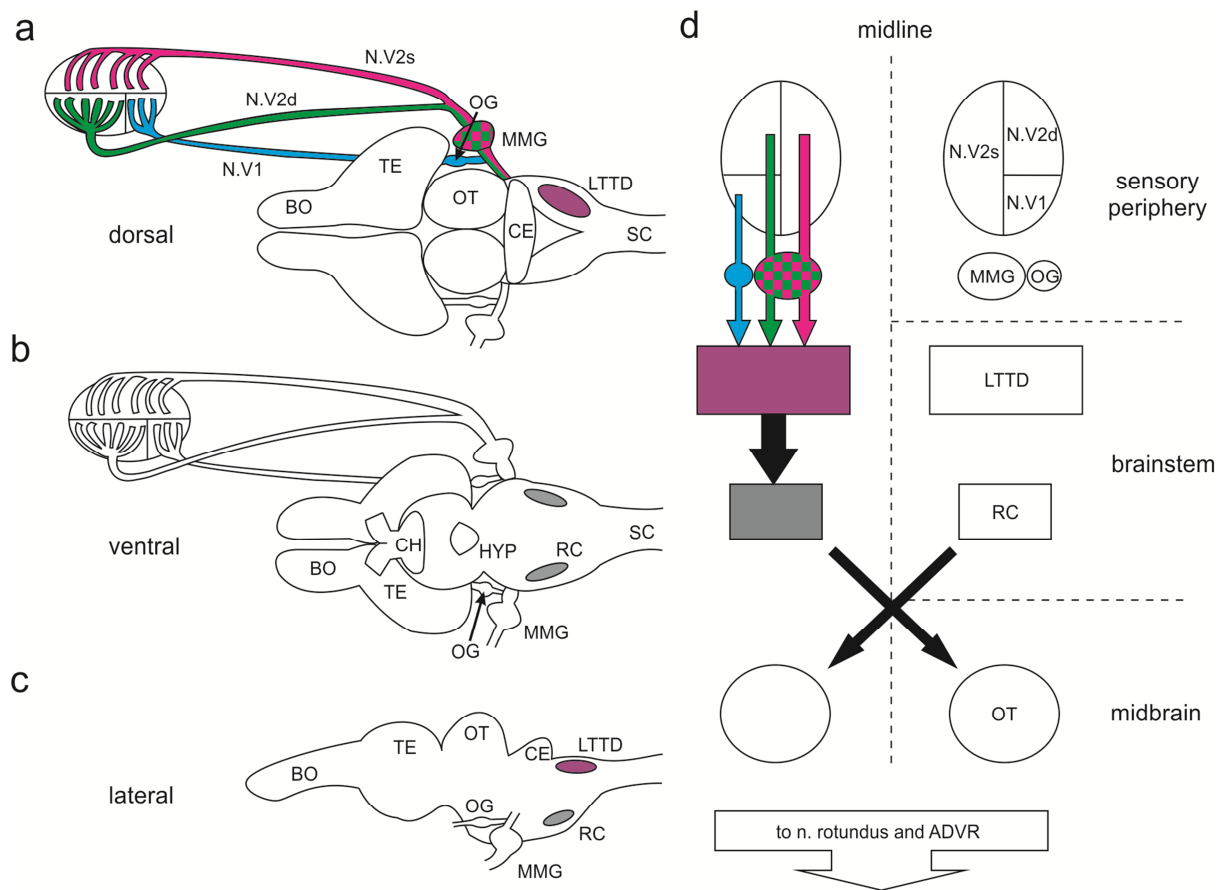


**Fig. 2: Schematics depicting anatomy and circuitry of the rattlesnake IR system. (a) Dorsal, (b) ventral and (c) lateral view of the rattlesnake brain and pit membrane. Upon entering the pit organ, N.V1 (blue), N.V2d (green) and N.V2s (magenta) ramify into smaller sub-branches which give rise to individual primary afferent dendrites that innervate distinct areas of the membrane. Somata of primary IR sensitive afferents lie in the maxillo-mandibular and ophthalmic ganglion, respectively. From here, axons project to the LTTD (violet in a, c, d). LTTD output is conveyed to the ipsilateral RC (gray in b,c,d), before it eventually reaches the contralateral OT. (d) Schematic depicting connections between the main compartments of the rattlesnake IR processing circuitry. ADVR, anterior dorsal ventricular ridge; BO, olfactory bulb; CB, cerebellum; CH, optic chiasm; HYP, hypophysis; LTTD, nucleus of the lateral descending trigeminal tract; MMG, maxillo-mandibular trigeminal ganglion; N.V1, ophthalmic trigeminal nerve; N.V2d, deep branch of the maxillary trigeminal nerve; N.V2s, superficial branch of the maxillary trigeminal nerve; OG, ophthalmic ganglion; OT, optic tectum; RC, nucleus reticularis caloridis; SC, spinal cord; TE, telencephalon.**

## Physiology of the crotaline IR system

### *The crotaline pit membrane as a heat intensity detector*

IR sensitive primary afferent fibers encode changes in the amount of heat energy, i.e. heat flux or intensity, that impact the pit membrane (Bullock & Diecke, 1956). To recognize an object it hereby is not important which temperature it has in relation to the pit membrane but that its

temperature differs from its environment and therefore provides thermal contrast (van Dyke & Grace, 2010). Objects whose IR emittance differs from their surroundings cause a change in heat flux on the part of the pit membrane their image is projected on. This change in heat flux is transduced into neural activity at the TNMs (Terashima et al., 1968). Net influx of heat energy causes primary afferents to increase their firing rate, while net efflux of heat energy causes decreased firing rates. Upon longer lasting stimuli, adaption of primary afferents towards temperature changes occurs (Bullock & Diecke, 1956; Goris & Nomoto, 1967). Bullock & Diecke, 1956 mathematically and experimentally determined the minimal temperature change the membrane needs to undergo to impose an influence on the firing rate of primary afferent fibers. They calculated that a temperature change as small as 0.003°C - 0.005°C could be sufficient to elicit activity in primary afferent fibers. In terms of stimulus intensity, Terashima & Goris, 1977 and 1979 in their experiments reported threshold sensitivities of primary IR sensitive afferents to lie between  $1.6 \frac{mW}{cm^2}$  -  $16 \frac{W}{cm^2}$ , depending on the individual recorded fiber. However, it has also been demonstrated that the sensitivity of primary afferent fibers is impacted by halogenated anesthesia and decreases with increasing depth of anesthesia (Moiseenkova et al., 2003). Therefore, threshold sensitivities might be even lower than those reported from anesthetized snakes so far. Primary afferent fibers of the crotaline IR system are spontaneously active. In the short-tailed mamushi (*Gloydius blomhoffii brevicaudus*) it has been shown that the primary afferent background activity is somehow variable and depends on the environmental temperature. Highest background activity could be recorded under typical temperatures the snakes encountered in their natural habitat (de Cock Buning et al., 1981). When compared to the spontaneous activity of other sensory systems, the background activity of primary IR sensitive afferents shows rather high variability and lies between 10 Hz and 30 Hz (Bullock & Diecke, 1956; de Cock Buning et al., 1981). In a study on the copperhead (*Agkistrodon contorix*) Moiseenkova et al. (2003) demonstrated that radiation from a broad spectrum between 400 nm and 10600 nm provides an adequate stimulus to elicit spikes in primary IR sensitive afferents. These results again indicate that the crotaline IR system is not tuned towards certain wavelengths of the IR spectrum but to changes of heat flux elicited by IR radiation. The intensity detector hypothesis is further emphasized by their finding that primary afferents showed peak response to stimulus wavelengths that are greatly absorbed by oxyhemoglobin (i.e. towards a 400 nm stimulus) and water (i.e. towards 3390 nm and 10600 nm stimuli). Both wavelengths have been previously demonstrated to also be best absorbed by the pit membrane (Bullock & Fox, 1957; Goris & Nomoto, 1967) and therefore are most effective in heating it up.

### *Electrophysiological properties of IR sensitive primary afferents*

Positive and negative changes in local membrane temperature are reflected in the activity of fibers that innervate the corresponding area by an in- and decrease of their firing rate, respectively. Heat flux as introduced by natural, i.e. ecologically relevant, stimuli is represented linearly in the firing rate of primary afferents (Bullock & Diecke, 1956; Goris & Nomoto, 1967). Intensity of such stimuli usually does not exceed threshold intensity by a factor of 10 (Bullock & Diecke, 1956) and elicits response frequencies below 100 Hz in individual primary afferents (Goris & Nomoto, 1967). Ongoing stimulation with moderate stimuli leads to an adaption of primary afferent firing and a drop to background activity over time. Stronger stimuli can cause more complex response characteristics. Stimulation with such stronger intensities causes an on-burst in primary afferents the frequency of which depends on stimulus strength. The on-burst is followed by a phase of silence that increases in duration with increasing strength of the stimulus. Cessation of stimulation in this phase causes an off-burst followed by reduced background activity that over time approaches the former background value again. Upon ongoing stimulation of the pit with strong intensities, activity will eventually recover with a second burst and settle at a new, slightly higher background level. Cessation of the stimulus after this adaption causes a phase of silence and a subsequent recovery of the former background activity (Bullock & Diecke, 1956). However, strong intensities that cause such more complex activity patterns have been suggested to be rather aversive stimuli a snake would avoid and orient away from (Goris & Nomoto, 1967). Different stimulus intensities are represented in individual primary afferents with different resolution. Dynamic ranges are quite variable and have been demonstrated to vary between 1:50 and 1:256 (threshold intensity : intensity at maximal excitation) (Bullock & Diecke, 1956). However, parts of this variability could be attributed to methodical implications of the experiments that have been performed to evaluate primary afferent resolution (for details refer to Bullock & Diecke, 1956). Maximum response frequency of IR sensitive primary afferents lies between 160 Hz and 180 Hz.

Given the large diameter of the pit-opening, the pinhole-camera optics of the pit organ provide a rather blurred, poorly resolved image of the IR environment (Bakken & Krochmal, 2007). Receptive fields of primary afferents have an average diameter of 65°, with some extending over up to 85° (Desalvo & Hartline, 1978). Calculations of theoretical receptive field sizes based on pit organ morphology mostly resulted in field sizes smaller than those experimentally measured. However, calculations were done under the assumption that a primary afferent fiber reflects only the area of the pit membrane its TNM lies in. Experimental data therefore point towards a rather broad integration of membrane temperature by primary afferents that includes membrane areas around

their respective TNMs (Desalvo & Hartline, 1978). A direct, neural interaction between individual primary afferents has not been demonstrated so far. Therefore, the findings described are most likely a result of heat spread over the membrane.

#### *Central processing of IR sensory input*

Primary central processing of IR input takes place in the LTTD. LTTD neurons are spontaneously active with frequencies around 10-20 Hz (Terashima & Goris, 1977). In vivo studies on anesthetized pitvipers revealed phasic rather than tonic responses of LTTD neurons upon stimulation with moderate IR stimuli. Initially excitatory responses are suppressed by secondary inhibition. The response threshold of IR sensitive LTTD units was measured to lie as low as 0.1 mw/cm<sup>2</sup>. This is a magnitude lower than described for primary afferents and may be attributed to the convergence of many primary afferents to single LTTD-neurons (Stanford & Hartline, 1984). Sub threshold stimuli might still provoke subtle changes, for example in the rhythm of the spontaneous activity of individual primary afferents. Such small effects might be integrated in the LTTD and cause response patterns upon stimuli that could not trigger or suppress spikes within individual primary afferents. With respect to primary afferent receptive fields, flanking inhibitory receptive fields reduce the size of excitatory fields in LTTD neurons. Thus, receptive fields of secondary LTTD neurons have average diameters between 29° and 35° and are much smaller than those measured for primary afferents (Stanford & Hartline, 1980, 1984). Other than for example in the retina, no center-surround architecture of excitatory and inhibitory receptive fields was found in the LTTD. Rather, inhibitory fields were horizontally flanking excitatory fields, thereby implementing lateral inhibition in the LTTD (Stanford & Hartline, 1984). The effects these receptive field properties impose on the processing of more transient, i.e. natural stimuli, have not been deciphered in detail yet.

Neurons in the RC respond with phasic excitation towards IR stimulation in vivo (Kishida et al., 1980; Newman et al., 1980). Apart from this, little is known about the physiological properties of the RC and its role in hindbrain processing of IR input. This is mainly due to the poor accessibility of the nucleus in vivo. Consequently, thorough studies on RC electrophysiology are missing. However, from the RC, IR input eventually reaches the contralateral lobe of the OT where it is integrated with visual information from the retina. Just as visual input, IR input is topographically mapped to the OT. Although the resolution of the IR map is much coarser than that of the visual map, both are still roughly aligned (Hartline et al., 1978). In addition to unimodal visual- and IR-responsive neurons, six types of bimodal neurons have been described in the OT: "OR" neurons which respond well to both,

IR and visual input; “AND” neurons which respond poorly to unimodal IR or visual stimulation but show reliable responses upon bimodal stimulation; IR-enhanced visual neurons; visual-enhanced IR neurons; IR-depressed visual neurons; visual depressed IR neurons (Newman & Hartline, 1981). From the OT, projections reach the ipsilateral and (to a lesser extent) the contralateral nucleus rotundus (Rt) (Berson & Hartline, 1988). IR sensory information is then further relayed to the anterior dorsal ventricular ridge (ADVR) in the forebrain, where IR is multimodally processed with visual and tactile information (Berson & Hartline, 1988).

## **Rational of the experiments performed for the presented PhD thesis**

Part of the crotaline trigeminal system has evolved into a highly specialized heat detection system. The pit organ itself resembles the physics of a pinhole camera. Combined with the greatly reduced thermal mass of the pit membrane, the pit organ is the only known somatosensory specialization that provides a basis for primary somatosensory afferents to function as low latency detectors of electromagnetic waves in the IR spectrum. Former studies in the LTTD of rattlesnakes have already revealed spatiotemporal sharpening of IR input by lateral inhibition. The aim of this thesis is to further decipher the neural mechanisms that are used to extract the precise spatiotemporal information from primary IR input that is needed to build up and integrate a spatiotopic representation of the IR environment with visual input in the optic tectum. The classic idea that the LTTD might function as a retina for the infrared system was the basis for the experimental design of the studies presented in this thesis. The main questions that were aimed to answer are:

- 1) Is the IR environment topographically represented in the LTTD?
- 2) What are the consequences of spatiotemporal sharpening in the LTTD for more complex, i.e. more natural, IR input?
- 3) Does lateral inhibition provide a basis for directional sensitivity of LTTD neurons as it is known from the retina?
- 4) What is the function of the RC in hindbrain processing of IR input?

The anatomical study presented in this thesis has already been published. Electrophysiological studies are presented in manuscript form and will be submitted for publication at a later point.

## Chapter 1

### **Organotopic organization of the primary Infrared Sensitive Nucleus (LTTD) in the western diamondback rattlesnake (*Crotalus atrox*)**

Tobias Kohl<sup>1\*</sup>, Maximilian S. Bothe<sup>1</sup>, Harald Luksch<sup>1</sup>, Hans Straka<sup>2</sup>, and Guido Westhoff<sup>3</sup>

<sup>1</sup> Chair of Zoology, Technical University Munich, Liesel-Beckmann-Str. 4, 85354 Freising-Weihenstephan, Germany Freising-Weihenstephan, Germany

<sup>2</sup> Department Biology II, Ludwig-Maximilians-University Munich, Großhaderner Str. 2, 82152 Planegg, Germany

<sup>3</sup> Institute for Zoology, University of Bonn, Meckenheimer Allee 169, 53115 Bonn, Germany

\*First-author

#### Contributions of Maximilian S. Bothe:

- Transfer of the whole-mount nerve staining technique to the rattlesnake in vitro preparation.
- Acquisition of data, except for nissl material (Figure 3)
- Analysis and interpretation of tracings
- Major part of the statistical analysis
- Preparation of Figures 1, 2, 4, 5, 6, 7
- Review and discussion of the manuscript

#### Contributions of other authors:

- Study concept and design: T.K., H.S., H.L., G.W.
- Establishment of the in vitro whole brain preparation: H.S., T.K., G.W.
- Review and discussion of data analysis and figures: T.K., H.S., H.L.
- Writing of the manuscript: T.K., H.S.
- Administrative, technical and material support: H.L., G.W., H.S., T.K.

*Permission for reuse granted by John Wiley & Sons, <https://www.wiley.com>*

Rightslink licence number: **4347670114730**

For online access refer to: <https://onlinelibrary.wiley.com/doi/epdf/10.1002/cne.23644>

# Organotopic Organization of the Primary Infrared Sensitive Nucleus (LTTD) in the Western Diamondback Rattlesnake (*Crotalus atrox*)

Tobias Kohl,<sup>1\*</sup> Maximilian S. Bothe,<sup>1</sup> Harald Luksch,<sup>1</sup> Hans Straka,<sup>2</sup> and Guido Westhoff<sup>3</sup>

<sup>1</sup>Chair of Zoology, Technische Universität München, Freising-Weihenstephan, Germany

<sup>2</sup>Department Biology II, Ludwig-Maximilians-Universität München, Planegg, Germany

<sup>3</sup>Institute for Zoology, University of Bonn, Bonn, Germany

## ABSTRACT

Pit vipers (Crotalinae) have a specific sensory system that detects infrared radiation with bilateral pit organs in the upper jaw. Each pit organ consists of a thin membrane, innervated by three trigeminal nerve branches that project to a specific nucleus in the dorsal hindbrain. The known topographic organization of infrared signals in the optic tectum prompted us to test the implementation of spatiotopically aligned sensory maps through hierarchical neuronal levels from the peripheral epithelium to the first central site in the hindbrain, the nucleus of the lateral descending trigeminal tract (LTTD). The spatial organization of the anatomical connections was revealed in a novel *in vitro* whole-brain preparation of the western diamondback rattlesnake (*Crotalus atrox*) that allowed specific application of multiple neuronal tracers to identified pit-organ-supplying trigeminal nerve branches. After adequate survival

times, the entire peripheral and central projections of fibers within the pit membrane and the LTTD became visible. This approach revealed a morphological partition of the pit membrane into three well-defined sensory areas with largely separated innervations by the three main branches. The peripheral segregation of infrared afferents in the sensory epithelium was matched by a differential termination of the afferents within different areas of the LTTD, with little overlap. This result demonstrates a topographic organizational principle of the snake infrared system that is implemented by maintaining spatially aligned representations of environmental infrared cues on the sensory epithelium through specific neuronal projections at the level of the first central processing stage, comparable to the visual system. *J. Comp. Neurol.* 522:3943–3959, 2014.

© 2014 Wiley Periodicals, Inc.

**INDEXING TERMS:** *in vitro* whole brain; pit viper; trigeminal nerve; topographic organization

Pit vipers perceive infrared (IR) radiation through a specialized structure known as the pit organ (Noble and Schmidt, 1937). The sensation of infrared radiation allows detection and avoidance of predators (Kardong and Mackessy, 1991; Roelke and Childress, 2007; Van Dyke and Grace, 2010), identification of optimal ecological environments for thermoregulation (Krochmal and Bakken, 2003), and precise strokes toward warm-blooded prey even in complete darkness (Kardong and Mackessy, 1991; Ebert and Westhoff, 2006; Chen et al., 2012). In contrast to the photochemical transduction process of visible electromagnetic radiation in the retina, infrared radiation raises the temperature of a thin membrane (pit membrane), which covers the cavity of the pit organ (Bullock and Diecke, 1956; Terashima et al., 1970). This change in temperature is

detected by free terminal endings of the trigeminal nerve by means of specialized heat-sensitive TRPA1-channels (Gracheva et al., 2010; Panzano et al., 2010).

H. Straka and G. Westhoff contributed equally to this work.

Grant sponsor: Dr. Leonhard-Lorenz Stiftung of the Technische Universität München; Grant number: 832/12 (to T.K.); Grant sponsor: Deutsche Forschungsgemeinschaft; Grant number: WE 2835/1-1 (to G.W.); Grant number: SFB 870, TP B12 (to H.S.); Grant sponsor: Bundesministerium für Bildung und Forschung; Grant number: 01RB0812B (to G.W.); Grant sponsor: Bourse Doctorale de Mobilité from the Université Paris Descartes (to T.K.).

Guido Westhoff's current address is Tierpark Hagenbeck gGmbH, Hamburg, Germany.

\*CORRESPONDENCE TO: Dr. Tobias Kohl, Lehrstuhl für Zoologie, Technische Universität München, Liesel-Beckmann-Str. 4, 85354 Freising-Weihenstephan, Germany. E-mail: tobias.kohl@wzw.tum.de

Received February 28, 2014; Revised June 25, 2014; Accepted June 30, 2014.

DOI 10.1002/cne.23644

Published online July 3, 2014 in Wiley Online Library (wileyonlinelibrary.com)

© 2014 Wiley Periodicals, Inc.

The infrared-receptive epithelium in the pit membrane thus consists of an arrangement of single free terminal nerve endings that each forms a terminal nerve mass (TNM) with a diameter of 30–50  $\mu\text{m}$  (Terashima et al., 1970; Amemiya et al., 1996). The pit membrane is innervated by two branches of the trigeminal nerve, the ophthalmic (V1) and the maxillary branch (V2), the latter of which splits into a deep branch (V2d) and a superficial branch (V2s). Each of these branches further ramifies into a distinct number of smaller fiber bundles, which were described in detail in the classic study by Lynn (1931). In addition to the transmission of infrared signals, the trigeminal nerve in these snakes also conveys other sensory information through several discrete V1 and V2 fiber bundles that bypass the pit membrane. These latter bundles along with the third branch of the trigeminal nerve (mandibular, V3) form the primary afferents of the common sensory trigeminal system, which in snakes closely resembles the trigeminal system of other vertebrates (Molenaar, 1978a,b).

Although the somata of the primary afferents of the infrared and the common trigeminal system are located within the trigeminal ganglion (Kishida et al., 1981), both signaling pathways are maintained separately at the level of the central nervous system (Meszler et al., 1981; Terashima and Liang, 1991, 1994). After entering the brainstem, infrared-sensitive primary afferent fibers form the lateral descending trigeminal tract (ltd) and project exclusively to the infrared-sensitive nucleus of the lateral descending trigeminal tract (LTTD; Meszler et al., 1981), which is unique to snakes capable of detecting infrared radiation (Schroeder and Loop, 1976). The LTTD is located in the dorsal hindbrain, lateral to the nucleus of the common trigeminal tract (TTD), which is the target of the primary afferent fiber bundle that forms the common trigeminal system (ttd) (Molenaar, 1974; Schroeder and Loop, 1976; Terashima and Liang, 1994).

In pit vipers, IR signals in LTTD neurons are relayed ipsilaterally to the nucleus reticularis calorificus (RC), a structure that is also exclusively sensitive to infrared radiation but is apparently absent in other infrared-sensitive snakes such as pythons and boas (Gruberg et al., 1979; Kishida et al., 1980; Newman et al., 1980; Stanford et al., 1981). IR-specific neurons in this latter nucleus project to the contralateral optic tectum of the midbrain, where the infrared information is obviously aligned with the spatiotopic map of the visual system (Hartline et al., 1978). This bimodal convergence onto sets of neurons allows an integration of signals from the infrared and visual environment (Hartline et al., 1978; Kass et al., 1978; Newman and Hartline, 1981).

A spatiotopic distribution of IR signals in the tectum has been demonstrated, but a corresponding

organizational principle for primary afferents in the periphery and secondary neurons in the LTTD remains elusive. Likewise, even though the infrared systems of pit vipers has been the focus of neuroanatomical and neurophysiological studies for more than 80 years, the computational calculations underlying IR signal processing in the LTTD are still poorly understood. A major reason for this lack of information is the difficult accessibility of the LTTD for in vivo experimentation in comparison with, e.g., the optic tectum. Consequently, there are few studies in which extracellular recordings were performed in the LTTD of pit vipers (Stanford and Hartline, 1980, 1984). These latter in vivo studies revealed an apparent convergence of primary infrared afferent inputs onto second-order infrared neurons in the LTTD; however, the excitatory receptive fields of the latter neurons were smaller than those of the primary afferents and were flanked by inhibitory areas. Even though this obvious contradiction was not entirely resolved, Stanford and Hartline (1980, 1984) suggested that the observed properties provide the basis for directional selectivity, motion sensitivity, and edge contrast in the infrared system.

To resolve the issue of afferent signal convergence in the LTTD and to elucidate the anatomical basis for a potential topographically organized signal processing along the hierarchical levels of the neuronal pathway in IR-sensitive snakes, we established an in vitro whole-brain preparation of the western diamondback rattlesnake (*Crotalus atrox*) for neuroanatomical tract tracing. This preparation permitted an unrestricted access to the trigeminal ganglion, LTTD, and RC as well as an unprecedented spatial specificity for tracer application to all sensory nerve branches. To delineate the peripheral and central projection patterns of primary infrared neurons, fluorescent tracers were applied to separate branches of the trigeminal nerve, with a subsequent survival of the isolated preparations for several days without any obvious deterioration. The staining identified the complete TNM termination pattern in the pit membrane as well as the axonal projection pattern within the LTTD. This allowed a direct correlation of distinctly innervated areas of the pit membrane by individual branches of the trigeminal nerve with the spatial distribution of the corresponding axon terminals in the LTTD.

## MATERIALS AND METHODS

In vitro experiments were performed on isolated brains of 24 juvenile western diamondback rattlesnakes (*Crotalus atrox*, Baird and Girard, 1853). The snakes (snout-vent length [SVL] 20–35 cm, weight 20–52 g)

were bred in captivity at the Chair of Zoology at the Technische Universität München. Snakes were kept on a 12:12-hour light:dark cycle with a 22–30°C temperature range and a diet of prekilled mice with water *ad libitum*. Care and maintenance of these animals followed the established guidelines for venomous snakes, and their use in these experiments was approved by the LANUV Nordrhein-Westfalen (8.87-50.10.45.08.080) and the Regierung von Oberbayern (55.2-1-54-2532.6-9-12). For isolation of the brains, specimens were placed in an induction chamber and preanesthetized with isoflurane until the tail-pinch reflex ceased. Snakes were mechanically secured with u-shaped needles to the Sylgard (Dow Corning, Wiesbaden, Germany) floor of a large petri dish and deeply anesthetized with a mixture of ketamine hydrochloride (40 mg/kg *i.m.*) and xylazine hydrochloride (20 mg/kg *i.m.*). After opening of the body by a ventral approach and exposure of the heart, the snakes were perfused transcidentally with 60 ml oxygenated ice-cold Ringer solution (in mM: 96.5 NaCl, 31.5 NaHCO<sub>3</sub>, 4 CaCl<sub>2</sub>, 2.6 KCl, 2 MgCl<sub>2</sub>, and 20 D-glucose, pH 7.4). After decapitation and removal of the lower jaw, the remaining dorsal part of the skull was transferred and fixed with needles upside down in a Sylgard-lined petri dish filled with cold Ringer solution that was permanently maintained at 4–8°C.

To access the peripheral and central infrared system, the maxillary bone on each side was removed at the level where the bone forms a depression that contains the pit organ. To expose the different branches of the trigeminal nerve, the overlying tissue, fangs, and venom glands were carefully removed. The skull was opened, and the brain was extracted with the pit organ attached to the trigeminal nerve. To facilitate Ringer diffusion into the nervous tissue, the meninges were opened. The individual trigeminal nerve branches innervating the pit membrane (V1, V2d, V2s; see Fig. 1) were identified and isolated for the application of fluorescent tracers. The employment of such an isolated *in vitro* snake whole-brain preparation thus provided the necessary accessibility to all relevant structural elements of the peripheral and central infrared system (Fig. 1),

comparable to the experimental condition previously described for the *in vitro* tracing of other sensory and motor systems in frogs (Luksch et al., 1996; Straka et al., 2006).

Application of neuronal tracers was performed immediately after isolation of the tissue. In these preparations, the pit organ remained attached to the trigeminal nerve branches for anterograde labeling of the free terminal nerve endings within the membrane. Two different dextran amines, conjugated to Alexa Fluor 488 or 546 (dextran, Alexa Fluor 488, 546; 10,000 MW, Invitrogen, Life Technologies, Darmstadt, Germany) were applied to two different sets of trigeminal nerve branches (V1–V3), respectively. This allowed correlating the area of the pit membrane innervated by each branch, as well as with the projection pattern in the hindbrain LTTD. For tracer application, a petroleum jelly (Vaseline weiss Ph.Eur., Bombastus-Werke, Freital, Germany) bowl was formed around an individual branch and sealed to avoid spread of tracer to neighboring tissue. The bowl was then filled with distilled water, and the nerve inside the bowl was cut with fine scissors and left for 30 seconds to prevent resealing of the cut ends. Subsequently, the distilled water was replaced with an Alexa Fluor dextran tracer (5% in phosphate buffer, 0.1 M) and incubated for 2 hours at 4°C. Thereafter, surplus tracer was removed, and the preparations were washed in cold Ringer solution and maintained at 8°C for up to 5 days. Different trigeminal nerve branches were stained separately with Alexa Fluor 488 and 546 dextran in four different combinations (Table 1) to outline the peripheral and central projections. In addition, neurons in the LTTD were retrogradely labeled to confirm the location of the LTTD in the isolated rattlesnake brain based on external landmarks (Gruberg et al., 1979). For this purpose, an incision was made at the lateroventral surface of the hindbrain at the level of the caudal end of the cerebellum to insert crystals of Alexa Fluor 546 dextran into the superficially located RC. The brain was subsequently incubated and processed as described for the nerve tracings. In addition, two brains were cut in either the transverse or the horizontal plane and processed

## Abbreviations

|      |  |     |   |
|------|--|-----|---|
| CB   | cerebellum   | rmx | maxillary root                                    |
| HB   | hindbrain  | RC  | nucleus reticularis caloris                       |
| ltd  | lateral trigeminal descending tract                | TNM | terminal nerve mass                               |
| LTTD | nucleus of the lateral descending trigeminal tract | TE  | telencephalon                                     |
| md   | mandibular part of MMG                             | TPR | principal nucleus of the common trigeminal system |
| MMG  | trigeminal ganglion                                | ttd | common descending trigeminal tract                |
| MT   | motor trigeminal nuclei                            | TTD | nucleus of the common descending trigeminal tract |
| mx   | maxillary part of MMG                              | Ve  | ventricle   |
| OG   | ophthalmic ganglion                                | V1  | ophthalmic trigeminal branch                      |
| OT   | optic tectum                                       | V2s | superficial maxillary trigeminal branch           |
| PC   | choroid plexus                                     | V2d | deep maxillary trigeminal branch                  |
| rmd  | mandibular root                                    | V3  | mandibular trigeminal branch                      |
| rmt  | motor trigeminal root                              |     |   |

for Nissl staining (cresyl violet; 1.5% in water) of the sections. These sections were used to outline the different common and infrared sensory nuclei of the trigeminal systems as a spatial reference for the labeled nuclei after application of neuronal tracers.

After incubation, preparations were fixed in 4% paraformaldehyde in phosphate buffer (PB; 0.1 M, pH 7.4) for 24 hours. Brains were immersed in 15% (2 hours) and 30% (24 hours) sucrose in 0.1 M PB, embedded in

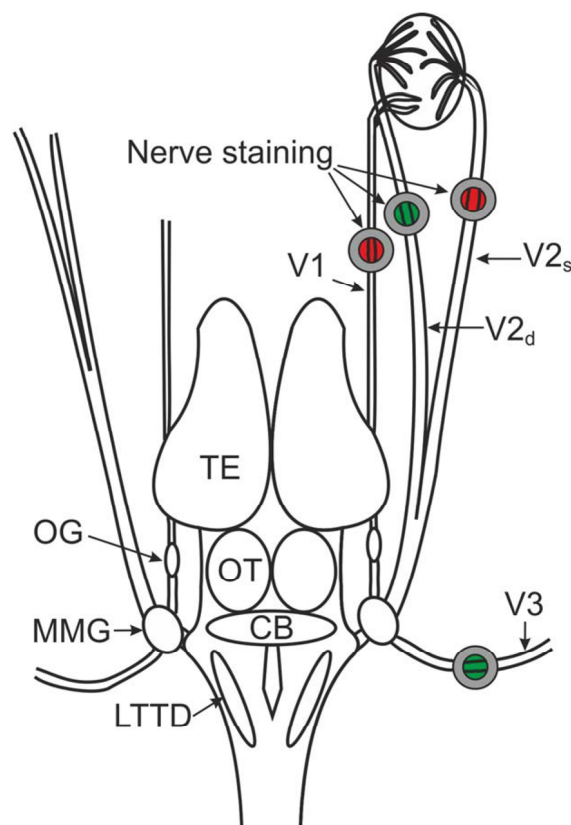


**Figure 1.** Schematic of the brain of the western diamondback rattlesnake and location of tracer application to different trigeminal nerve branches. The pit membrane and different trigeminal nerve branches (V1–V3) remained intact for tracer application. Fluorescent tracers (Alexa Fluor dextran 488, 546) were applied to combinations of individual branches of the trigeminal nerve (V1, V2s, V2d, V3). For abbreviations see list.

Cryomatrix (Thermo Shandon Limited, Cambridge, United Kingdom), and sectioned on a cryostat at  $-20^{\circ}\text{C}$ . Brains were cut in the horizontal, sagittal, or transverse plane at a thickness of  $40\ \mu\text{m}$ . Sections were mounted onto slides, washed in 0.1 M PB, and coverslipped with an antifade mounting medium (propyl gallat 0.2% [Sigma-Aldrich, Darmstadt, Germany], DMSO 1% [Sigma-Aldrich], glycerol 90%, dissolved in PBS 1 M, pH 7.4). The limited thickness of the pit membrane ( $\sim 25\ \mu\text{m}$ ) allowed scanning of the epithelial structure in whole-mount preparations of the entire organ. Stained terminations in the pit membrane, labeled neurons in the trigeminal ganglion, and axonal projections and neurons in the LTTD were reconstructed from stacks of 10–20 consecutive optical sections after scanning on a Leica SP-5 confocal microscope (Leica, Wetzlar, Germany) at  $1.5\text{--}3.5\text{-}\mu\text{m}$  z-axis intervals. Images were produced by a projection of the entire stack. For reason of clarity, color channels were digitally converted to blue (V1), green (V2d), and magenta (V2s). The diameter of labeled TNMs was determined by fitting a circle to each TNM and calculating its diameter. For a comparison with previous studies related to the trigeminal ganglion of infrared-sensitive snakes (Kishida et al., 1981; Terashima and Liang, 1991), soma diameters of primary afferents were calculated. In accordance with these studies, an ellipsoid was fitted to each soma, and the major axis was determined. All measurements were performed with public-domain image processing software (Fiji plugin, <http://www.fiji.sc>, RRID:nif-0000-30467).

## RESULTS

Tracer application to the peripheral branches of the trigeminal nerve and a survival of the *in vitro* whole-brain preparation for up to 5 days outlined the afferent termination pattern in the pit membrane as well as the first central infrared nucleus, the LTTD.

### Anterograde labeling of terminal nerve endings in the pit membrane

Application of Alexa Fluor dextran to the V1, V2d, and V2s nerve branches ( $n = 17$ ) resulted in labeling of

**TABLE 1.**

**Summary of Combinations of Injected Trigeminal Nerve Branches With Alexa Fluor Dextran Conjugates**

| N | V1 (blue)   | V2d (green)   | V2s (magenta)                                     | V3 (green)      |
|---|---|---|---|-----------------|
| 8 | Alexa Fluor 546                                   | Alexa Fluor 488                                     |   |                 |
| 8 |   | Alexa Fluor 488                                     | Alexa Fluor 546                                   |                 |
| 3 |   |   |   | Alexa Fluor 488 |
| 1 | <b>V2s<sub>2</sub> (green)</b><br>Alexa Fluor 488 | <b>V2s<sub>3</sub> (magenta)</b><br>Alexa Fluor 546 | <b>V2s<sub>4</sub> (green)</b><br>Alexa Fluor 488 |                 |

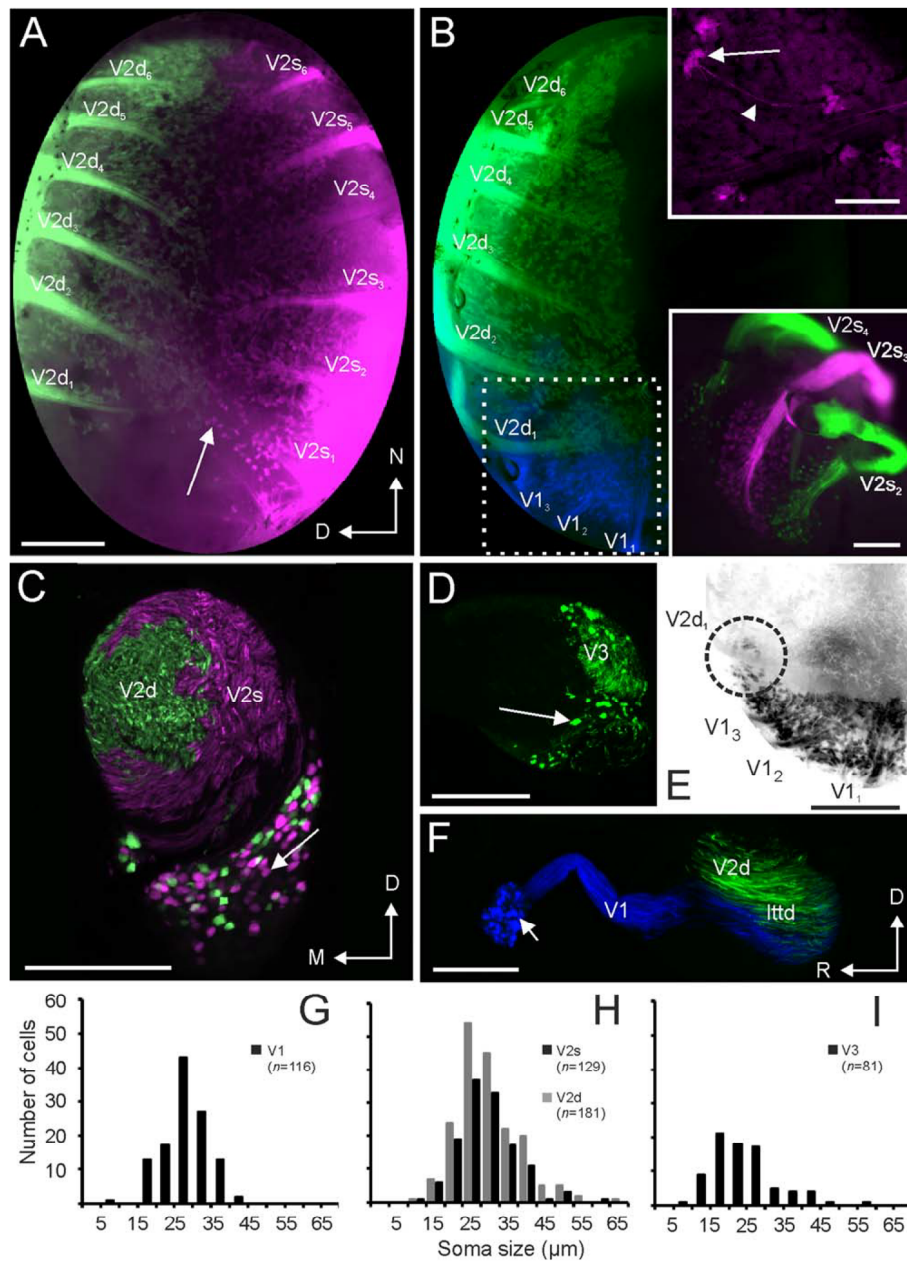


**Figure 2.** Anterograde tracing of TNMs in the pit membrane and retrograde labeling of corresponding cell bodies in the trigeminal ganglion. **A,B:** Application of fluorescent tracer to V1 (blue), V2d (green), and V2s (magenta) outlined trigeminal nerve projections in the pit membrane. Labeled branches ramified into smaller fiber bundles ( $V1_{1-3}$ ,  $V2d_{1-6}$ ,  $V2s_{1-6}$ ) and further split into individual fibers (arrowhead in **B**, **upper inset**) to form single TNMs (arrow in **A**; for details see arrow in **B**, **upper inset**); nonoverlapping innervations of distinct areas were maintained at the level of smaller fiber bundles (**lower inset** in **B**:  $V2s_{2-4}$ ). **C,D:** Distribution of somata (arrow) of V2d and V2s fibers in the rostral part of the maxillomandibular ganglion (**C**) and of V3 fibers in the caudal maxillomandibular ganglion (**D**). **E:** Higher magnification of the outlined area in **B**, illustrating the limited overlap of projections from V1 and V2d (dashed circle); for the visual presentation, the blue color channel was converted and inverted to black and white to enhance the contrast of labeled TNMs. **F:** Somata of V1 fibers in the ophthalmic ganglion (arrow); ascending afferent fibers (blue) entered the hindbrain to form the lttid conjointly with fibers from V2d (green). **G–I:** Distribution of ganglion cell soma size for V1 (**G**), V2s/V2d (**H**), and V3 (**I**) branches of the trigeminal nerve. The spatial orientation of the pit organ is indicated by the arrows in **A** (also applies to **B**). Orientation of sections in **C,D,F** is indicated by arrows in **C** and **F**. Orientation bars in **C** also apply to **D**. D, dorsal; M, medial; R, rostral. For abbreviations see list. Scale bars = 0.5 mm in **A** (applies to **A,B**); 100  $\mu$ m in **B**, upper inset; 0.5 mm in **B**, lower inset; 0.5 mm in **C,D,E,F**.

individual trigeminal nerve fibers within the pit membrane, arising from the nerve branches after entering the pit membrane (Fig. 2A,B,E). Each fiber terminated as a single free terminal nerve ending that formed a densely packed TNM (Fig. 2B, upper inset). With the exception of the vascular bed, the entire pit area was densely covered with labeled TNMs, confirming that the tracer was taken up by virtually all fibers of the individual nerve branches. Even though the outline of individual TNMs was not clearly distinguishable in most preparations, mostly because of the packing density, the tracing yielded the complete projection pattern throughout the pit membrane. In one case, however, application of Alexa Fluor dextran to V2s and V2d caused an incomplete staining of the pit membrane. In this case, single TNMs distributed throughout the whole membrane except the area innervated by V1 were discernible. The limited visual delineation of the TNMs in this experiment made it possible to determine more precisely the diameter of individual TNMs. Measurements indicated that the size of TNMs (30–50  $\mu\text{m}$ ) formed by either fibers of the V2s (mean  $\pm$  SD,  $41 \pm 5 \mu\text{m}$ ;  $n = 19$ ) or the V2d nerve branch (mean  $\pm$  SD,  $38 \pm 6 \mu\text{m}$ ;  $n = 19$ ) was similar and not significantly different ( $P = 0.116$ , Kolmogorov-Smirnov test).

In general, tracing of adjacent branches of the trigeminal nerve with different fluorescent dyes of complementary color showed that each branch innervates a distinct area of the pit membrane. Accordingly, application of Alexa Fluor dextran 546 to V2s resulted in staining of TNMs located in the ventral area of the pit membrane (Fig. 2A), whereas TNMs in the remaining dorsal area of the pit membrane were outlined by a simultaneous application of Alexa Fluor dextran 488 to V2d. The border between these two regions was clearly delineated, with minimal if any overlap between the outlined areas, compatible with the implementation of a topographic principle for the signal processing in the infrared system. Figure 2A also shows that the dorso-temporal part of the pit membrane remained unlabeled after tracer application to both V2 branches of the trigeminal nerve. TNMs in this area, however, were labeled after application of Alexa Fluor dextran 546 to V1 (Fig. 2B, blue). When Alexa Fluor dextran 488 was additionally applied to V2d, the complementary part to the area innervated by V2s was outlined. However, in three preparations in which V1 and V2d were labeled conjointly, a small area of overlap was encountered (Fig. 2B,E). In contrast, and as expected, tracer application to V3 did not label TNMs in the pit membrane, confirming that this trigeminal nerve branch innervates targets other than the pit membrane. In summary, the pit membrane can be divided into three distinct areas

that are innervated exclusively by single branches of the trigeminal nerve, with a spatially limited region of overlap between the areas supplied by V1 and V2d. The general separation at the gross morphological level of the different trigeminal nerve branches appears to be continued at the next lower branching level. In fact, alternate staining of discrete neighboring fiber bundles of, e.g., the V2s branch (V2s<sub>2–4</sub>) with Alexa Fluor dextran 488 and 546 after the final ramification of the branches within the pit membrane revealed a distinct, nonoverlapping spatial arrangement of the regional projection and the formation of the TNMs (lower inset in Fig. 2B).

### Labeling of cell bodies in the trigeminal ganglion

The use of an isolated whole-brain preparation for *in vitro* experimentation allowed separate tracing of primary afferent neurons within specific branches from the pit membrane to the axon terminals in the first central nucleus of the common trigeminal (TTD) and the infrared-sensitive system (LTTD). The cell bodies of all peripherally labeled afferent fibers were located in the trigeminal ganglionic complex, which formed two anatomically separate entities (see Fig. 1). The ophthalmic ganglion, situated most rostrally (OG in Fig. 1), contained medium-sized to large cell bodies (Fig. 2G) of fibers in the V1 branch innervating part of the pit organ (Fig. 2F). In contrast, the predominantly small cell bodies (Fig. 2I) of the common trigeminal system within the mandibular branch (V3) were located caudally within the considerably larger maxillo-mandibular ganglion (MMG in Figs. 1, 2D). In a complementary fashion, the rostral part of the maxillomandibular ganglion contained the relatively large cell bodies of the V2d and V2s trigeminal nerve branches (Fig. 2H), both of which innervate specific areas of the pit membrane (Fig. 2A,B). At variance with the separate location of somata of fibers in the V1 and V2 branch in two ganglia, cell bodies of the latter two V2 (V2s, V2d) branches were largely intermingled and randomly distributed within the rostral part of the maxillomandibular ganglion, without any double-labeled neurons projecting into both branches (Fig. 2C). Ganglion cells of fibers of the common trigeminal system traversing the mandibular branch (V3; Fig. 2I) were significantly smaller compared with soma diameters of pit-membrane-supplying fibers in the V1 and V2s/V2d (Fig. 2G,H;  $P = 0.001$ , Kruskal-Wallis test, Bonferroni corrected).

### Neuroanatomical localization of the TTD and LTTD

Transverse (Fig. 3A–C) and horizontal (Fig. 3D<sub>1,2</sub>) Nissl-stained sections revealed a clear demarcation of

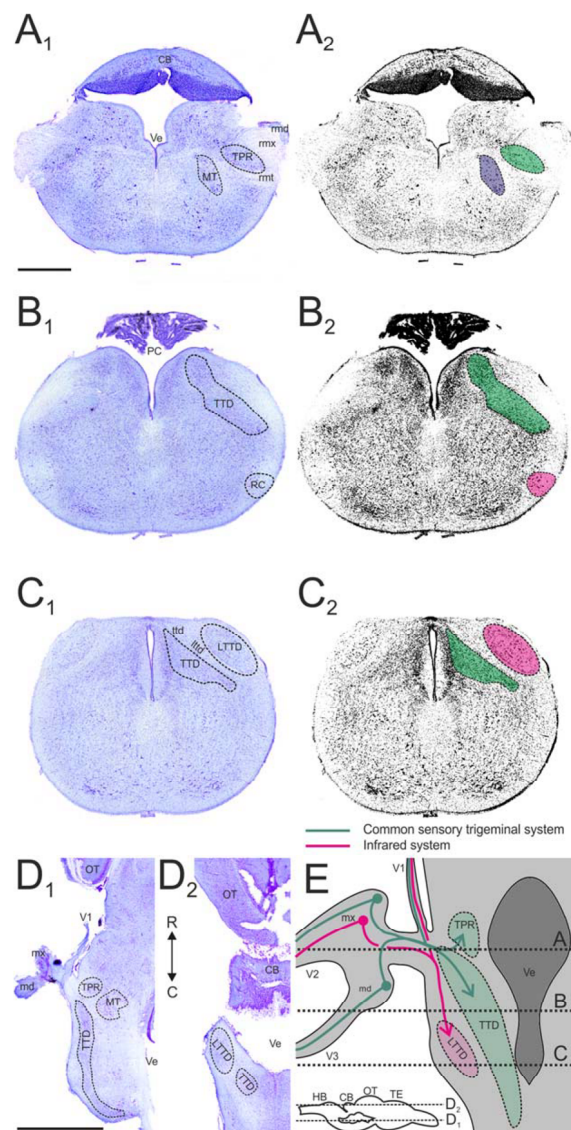


**Figure 3.** Anatomical organization of the trigeminal nuclear complex. **A–C:** Nissl-stained transverse sections through the hindbrain at three rostrocaudal levels ( $A_1$ – $C_1$ ) depicting the different trigeminal sensory and motor nuclei; color-coded demarcation of the common sensory (green) and infrared recipient nuclei (red) as well as the motor nucleus (blue) in black-and-white versions ( $A_2$ – $C_2$ ) of the same sections shown in  $A_1$ – $C_1$ ; rostrocaudal levels of the sections are indicated in **E**. **D:** Nissl-stained horizontal sections at a ventral ( $D_1$ ) and a more dorsal ( $D_2$ ) level of the hindbrain (levels are indicated by dashed lines in the scheme in **E**) illustrating the longitudinal extension of the common sensory (TTD) and infrared (LTTD) trigeminal nuclei. **E:** Schematic drawing indicating trajectories and projections of trigeminal sensory afferents to the central nuclei; dashed lines represent the levels of transverse sections in **A–C**; green and red mark the common sensory and infrared trigeminal system, respectively; the **inset** in **E** is a sagittal view of the brain indicating the dorsoventral levels of the horizontal sections in  $D_{1,2}$ . C, caudal; R, rostral. For abbreviations see list. Scale bars = 1 mm in  $A_1$  (applies to  $A_{1,2}$ ,  $B_{1,2}$ ,  $C_{1,2}$ ); 2 mm in  $D_1$  (applies to  $D_{1,2}$ ).

the nuclei of the common sensory system from those of the infrared system (Fig. 3E). The trajectory of the labeled primary trigeminal afferent axons could be followed to their termination sites in the ipsilateral hindbrain. Labeled axonal processes and terminals outlined a region in the dorsolateral hindbrain (Figs. 3A–C, 4A,B). To demarcate the location of the nucleus related to the common trigeminal sensory system (TTD) from that of the infrared system (LTTD) clearly, two control experiments were performed. First, Alexa Fluor dextran 488 was injected into V3, which innervates the lower jaw and has no relation to the pit membrane in this group of snakes. Labeled fibers of the ttd entered the hindbrain at the dorsal surface and turned centrally to form axon terminals, thereby outlining the TTD (Fig. 4B). This termination pattern clearly delimited this latter area from the more laterally located area delineated by labeled fibers from V1 and V2d (Fig. 4A). Second, application of Alexa Fluor dextran 546 into the ipsilateral RC (Fig. 4C), which is an exclusive target area for projections originating in the LTTD, resulted in retrograde labeling of neurons close to the dorsolateral surface of the hindbrain (Fig. 4C,D). This area coincided with the axon terminal field of fibers labeled from the V1 and V2d nerve branches (Fig. 4A). Labeled neurons were relatively small (mean diameter  $\pm$  SD  $21 \pm 4 \mu\text{m}$ ;  $n = 56$ ) and scattered throughout this area. In contrast, no labeled neurons were encountered in the TTD, compatible with a separation of common and infrared central trigeminal pathways. The unstained area between the TTD and the LTTD (ltd in Fig. 4B,D) corresponds to the tract formed by the ventrodorsally traversing IR-sensitive afferent fibers.

### Projection pattern of primary infrared neurons

To reveal a potential topographic organization of primary infrared afferent projections in the LTTD, neuronal tracers were injected into different branches of the trigeminal nerve (V1, V2s, and V2d). Parasagittal sections through the brainstem showed a dense labeling of axonal processes and terminals in the dorsal hindbrain (Fig. 5A), which extended from the level of the caudal end of the cerebellum to the obex. Labeled axonal processes were clearly distinguishable from fine axon terminals, which extended throughout the entire area, but with different patterns following tracing of the different trigeminal nerve branches (Fig. 5B,C). Axons from V2d entered the LTTD at the most rostradorsal aspect and traversed caudally, giving off ventrally projecting collaterals (Fig. 5B, green) that terminated as relatively large bouton-like endings throughout the

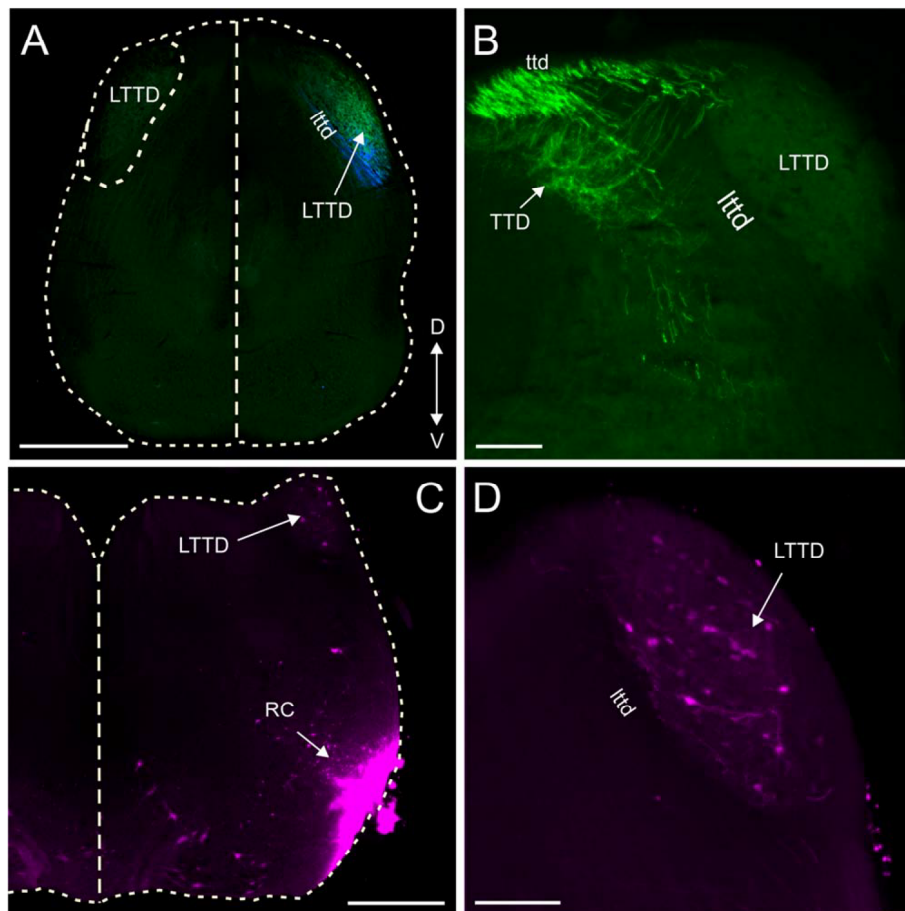


**Figure 4.** Anatomical delineation of the infrared (LTTD) and common trigeminal central nuclei (TTD) on transverse sections through the hindbrain. **A:** Fibers, labeled from V1 (blue) and V2d (green), enter the hindbrain at the dorsolateral edge and outline the laterally located LTTD. **B:** Fibers, labeled from V3 (green), terminate in a more medially located area and delineate the TTD. **C,D:** Injection of Alexa Fluor dextran into the infrared-sensitive RC retrogradely labeled neurons in the LTTD, thus overlapping with projections of fibers from V1 and both V2 branches. The orientation of the sections is indicated in A (applies to A–C). The outline of the sections in A,C and the LTTD and midline are indicated by dashed lines. D, dorsal; V, ventral. For abbreviations see list. Scale bars = 1 mm in A; 200  $\mu$ m in B,D; 500  $\mu$ m in C.

dorsal part of the LTTD (Fig. 5C). In contrast, fibers of V1 entered the LTTD from ventral and coursed caudally toward their final termination site in the ventral area of the LTTD (Fig. 5B, blue), delineating a small area of overlap with V2d fiber terminals. In parasagittal sections, no V1 axon terminals were found at the most lateral edge of the LTTD (Fig. 5D). From laterally to medially, the area with stained axon terminals of V2d and V1 increased in size (Fig. 5B), whereas the most medial sections contained only few axon terminals from fibers of both nerve branches (Fig. 5E).

In comparison, parasagittal sections with afferent fibers stained separately from V2s (magenta) and V2d (green) displayed a more pronounced lateromedial differentiation of their termination areas with minor dorsoventral differences (Fig. 5F–H). Accordingly, axon terminals

of V2d fibers were particularly abundant in the most lateral part of the LTTD, a region where terminals of V2s fibers were absent (Fig. 5F). Sections from more medial areas showed axon terminals of both branches, with terminals from V2d fibers located dorsal to those of V2s axons (Fig. 5G). The extent of lateromedial differentiation became particularly apparent in the most medial aspect of the nucleus, where mostly terminals of V2s were found with only few terminals of V2d (Fig. 5H).

The differential dorsoventral organization of V2d and V1 axonal terminations within the LTTD as well as the lateromedial separation of V2d and V2s axonal terminals was corroborated by results obtained from transverse sections through the nucleus (Fig. 6). Fibers and axon terminals of V2d (green in Fig. 6B–L) were particularly abundant at ventrolateral positions of the rostral

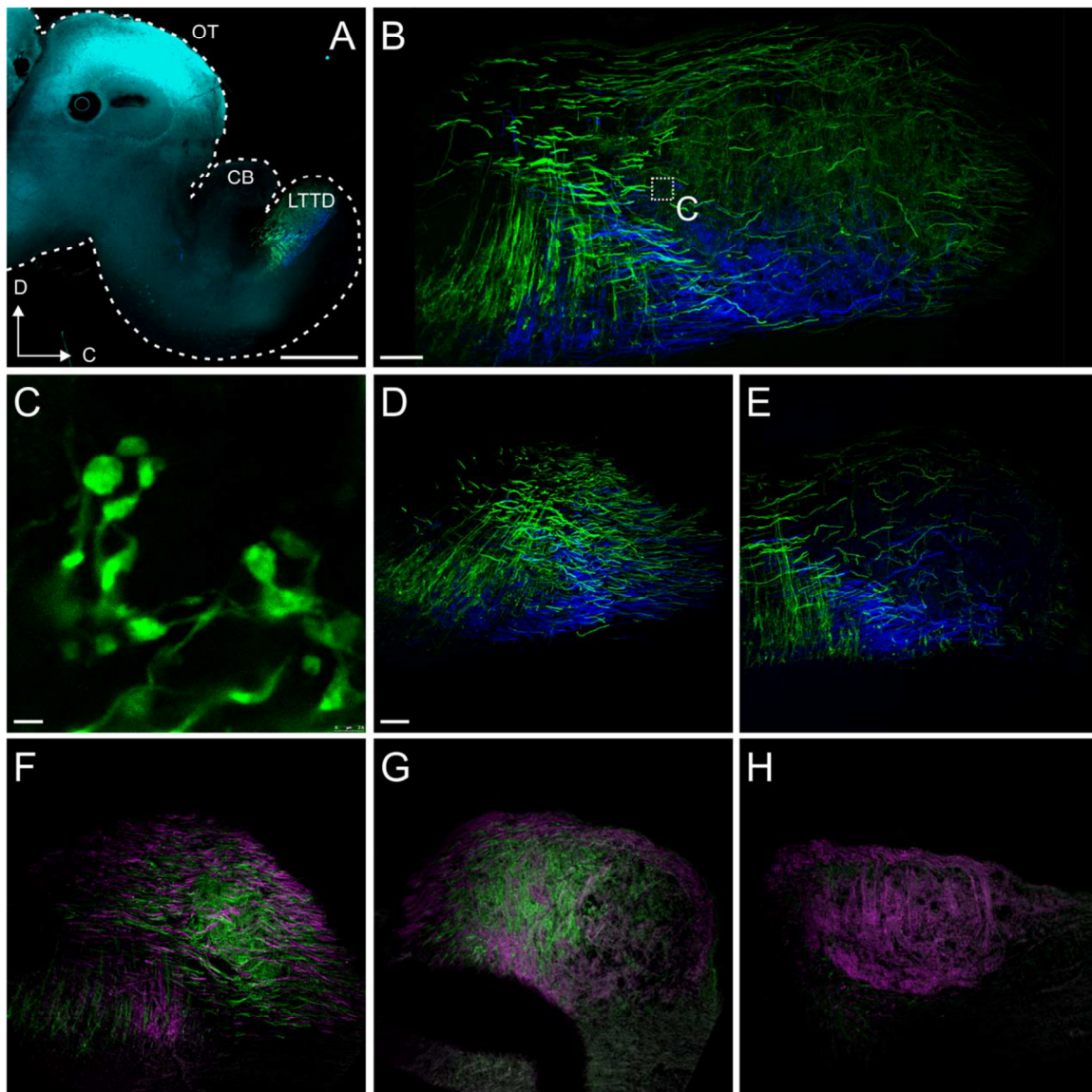


**Figure 5.** Sagittal view of primary infrared afferent projections within the LTTD. **A:** Parasagittal section through the brain depicting the location of the LTTD within the hindbrain. **B–H:** Two separate series of parasagittal sections (40  $\mu\text{m}$ ) through the LTTD from lateral to medial (D,B,E; F–H), illustrating differential projections of afferent fibers and axonal terminations from V1 (blue) and V2d (green) nerve branches (B–E) and from V2s (magenta) and V2d (green) nerve branches (F–H); higher magnification (C) of the outlined area in B illustrating axon terminals of V2d nerve fibers. The outline of the section in A is indicated by a dashed line. C, caudal; D, dorsal. For abbreviations see list. Scale bars = 1 mm in A; 100  $\mu\text{m}$  in B,D (applies to D–H); 2.5  $\mu\text{m}$  in C.

LTTD. A limited spatial overlap with projections from the latter nerve branch in ventral areas of the LTTD was observed for axon terminals of V1 fibers (blue in Fig. 6), which extended mainly ventromedially (Fig. 6E–G). From caudal to rostral, the area with axon terminations of V2d fibers increased until the entire area of the LTTD was covered (Fig. 6B–I).

The dorsomedial area of the LTTD (asterisk in Fig. 6F), which remained relatively devoid of fibers and

axonal terminations after a combined labeling of the V1 and V2d branches, contained axonal terminations from V2s nerve fibers (Fig. 6K,L), as evidenced by the separate staining of V2d and V2s. At the most caudal aspect of the LTTD, the entire area was covered only by axon terminals from the V2s nerve branch (Fig. 6L). At more rostral levels of the LTTD, this area extended dorsomedially within the LTTD (asterisk in Fig. 6K), which corresponds to the fiber-free area depicted in

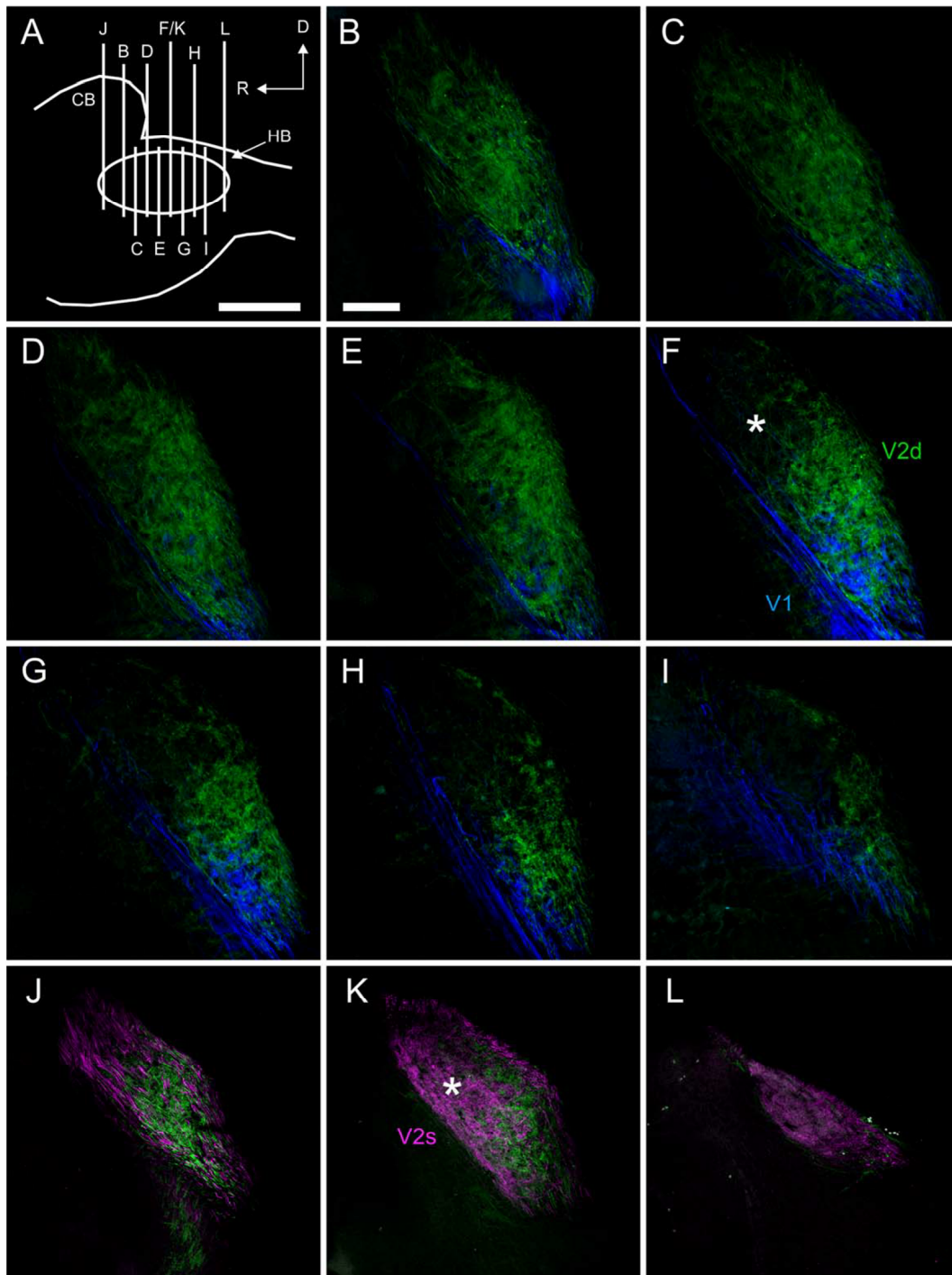


**Figure 6.** Primary infrared afferent projections within the LTTD. **A:** Schematic sagittal view of the brain depicting the location of the transverse sections shown in B–L. **B–L:** Two separate series of cross sections (40  $\mu\text{m}$ ) through the LTTD (B–I; J–L) from rostral to caudal, respectively, illustrating differential projections of afferent fibers and axonal terminations from V1 (blue) and V2d (green) nerve branches (B–I) and from V2s (magenta) and V2d (green) nerve branches (J–L); asterisk in F,K depicts the corresponding area devoid of axon terminals of fibers from the V2d and V1 nerve branches but abundant terminations of fibers from the V2s nerve branch. D, dorsal; R, rostral. For abbreviations see list. Scale bars = 500  $\mu\text{m}$  in A; 200  $\mu\text{m}$  in B (applies to B–L).

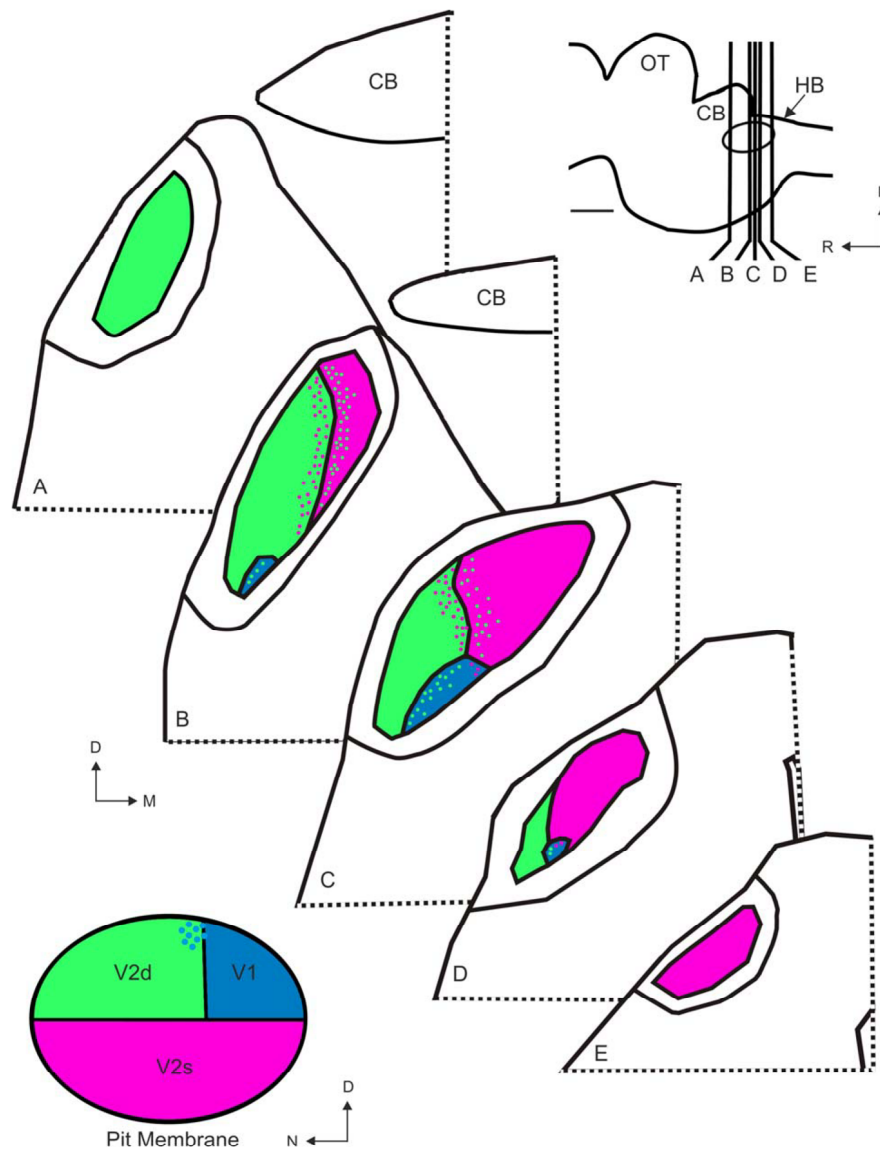


**Figure 7.** Diagram summarizing the corresponding peripheral and central topographic organization of infrared afferent projections. Series of schematic transverse sections (A–E) through the LTTD (section levels indicated at upper right). The distinct spatiotopic innervation of the pit membrane by different trigeminal nerve branches is reflected centrally by a similar differential projection pattern along the rostro-caudal extent of the LTTD. Boundaries between adjacent areas of axonal innervations were distinct, with restricted areas of overlap (colored dots). Blue: V1; green: V2d; magenta: V2s nerve branch. D, dorsal; M, medial; N, nasal; R, rostral. For abbreviations see list. Scale bar = 1 mm.

Figure 6F (asterisk). Even though the central projection in the hindbrain is dominated by separate terminal fields, a prominent but restricted overlap was present along the border of areas differentially innervated by the V2s and V2d branches (Fig. 6K) and V2s and V1 (Fig. 6F). Despite this limited overlap, the notion of a general spatial segregation of IR-sensitive afferent projections from different areas of the pit membrane within the LTTD prevailed, in agreement with a topographic

organizational pattern of afferent inputs within the first central nucleus (Fig. 7), and suggests a limited synaptic convergence of signals from different areas of the sensory periphery.

## DISCUSSION

Separate staining of trigeminal nerve branches in isolated whole brains of the pit viper yielded a spatially

aligned and topographically organized termination pattern of afferent fibers in the sensory epithelium as well as the first central nucleus in the brainstem. The limited peripheral and central overlap of the spatiotopic infrared signal representations suggests the presence of a segregated organotopic representation that is similar to that in the visual system and relies on the transfer of the spatial maps through ascending hierarchical levels of sensory signal processing. The current results will serve as the anatomical basis for understanding how dynamic environmental infrared signatures are spatially encoded, fine-tuned, and integrated with signals related to the visual world in IR-sensitive snakes.

### In vitro snake whole brains for neuroanatomical tract tracing

This study used an *in vitro* whole brain of an infrared-sensitive snake that allowed unrestricted experimental access for the application of multiple tracer substances to all relevant neuronal structures in the sensory periphery as well as the central nervous system. The survival of the brain after isolation for several days without any noticeable deterioration along with the complete staining of all trigeminal nerve afferents at the level of the sensory periphery and central termination site indicates the suitability of such a preparation for delineating neuronal pathways. Although this *in vitro* brain preparation is novel for infrared-sensitive snakes, similar isolated preparations of adult anamniote and amniote vertebrate species have been used previously for a number of morphophysiological studies (see, e.g., Luksch et al., 1996; Vibert et al., 1997; Kogo et al., 2002; Straka and Simmers, 2012). In fact, comparable isolated whole brains have been established for lamprey (see, e.g., Brodin and Grillner, 1990), anurans (see, e.g., Straka et al., 2001, 2006), reptiles (see, e.g., Keifer and Houk, 1989; Perez-Santana et al., 1997), and guinea pigs (Mühlethaler et al., 1993) and shown to be excellent experimental model systems that circumvent several methodical drawbacks of *in vivo* approaches such as bleeding, pulsations from the blood flow, and the necessity to maintain a particular anesthetic level (Luksch et al., 1996; Moiseenkova et al., 2003). The main advantages of the isolated central nervous system for the current study was the unprecedented accessibility of the different cranial nerve branches, the sensory epithelium as well as the brainstem nuclei, for the application of neuronal tracers to specific target sites or fiber bundles, which would have been impossible to accomplish under *in vivo* conditions. The development of such a preparation for successful *in vitro* anatomical tract tracing of the infrared system in snakes is only a

first step in understanding the signal processing within this sensory system. Future studies extending the use of this preparation and combining neurophysiological and pharmacological approaches at the single-cell level (Kohl, 2011) will allow deciphering the computational steps at the different synaptic levels from the sensory periphery to the optic tectum, where infrared signals fuse with visual signals in a spatially and dynamically specific manner that has yet to be determined in detail.

### Functional organization of the infrared sensory periphery

In pit vipers, in which the pit organ is located in the upper jaw, the membrane is innervated by the V1, V2d, and V2s but not the V3 trigeminal nerve branch (Lynn, 1931; Bullock and Fox, 1957; Kohl et al., 2012; Figs. 2A,B, 3E). In contrast, besides supralabial pits, boids and pythons have in addition infralabial pits, which in these snakes are innervated by the mandibular branch (V3), compatible with the evolutionarily conserved projection of this trigeminal nerve branch to the lower jaw (Molenaar, 1992). Thus, the different innervation patterns of pit organs in pit vipers and boids/pythons by different sets of trigeminal nerve branches comply with the cranial locations of infrared organs in the different groups of snakes. The multiple innervation of the pit membrane in pit vipers by V1, V2d, and V2s, however, is not arbitrary; each of these branches supplies a specific area of the pit organ, as indicated by the separate fields of TNMs in the membrane, with a limited amount of overlap (Figs. 2A,B, 7). Our findings thus extend the results of previous studies using a degeneration technique (Bullock and Fox, 1957) or succinate dehydrogenase staining (Goris et al., 1989). The apparent clear demarcation of pit areas innervated by individual trigeminal nerve branches in the latter studies, however, is likely overestimated given the limited but clear overlap of areas innervated by, e.g., V1 and V2d. Nonetheless, the distinct mapping of infrared cues in the environment onto the sensory epithelium in the pit is matched by a clear segregation of trigeminal nerve afferents that innervate specific areas. This pattern indicates the implementation of a topographic principle that originates in the arrangement of the TNMs and is continued and extended by the cranial nerve supply of the different peripheral regions.

The anatomically segregated innervation pattern, however, remains so far without any physiological correlate or functional implication. The aperture of the pit organ implements the function of a pinhole lens, so the resulting image on the pit membrane is inverted (Sichert et al., 2006). Given the orientation of the pit

membrane in situ, the areas innervated by V2s (ventral) and V2d (dorsal) appear to receive infrared radiation from sources above (V2s) and below (V2d) the snake, respectively, thus separating the sensory field in the vertical plane into two major regions. Accordingly, the region below the horizon is represented in the area of the pit membrane innervated by V2d, whereas the region above the horizon is represented in the area of V2s. The area innervated by V1 specifically receives environmental information from frontal regions with the receptive field extending onto the contralateral side. Although sensory fields in rattlesnakes show little binocular overlap ( $<10^\circ$ ; Bakken et al., 2012), areas innervated by V1 might play a fundamental role in stereoscopic infrared vision. This hypothesis is supported by previous findings (Amemiya et al., 1999) demonstrating that the capillary network of the area innervated by V1 is considerably denser than those areas innervated by V2s and V2d, suggesting a particular functional importance. However, if this anatomical peculiarity is in fact indicative of a putative stereoscopic infrared vision remains to be evaluated. Although infrared sensitive snakes with both eyes and one pit occluded are still able to perform successful strikes, the precision of this motor reaction is considerably reduced (Chen et al., 2012), compatible with an improvement of spatial sensory specificity when infrared signals are detected through bilateral pit organs.

Even though TNMs in the epithelium are formed by different nerve branches, the diameters of all TNMs are very similar, compatible with the measurements of earlier reports (Bullock and Fox, 1957; Terashima et al., 1970). Furthermore, the number of labeled TNMs in our study of  $\sim 5,000$  for a pit area of  $\sim 6 \text{ mm}^2$  was comparable to the number of TNMs (Hisajima et al., 2002) and the number of infrared-sensitive cell bodies in the trigeminal ganglia reported for *Gloydus brevicaudus* (Kishida et al., 1982) as well as for *Crotalus horridus* (Bullock and Fox, 1957) after correction for noninfrared-sensitive C-fibers in the latter study. Although the peripheral innervation of the pit membrane by V2s and V2d is separated, there is considerable intermingling of the cell bodies in the maxillomandibular ganglionic complex, compatible with the inference from previous studies (Kishida et al., 1982; Terashima and Liang, 1991). The absence of double-labeled ganglion cells and fibers in our specific tracing study complies with results of histological (Terashima et al., 1970) and electrophysiological (Terashima and Goris, 1979) experiments and rejects earlier suggestions that individual primary afferent fibers secondarily branch within the pit membrane to innervate multiple areas (Desalvo and Hartline, 1978).

Previous studies classified primary afferent neurons in the trigeminal ganglia of different species of pit vipers according to morphological characteristics (Kishida et al., 1982; Terashima and Liang, 1994; Liang et al., 1995), general appearance in Nissl-stained material (Kishida et al., 1982), and immunohistochemistry (Moon et al., 2003, 2004). Infrared-sensitive ganglion cells in pit vipers are comparable in size to nociceptive A- $\delta$  neurons, smaller than tactile neurons, and larger than mechanical nociceptive neurons (Liang et al., 1995). This classification appears to be species independent given the fact that in *Gloydus blomhoffi* a comparable differentiation of identified infrared neurons was observed (Kishida et al., 1982). Since the somata of the noninfrared-sensitive V3 trigeminal branch were considerably smaller than somata of fibers in the V1 and V2s/V2d nerve branch in the present study, this general notion was confirmed, extending its validity across different snake species. Accordingly, in all infrared snakes, primary trigeminal afferents and ganglion cells of those neurons that supply the infrared organ appear to be generally larger, with the exception of tactile neurons, in comparison with those of the common trigeminal system. However, whether this size correlation has any functional relevance remains to be determined.

### Central topographic organization of primary infrared afferent fibers

Central projections of the trigeminal nerve enter the hindbrain and immediately segregate into two distinct tracts that project either to the nucleus of the common trigeminal system (TTD) or to the nucleus of the infrared system (LTTD; Fig. 3E; Terashima and Liang, 1991, 1994). This separation into a first central nucleus for the common trigeminal and the specific infrared system (Meszler et al., 1981) was confirmed by the anterograde labeling of fibers within the TTD from the noninfrared-sensitive mandibular branch (V3) and by the retrograde labeling of the neurons in the LTTD following tracer application into the infrared-sensitive RC. Trigeminal projections from the V1, V2s, and V2d nerve branches were mostly restricted to the LTTD with only few axon terminals labeled outside this area, supporting the hypothesis that infrared-related signals from the pit organ are processed predominantly within the latter nucleus (Lynn, 1931; Bullock and Fox, 1957).

Combinatorial tracer applications with dextrans conjugated to two different fluorophores outlined a differential spatial termination pattern of infrared-related trigeminal inputs from different areas of the sensory periphery in the LTTD. The simultaneous anterograde

and retrograde transport of tracer allowed correlating the region within the pit membrane innervated by each nerve branch with its projection area in the LTTD. The delineation of an organotopic organization in the latter nucleus with respect to the afferent origin within the pit membrane will serve as the basis for understanding the spatiotopic organization of infrared information at higher levels including the optic tectum and is summarized in Figure 7. Even though the spatial distribution of axonal terminations from different trigeminal nerve branches within the LTTD deviates from a simple rectangular scheme along rostrocaudal or dorsoventral axes, the pattern illustrates a clear regional preference of afferent projections with limited overlap (Fig. 7), compatible with the implementation of a topographic map that reflects the spatial arrangement of infrared cues in the environment.

A comparable topographic map of primary trigeminal afferents has been studied in detail in species that have either a rather general (turtle, chicken: Rhinn et al., 2012; pigeon: Wild and Ziegler, 1996) or a more specialized (mouse: Pokay, 1991; star-nosed mole: Sawyer et al., 2014) somatosensory system. The somatotopic organization of the principal nucleus of the trigeminal system in turtle is comparable to that of mice, whereas the central terminal areas of the maxillary and mandibular branches appear to be inverted in chicken (Rhinn et al., 2012) but not in pigeon (Wild and Ziegler, 1996). Rhinn et al. (2012) suggested, based on comparative sets of data, that the basic spatial organization of central trigeminal projections is rather well conserved among amniotes, although specific modifications occur in some amniote groups during vertebrate evolution. Such specific modifications are evident in somatosensory specialists such as mice or star-nosed moles (Pokay, 1991; Sawyer et al., 2014). In mice, the vibrissae are topographically represented in the principal trigeminal nucleus and two distinct subnuclei of the descending trigeminal complex (interpolaris and caudalis). These representations form cytoarchitectonically discernible subunits, called *barrelettes*, based on their cylindroid appearance. The arrangement of these barrelettes in the trigeminal nuclei forms a spatiotopic sensory map that matches the alignment of the mystacial vibrissae on the snout (Pokay, 1991). Such an organotopic arrangement is also found in the somatosensory highly specialized star-nosed mole (Sawyer et al., 2014). In these animals, the topographic organization of the trigeminal nuclei is shaped by the central representation of the 22 rays of the star, which are nasal appendages used for tactile sensation. These rays, as with the vibrissae in mice, are spatiotopically represented, although in a differential organizational pattern in the

same trigeminal subnuclei (principalis, interpolaris, and caudalis; Catania et al., 2011; Sawyer et al., 2014), indicating a considerable adaptive plasticity of the organotopic organization of these subnuclei depending on the peripheral sensory structure. Assuming that the infrared-sensitive nucleus (LTTD) of snakes in fact derives from the caudal subnucleus of the trigeminal nuclear complex as suggested earlier (Gruberg et al., 1979), this latter region potentially offers an ideal substrate for adaptive transformations of intrinsic organizational patterns into respective image-forming structural cytoarchitectonics in different vertebrate groups. However, the mere occurrence of spatiotopically organized trigeminal nuclear regions in reptiles and mammals is no proof for a homology of these areas but might simply be the expression of a coincidence resulting from the functional necessity to represent sensory signals topographically in central circuits mediated by trigeminal sensory afferent fibers.

So far, only one study has examined the spatial organization of the LTTD in a pit viper (*Gloydius brevicaudus*; Terashima and Goris, 1977), including an anecdotal report that units recorded in deep layers of the LTTD were driven by stimulation of dorsal parts of the pit membrane, whereas more superficially recorded units received inputs from ventral parts of the membrane. Despite the lack of a systematic analysis of peripheral-central correlations of connectivity, the general notion of an organotopic neuronal activity in the latter study complies with the present anatomical data. This is based on the assumption that in the previous study a particular electrode track first penetrated superficial areas in the LTTD with V2s nerve projections from the ventral part of the pit membrane and subsequently sampled units in deeper regions of the LTTD innervated by V2d and V1 afferent fibers from the dorsal part of the pit membrane. A similar topographic arrangement of the LTTD with dorsoventrally segregated inputs has also been described for infrared-sensitive pythons, which have pit organs in both the lower and the upper jaws (Molenaar, 1978b). In contrast to pit vipers, however, fibers of the mandibular nerve branch, which in pythons innervates the lower jaw pit organ, also project to the dorsal LTTD. A prominent area of overlap with fibers from the mandibular branch and both maxillary branches that innervate the pit organ of the upper jaw in these animals was found in central areas of the LTTD (Molenaar, 1978b). This anatomical pattern of afferent fiber terminations is completed by inputs from the ophthalmic branch to ventral areas of the LTTD, compatible with the current findings in pit vipers and the organization of the common trigeminal system of reptiles in general (Rhinn et al., 2013). The presence of areas in

the LTTD with overlapping projections from the pit organs of the lower and upper jaws in pythons might be explained by the fact that certain regions of both pit organs have a matching spatial correspondence of environmental cues, potentially explaining a central convergence of signals from the respective areas of the dual pit organs that benefits from common termination areas.

Although this latter overlap of afferent projections in pythons might be interpreted by matching spatial specificities of sensory signals, the significance of the overlap of afferent fiber terminations from a single organ in pit vipers in the current study is less clear. The overlap of afferent projections in the latter snakes, however, does not necessarily imply the presence of a considerable monosynaptic convergence of signals from different nerve branches. In fact, in other sensory systems (e.g., the vestibular system), afferent fibers from different semicircular canals also overlap to a large extent at the level of the first central nucleus (Birinyi et al., 2001), whereas the majority of second-order vestibular neurons accept monosynaptic inputs from only one canal organ (Straka and Dieringer, 2004). Thus, the limited intermingling of afferent infrared signals might not have a functional impact for the synaptic processing and convergence. Apart from the afferent excitation of second-order neurons in the LTTD, inhibitory interactions have been reported (Stanford and Hartline, 1980, 1984) and might be related to a spatial tuning or sharpening, potentially mediated by the previously observed axodendritic and axoaxonic synapses (Meszler et al., 1981). However, the underlying synaptic network for infrared signal processing in the LTTD requires further investigation. An extension of the novel in vitro whole-brain preparation of pit vipers to physiological studies will allow deciphering the synaptic signal processing and computational processes in central infrared nuclei, including a potential fusion with visual signal in the optic tectum.

## ACKNOWLEDGMENTS

We thank Slawa Braun for animal care; Birgit Seibel, Yvonne Schwarz, and Gaby Schwabedissen for technical assistance; Roberto Banchi for assistance with the confocal scanning; and Dr. Horst Bleckmann for material support and study supervision.

## CONFLICT OF INTEREST STATEMENT

The authors declare no conflicts of interest.

## ROLE OF AUTHORS

All authors had full access to all data in the study and take responsibility for the integrity of the data and

the accuracy of the data analysis. Study concept and design: TK, HS, HL, GW. Establishment of the in vitro whole brain preparation: HS, TK, GW. Acquisition of data: MB, TK. Analysis and interpretation of data: TK, MB, HL, HS. Drafting of the manuscript: TK, HS. Statistical analysis: MB, TK. Critical revision of the manuscript: HL, HS, MB, GW. Administrative, technical, and material support: HL, GW, HS, TK.

## LITERATURE CITED

- Amemiya F, Ushiki T, Goris RC, Atobe Y, Kusunoki T. 1996. Ultrastructure of the crotaline snake infrared pit receptors: SEM confirmation of TEM findings. *Anat Rec* 246: 135–146.
- Amemiya F, Nakano M, Goris RC, Kadota T, Atobe Y, Funakoshi K, Hibiya K, Kishida R. 1999. Microvasculature of crotaline snake pit organs: possible function as a heat exchange mechanism. *Anat Rec* 254:107–115.
- Bakken GS, Colayori SE, Duong T. 2012. Analytical methods for the geometric optics of thermal vision illustrated with four species of pit vipers. *J Exp Biol* 215:2621–2629.
- Birinyi A, Straka H, Matesz C, Dieringer N. 2001. Location of dye-coupled second order and of efferent vestibular neurons labeled from individual semicircular canal or otolith organs in the frog. *Brain Res* 921:44–59.
- Brodin L, Grillner S. 1990. The lamprey CNS in vitro, an experimentally amenable model for synaptic transmission and integrative functions. In: Jahnsen H, editor. Preparations of vertebrate central nervous system in vitro. Chichester: Wiley. p 103–153.
- Bullock TH, Diecke FPJ. 1956. Properties of an infra-red receptor. *J Physiol* 134:47–87.
- Bullock TH, Fox W. 1957. The anatomy of the infra-red sense organ in the facial pit of pit vipers. *J Cell Sci* 3:219–234.
- Catania KC, Leitch DB, Gauthier D. 2011. A star in the brainstem reveals the first step of cortical magnification. *PLoS One* 6:e22406.
- Chen Q, Deng H, Brauth SE, Ding L, Tang Y. 2012. Reduced performance of prey targeting in pit vipers with contralaterally occluded infrared and visual senses. *PLoS One* 7: e34989.
- Desalvo JA, Hartline PH. 1978. Spatial properties of primary infrared sensory neurons in Crotalidae. *Brain Res* 142: 338–342.
- Ebert J, Westhoff G. 2006. Behavioural examination of the infrared sensitivity of rattlesnakes (*Crotalus atrox*). *J Comp Physiol A* 192:941–947.
- Goris RC, Kadota T, Kishida R. 1989. Innervation of snake pit organ membranes mapped by receptor terminal succinate dehydrogenase activity. In: Matsui M, Hikida T, Goris RC, editors. Current herpetology in East Asia. Kyoto: Herpet. Soc. Japan. p 8–16.
- Gracheva EO, Ingolia NT, Kelly YM, Cordero-Morales JF, Hillopeter G, Chesler AT, Sánchez EE, Perez JC, Weissman JS, Julius D. 2010. Molecular basis of infrared detection by snakes. *Nature* 464:1006–1011.
- Gruberg ER, Kicliter E, Newman EA, Kass L, Hartline PH. 1979. Connections of the tectum of the rattlesnake *Crotalus viridis*: an HRP study. *J Comp Neurol* 188:31–42.
- Hartline PH, Kass L, Loop MS. 1978. Merging of modalities in the optic tectum: infrared and visual integration in rattlesnakes. *Science* 199:1225–1229.
- Hisajima T, Kishida R, Atobe Y, Nakano M, Goris RC, Funakoshi K. 2002. Distribution of myelinated and unmyelinated nerve fibers and their possible role in

- blood flow control in crotaline snake infrared receptor organs. *J Comp Neurol* 449:319–329.
- Kardong KV, Mackessy SP. 1991. The strike behavior of a congenitally blind rattlesnake. *J Herpetol* 25:208–211.
- Kass L, Loop MS, Hartline PH. 1978. Anatomical and physiological localization of visual and infrared cell layers in tectum of pit vipers. *J Comp Neurol* 182:811–820.
- Keifer J, Houk JC. 1989. An in vitro preparation for studying motor pattern generation in the cerebellorubrospinal circuit of the turtle. *Neurosci Lett* 97:123–128.
- Kishida R, Amemiya F, Kusunoki T, Terashima S. 1980. A new tectal afferent nucleus of the infrared sensory system in the medulla oblongata of crotaline snakes. *Brain Res* 195:271–279.
- Kishida R, Kusunoki T, Terashima S, Goris RC. 1981. Thermal neurons in the trigeminal ganglia of crotaline snakes. *Neurosci Lett Suppl* 6:S91.
- Kishida R, Terashima S, Goris RC, Kusunoki T. 1982. Infrared sensory neurons in the trigeminal ganglia of crotaline snakes: transganglionic HRP transport. *Brain Res* 241:3–10.
- Kogo N, Fan TX, Ariel M. 2002. Synaptic pharmacology in the turtle accessory optic system. *Exp Brain Res* 147:464–472.
- Kohl T. 2011. Elektrophysiologische Untersuchungen am Infrarotsinn der westlichen Diamantklapperschlange (*Crotalus atrox*) im Vergleich mit dem optischen Sinn der Schlangen (PhD Thesis). Bonn: University of Bonn. p 1–118.
- Kohl T, Colayori SE, Westhoff G, Bakken GS, Young BA. 2012. Directional sensitivity in the thermal response of the facial pit in western diamondback rattlesnakes (*Crotalus atrox*). *J Exp Biol* 215:2630–2636.
- Krochmal AR, Bakken GS. 2003. Thermoregulation is the pits: use of thermal radiation for retreat site selection by rattlesnakes. *J Exp Biol* 206:2539–2545.
- Liang YF, Terashima S, Zhu AQ. 1995. Distinct morphological characteristics of touch, temperature, and mechanical nociceptive neurons in the crotaline trigeminal ganglia. *J Comp Neurol* 360:621–633.
- Luksch H, Walkowiak W, Munoz A, ten Donkelaar HJ. 1996. The use of in vitro preparations of the isolated amphibian central nervous system in neuroanatomy and electrophysiology. *J Neurosci Methods* 70:91–102.
- Lynn WG. 1931. The structure and function of the facial pit of the pit vipers. *Am J Anat* 49:97–139.
- Meszler RM, Auker CR, Carpenter DO. 1981. Fine structure and organization of the infrared receptor relay, the lateral descending nucleus of the trigeminal nerve in pit vipers. *J Comp Neurol* 196:571–584.
- Moiseenkova V, Bell B, Motamedi M, Wozniak E, Christensen B. 2003. Wide-band spectral tuning of heat receptors in the pit organ of the copperhead snake (*Crotalinae*). *Am J Physiol Reg I* 284:598–606.
- Molenaar GJ. 1974. An additional trigeminal system in certain snakes possessing infrared receptors. *Brain Res* 78:340–344.
- Molenaar GJ. 1978a. The sensory trigeminal system of a snake in the possession of infrared receptors. I. The sensory trigeminal nuclei. *J Comp Neurol* 179:123–136.
- Molenaar GJ. 1978b. The sensory trigeminal system of a snake in the possession of infrared receptors. II. The central projections of the trigeminal nerve. *J Comp Neurol* 179:137–151.
- Molenaar GJ. 1992. Anatomy and physiology of infrared sensitivity of snakes. In: Gans C, editor. *Biology of the reptilia*, vol 17. Chicago: University of Chicago Press. p 367–453.
- Moon C, Terashima S, Shin T. 2003. Immunohistochemical localization of the delta subspecies of protein kinase C in the trigeminal sensory system of *Trimeresurus flavoviridis*, an infrared-sensitive snake. *Neurosci Lett* 338:233–236.
- Moon C, Terashima S, Shin T. 2004. Immunohistochemical study of endothelial nitric oxide synthase in the trigeminal ganglia of a crotaline snake *Trimeresurus flavoviridis*. *J Vet Med Sci* 66:1007–1009.
- Mühlethaler M, Curtis M, Walton K, Llinás R. 1993. The isolated and perfused brain of the guinea-pig in vitro. *Eur J Neurosci* 5:915–926.
- Newman EA, Hartline PH. 1981. Integration of visual and infrared information in bimodal neurons in the rattlesnake optic tectum. *Science* 213:789–791.
- Newman EA, Gruberg ER, Hartline PH. 1980. The infrared trigemino-tectal pathway in the rattlesnake and in the python. *J Comp Neurol* 191:465–477.
- Noble G, Schmidt A. 1937. The structure and function of the facial and labial pits of snakes. *Proc Am Phil Soc* 77:263–288.
- Panzano VC, Kang K, Garrity PA. 2010. Infrared snake eyes: TRPA1 and the thermal sensitivity of the snake pit organ. *Sci Signal* 3:pe22.
- Perez-Santana L, Marín O, Smeets WJ. 1997. Afferent connections of the nucleus accumbens of the snake *Elaphe guttata* studied by means of in vitro and in vivo tracing techniques in combination with TH immunohistochemistry. *Neurosci Lett* 225:101–104.
- Pokay MM. 1991. The barrelettes-architectonic vibrissal representations in the brainstem trigeminal complex of the mouse. I. Normal structural organization. *J Comp Neurol* 309:161–199.
- Rhinn M, Miyoshi K, Watanabe A, Kawaguchi M, Ito F, Kuratani S, Baker CVH, Murakami Y, Rijli FM. 2013. Evolutionary divergence of trigeminal nerve somatotopy in amniotes. *J Comp Neurol* 521:1378–1394.
- Roelke CE, Childress MJ. 2007. Defensive and infrared reception responses of true vipers, pitvipers, *Azemiops* and colubrids. *J Zool* 273:421–425.
- Sawyer EK, Leitch DB, Catania KC. 2014. Organization of the spinal trigeminal nucleus in star-nosed moles. *J Comp Neurol* doi: 10.1002/cne.23605.
- Schroeder DM, Loop MS. 1976. Trigeminal projections in snakes possessing infrared sensitivity. *J Comp Neurol* 169:1–14.
- Sichert AB, Friedel P, van Hemmen JL. 2006. Snake's perspective on heat: reconstruction of input using an imperfect detection system. *Phys Rev Lett* 97:068105–068109.
- Stanford LR, Hartline PH. 1980. Spatial sharpening by second-order trigeminal neurons in crotaline infrared system. *Brain Res* 185:115–123.
- Stanford LR, Hartline PH. 1984. Spatial and temporal integration in primary trigeminal nucleus of rattlesnake infrared system. *J Neurophysiol* 51:1077–1090.
- Stanford LR, Schroeder DM, Hartline PH. 1981. The ascending projection of the nucleus of the lateral descending trigeminal tract: a nucleus in the infrared system of the rattlesnake, *Crotalus viridis*. *J Comp Neurol* 201:161–173.
- Straka H, Dieringer N. 2004. Basic organization principles of the VOR: lessons from frogs. *Prog Neurobiol* 73:259–309.
- Straka H, Simmers J. 2012. *Xenopus laevis*: an ideal experimental model for studying the developmental dynamics of neural network assembly and sensory-motor computations. *Dev Neurobiol* 72:649–663.

- Straka H, Baker R, Gilland E. 2001. Rhombomeric organization of vestibular pathways in larval frogs. *J Comp Neurol* 437:42–55.
- Straka H, Baker R, Gilland E. 2006. Preservation of segmental hindbrain organization in adult frogs. *J Comp Neurol* 494: 228–245.
- Terashima S, Goris RC. 1977. Infrared bulbar units in crotaline snakes. *Proc Jpn Acad Ser B Phys Biol Sci* 53:292–296.
- Terashima S, Goris RC. 1979. Receptive areas of primary infrared afferent neurons in crotaline snakes. *Neuroscience* 4:1137–1144.
- Terashima S, Liang YF. 1991. Temperature neurons in the crotaline trigeminal ganglia. *J Neurophysiol* 66:623–634.
- Terashima S, Liang YF. 1994. Touch and vibrotactile neurons in a crotaline snake's trigeminal ganglia. *Somat Mot Res* 11:169–181.
- Terashima S, Goris RC, Katsuki Y. 1970. Structure of warm fiber terminals in the pit membrane of vipers. *J Ultrastruct Res* 31:494–506.
- Van Dyke JU, Grace MS. 2010. The role of thermal contrast in infrared-based defensive targeting by the copperhead, *Agkistrodon contortrix*. *Anim Behav* 79:993–999.
- Vibert N, de Waele C, Serafin M, Babalian A, Mühlethaler M, Vidal P.P. 1997. The vestibular system as a model of sensorimotor transformations. A combined in vivo and in vitro approach to study the cellular mechanisms of gaze and posture stabilization in mammals. *Prog Neurobiol* 51:243–286.
- Wild JM, Ziegler HP. 1996. Central projections and somatotopic organization of trigeminal primary afferents in pigeon (*Columba livia*). *J Comp Neurol* 368:136–152.

## Chapter 2

### **Physiological basis for infrared motion detection in the brainstem of the western diamondback-rattlesnake (*Crotalus atrox*)**

Maximilian S. Bothe<sup>1,2\*</sup>, Harald Luksch<sup>1</sup>, Hans Straka<sup>3</sup>, and Tobias Kohl<sup>1</sup>

<sup>1</sup> Chair of Zoology, Technical University Munich, Liesel-Beckmann-Str. 4, 85354 Freising-Weihenstephan, Germany Freising-Weihenstephan, Germany

<sup>2</sup> Graduate School of Systemic Neurosciences, Ludwig-Maximilians-University Munich, Großhaderner Str. 2, 82152 Planegg

<sup>3</sup> Department Biology II, Ludwig-Maximilians-University Munich, Großhaderner Str. 2, 82152 Planegg

\*First-author

#### Contributions of Maximilian S. Bothe:

- Participated in the development of study concept and design
- Extension of the in vitro whole brain preparation to the pit organ attached state
- Setup of the IR emitter stimulus and inclusion in the in vitro recording chamber
- Acquisition of data
- Analysis of data
- Preparation of all figures
- Writing of the first draft of the manuscript
- Major part of the statistical analysis
- Review and discussion of the manuscript

#### Contributions of other authors:

- Study concept and design: T.K., H.S.
- Review and discussion of data analysis and figures: T.K., H.S.
- Review and discussion of the manuscript: T.K., H.S., H.L.
- Administrative, technical and material support: H.L., H.S., T.K.

## **Physiological basis for infrared motion detection in the brainstem of the western diamondback-rattlesnake (*Crotalus atrox*)**

### **Abstract**

Pitvipers have a specialized sensory system in the upper jaw to detect infrared (IR) radiation. The bilateral pit organs are simple pinhole cameras that map IR objects onto the sensory epithelium as blurred images. Trigeminal afferents transmit information about these images as neuronal spike patterns in a topographic manner to the hindbrain nucleus of the lateral descending trigeminal tract (LTTD). LTTD output is conveyed to the ipsilateral nucleus reticularis caloris (RC) of the hindbrain. Intracellular recordings of LTTD neurons in isolated rattlesnake brains allowed deciphering the patterns of excitatory and inhibitory responses following sensory stimulation. Electrically simulated and real IR motion in preparations with an intact sensory periphery revealed complex spike sequences in LTTD neurons. These patterns comply with a central excitation flanked by a lateral inhibition thereby enhancing the IR-image contrast. Direction-specific discharge patterns recorded from RC neurons during bi-directional IR object motion indicates that through convergence of the population code of neurons in the LTTD, individual neurons in the RC are capable of differentiating IR motion directions. This assigns a retina-like function to the early level of rattlesnake IR signal processing.

## Introduction

Pitvipers (*Crotalinae*) are able to detect infrared (IR) radiation with loreal pit organs (Noble & Schmidt, 1937). The pits are located bilaterally on the upper jaw between the eyes and the nostrils and allow the perception of electromagnetic radiation from 3-10  $\mu\text{m}$  (Bullock & Diecke, 1956; Goris & Nomoto, 1967; Moiseenkova et al., 2003). Pitvipers use IR detection for e.g. thermoregulation (Bakken & Krochmal, 2007), predator avoidance (Roelke & Childress, 2007; van Dyke & Grace, 2010) or precise strikes towards warm-blooded prey (Chen et al., 2012; Haverly & Kardong, 1996; Kardong & MacKessy, 1991; Westhoff et al., 2006). Based on the principle of a simple pinhole camera, IR objects are mapped onto the pit membrane (Bakken & Krochmal, 2007; Otto, 1972). This thin sensory layer is innervated by the ophthalmic (N.V1) and the deep (N.V2d) and superficial maxillary (N.V2s) branch of the trigeminal nerve (Bullock & Fox, 1957; Kohl et al., 2014; Lynn, 1931). Each of these pit organ-innervating fiber bundles supplies a distinct sensory region with little overlap of the termination areas. Accordingly, N.V1 innervates the dorso-caudal, N.V2d the dorso-rostral and N.V2s the ventral part of the pit membrane (Bullock & Fox, 1957; Goris et al., 1989; Kohl et al., 2014). Before ramifying within the sensory epithelium, each of these branches split into multiple smaller sub-branches that are interconnected through anastomoses (Kohl et al., 2014). Individual fibers within these sub-branches form brush-like terminal nerve masses (Amemiya et al., 1996; Bullock & Fox, 1957; Goris et al., 1989; Kohl et al., 2014; Terashima et al., 1970) that contain TRPA1 channels for the transduction of IR radiation into electrical signals (Gracheva et al., 2010).

Afferent fibers within the N.V1, N.V2s and N.V2d form part of the trigeminal nerve and project into a designated area in the rostral hindbrain (Kishida et al., 1982). After entering the brainstem in rhombomere 2 (Gilland & Baker, 2005), afferent axons from the pit organ form the lateral descending trigeminal tract (ltd) and terminate within the nucleus of the ltd (LTTD) (Meszler et al., 1981; Newman et al., 1980; Schroeder & Loop, 1976; Terashima & Liang, 1991). Within the latter nucleus, afferents terminate in a topographical organization that represents the spatial origin of the fibers in the pit membrane (Kohl et al., 2014). Accordingly, N.V1, N.V2s and N.V2d afferents terminate in distinct areas of the LTTD with little overlap at border regions (Kohl et al., 2014). Throughout the LTTD, IR afferents form a dense neuropil, within which the somata and dendrites of LTTD neurons are tightly embedded (Kohl et al., 2014; Meszler et al., 1981). Based on morphological studies in different *Crotaline* species, LTTD neurons distinctly subdivide into a population of medium to large-sized neurons and a population of smaller cells (Meszler et al., 1981; Newman et al., 1980). This likely correlates with different functional roles in sensory processing. Extracellular recordings of LTTD neurons indicated that IR stimulation elicits spikes in most cells with relatively broad receptive fields (Terashima & Goris, 1977). A flanking inhibition (Stanford & Hartline, 1980, 1984) appears to

reduce the size of excitatory receptive fields with respect to presynaptic afferent receptive fields (Desalvo & Hartline, 1978). This computation is reminiscent of retinal signal processing (Stanford & Hartline, 1984), even though definitive proof of principle experiments are still lacking. Secondary neurons from the LTTD project towards the hindbrain “nucleus reticularis caloris” (RC). Other than the LTTD, the RC lies on the ventral surface of the hindbrain at a slightly more rostral position. Besides its excitability through IR stimulation of the ipsilateral pit organ, little is known about RC physiology. From the RC, neurons project to the contralateral lobe of the optic tectum (OT) where they innervate layers 7a and b of Cajal (Kass et al., 1978). Similar to the visual environment, IR input is topographically represented in the OT of rattlesnakes and roughly aligned with the visual map (Hartline et al., 1978).

Here, we studied the signal processing in LTTD and RC neurons following electrical and IR motion stimulation in semi-intact preparations of rattlesnakes with an intact brain and attached pit organ. Extra- and intracellular recordings of LTTD and RC neurons during real and electrically simulated IR object motion revealed the spatial representation of sensory signals and excitatory and inhibitory signal convergence in the LTTD. The response dynamics depended on the temporal sequence of afferent spike activity from adjacent pit areas during electrical stimulation. This suggests that excitatory inputs in LTTD neurons are contrast-enhanced by asymmetric inhibitory inputs. While individual LTTD neurons only showed slight directional tuning caused by these asymmetric input components, neurons in the RC exhibited clear stimulus direction dependent differences in their response characteristics. Based on these results, the IR processing brainstem circuitry of rattlesnakes can be divided into two parts. The strong secondary inhibition that characterizes responses of LTTD neurons leads to clear spatiotemporal contrast enhancement of primary input signals. Presumably via convergence of multiple LTTD units onto individual neurons in the RC, the stimulus motion direction dependent asymmetry of excitatory and inhibitory LTTD response components provides the basis for directional sensitivity of individual RC neurons.

## **Material and methods**

### *Animals and experimental preparation*

In vitro experiments were performed on isolated brain preparations of 22 juvenile western diamondback rattlesnakes (*Crotalus atrox*). Snakes of either sex and a body weight of 23-69 g were obtained from the in house animal breeding facility at the Chair of Zoology at the Technical University of Munich. Snakes were kept at a temperature of 22-30°C at a 12h/12h light/dark cycle. Animals were fed weekly with pre-killed mice and water was provided *ad libitum*. Care and

maintenance of the animals followed the established guidelines for venomous snakes (Westhoff, 2014). Electrophysiological experiments were performed in vitro on isolated, semi-intact preparations and complied with the "Principles of animal care", publication No. 86-23, 212 revised 1985 of the National Institute of Health. Permission for the experiments was granted by the respective governmental institution at the Regierung von Oberbayern (55.2-1-54-2532.6-9-12).

For all experiments, animals were initially anesthetized with isoflurane in an induction chamber. After the tail-pinch reflex ceased, snakes were secured with u-shaped pins to the Sylgard® (Dow Corning, Wiesbaden, Germany) floor of a large petri dish. Intramuscular injection of a combination of Ketamine hydrochloride (40 mg/kg; Ketamine 100 mg/ml, Ketavet, Zoetis Deutschland GmbH, Berlin, Germany) and Xylazine hydrochloride (20 mg/kg; Rompun 2%, Bayer Vital GmbH, Leverkusen, Germany) ensured deep anesthesia for the subsequent surgical procedure. The body was opened ventrally at the level of the heart and snakes were perfused transcardially with 30-70 ml of ice-cold snake Ringer solution (in mM: 96.5 NaCl, 31.5 NaHCO<sub>3</sub>, 4 CaCl<sub>2</sub>, 2.6 KCl, 2 MgCl<sub>2</sub>, and 20 D-glucose, pH 7.4). Thereafter, the animals were decapitated and the lower jaws including muscle and connective tissue were removed. The bilateral pit organs in the upper jaw and the innervating trigeminal nerve branches on both sides were maintained intact. The skull was then carefully opened ventrally to isolate the entire brain with the trigeminal nerve branches and the pit organs on both sides attached (Fig. 1a,b). To mechanically stabilize the trigeminal ganglia, the bone surrounding them was kept intact. After completion of the isolation procedure, preparations were stored in ice-cold Ringer solution. For all experiments, the preparations were placed in a recording chamber (2 x 3 cm) with a volume of ~6 ml and fixed with insect pins to the Sylgard® floor. Preparations were continuously superfused with oxygenated snake Ringer solution, however, with a lower magnesium concentration (in mM: 0.4 MgCl<sub>2</sub>) for facilitated activation of NMDA receptors (Nowak et al., 1984). For experiments that employed natural IR object motion, the concentration of CaCl<sub>2</sub> was lowered to 2 mM, providing a temporally more stable resting discharge. Throughout the experiments, the temperature of the Ringer solution in the chamber was electronically controlled and maintained at 14.0 ± 0.2°C. Whole-brain preparations were used for up to 4 days and kept overnight at 4°C in oxygenated Ringer solution with standard magnesium concentration. No noticeable differences in response parameters were encountered during the daily recording sessions over this period.

### *Recording of trigeminal nerve afferents and central neurons in the LTTD and RC*

At the beginning of each experiment, compound spikes of pit organ-innervating trigeminal afferent fibers or pre- and postsynaptic field potentials in the LTTD were recorded extracellularly. Glass microelectrodes for these recordings were fabricated with a micropipette puller (P-87 Micropipette Puller, Sutter Instrument, Novato California, USA). After breaking the tip, electrodes were filled with 2 M sodium chloride to reach a final resistance of 3-5 M $\Omega$ . Intracellular recordings from LTTD neurons were performed with glass micropipettes, which after pulling were directly filled with a mixture of 3 M potassium acetate and 2 M potassium chloride at a ratio of 9:1, to reach a final resistance of 50-60 M $\Omega$ . Electrodes for trigeminal nerve recordings were manually positioned onto the nerve branch by 3-axis micromanipulators (U-31 CF, Narishige Group, Tokyo, Japan). For extra- and intracellular recordings of neuronal activity in the LTTD and RC, electrodes were stereotactically positioned in the horizontal plane and advanced stepwise within the brainstem target area with a 3-axis piezo-stepper (Triple Axis Micromanipulator, Sensapex, Oulu, Finland) in dorso-ventral and ventro-dorsal direction, respectively. Neuronal activity of the trigeminal nerve and LTTD and RC neurons was recorded (BA-03X, npi electronic GmbH, Tamm, Germany; DAM80, WPI, Sarasota Florida, USA) and digitized (NI USB-6211, National Instruments, Austin Texas, USA) with a sampling rate of 20 kHz using a custom built Matlab-script (Matlab2014a, The MathWorks Inc., Natick Massachusetts, USA). To reduce high-frequency noise, signals were filtered prior to digitizing by low-pass filtering with a cutoff frequency of 13 kHz. Depending on the current intensity, stimulus artefacts were clipped for the presentation in the figures.

### *Electrical stimulation of trigeminal nerve afferent fibers*

To access single trigeminal nerve branches, the surrounding connective tissue was removed. For different sets of experiments, either the main branches (N.V1, N.V2d and N.V2s; color-coded in Fig. 1b) or up to three adjacent sub-branches of the N.V2s were cut with a fine scissor and their blunt ends were sucked into glass micropipettes, respectively (Fig. 1c,d). The average distance between the stimulus site of a main nerve branch and the recording site in the central region of the LTTD was  $7.7 \pm 0.3$  mm ( $n = 4$ ). N.V2s sub-branches were stimulated more peripherally at an average distance of  $12.2 \pm 0.8$  mm ( $n = 4$ ) between the stimulus site and central LTTD neurons. These values were used to estimate the earliest latency of evoked afferent spike discharge in the brainstem nucleus. The micropipettes were pulled with an electrode puller (P-87 Micropipette Puller, Sutter Instrument, Novato California, USA) and the tip diameters were individually adjusted to the size of each nerve branch by tip cutting and fire polishing. Bipolar single current pulses (0.2 ms, 4-30  $\mu$ A)

were produced by a stimulus isolation unit (Isolated Pulse Stimulator, Model 2100, A-M Systems, Sequim Washington, USA) and applied at a rate of 0.5 Hz. Trains of single electrical pulses were generated by a multichannel stimulation system (STG 1008, multichannel systems, Reutlingen, Germany) that allowed adjusting the dynamics of the pulse sequence. Prior to each recording session, the stimulus threshold of each nerve branch was determined either by recording the spike discharge of the respective nerve branch at a level proximal to the stimulation site (Fig. 1e) or by recording field potentials within the LTTD (Fig. 2). For all intracellularly recorded neurons in the LTTD, nerve branches were stimulated at a current intensity three times the threshold ( $\times T$ ).

To differentiate between pre- and postsynaptic responses in the LTTD and to calculate the synaptic delay, the conduction velocity of pit organ-innervating afferent fibers was determined. Two glass electrodes were separately placed onto the same nerve branch at defined distances from the stimulus electrode (Fig. 1e). The two electrodes simultaneously recorded evoked compound action potentials following single pulse stimulation of the nerve branch at the entrance of the fibers into the pit organ (Fig. 1e). The distance between both recording electrodes (Fig. 1e,  $\Delta s$ ) and the difference in the latency of the first negative peak (Fig. 1f,  $\Delta t$ ) at the two sites, respectively, were used to calculate the conduction velocity of the fastest trigeminal nerve afferent fibers. The time difference of the responses was independent of stimulus intensity (see results) even though the amplitude increased gradually with increasing current (Fig. 1g). The latency measurements of the compound spikes recorded by the two electrodes also served to calculate the recruitment time for eliciting spikes in trigeminal afferents (Fig. 1h).

A putative organotopic arrangement of second-order IR-sensitive neurons in the LTTD was tested by systematic recording of the field potential profile along the rostral-caudal extent of the nucleus following separate stimulation of N.V1, N.V2d and N.V2s (Fig. 1b,c). To distinguish between pre- and postsynaptic response components of the field potential, the glutamate blocker NBQX (10  $\mu$ M; NBQX disodium salt, Abcam plc, Cambridge, United Kingdom) was bath-applied. A complete block of the evoked postsynaptic responses was usually achieved after 25 min. At three rostral-caudal positions, field potentials were acquired along dorso-ventral depth tracks in steps of 50  $\mu$ m from the dorsal surface (Fig. 2a-d). The rostral-caudal positions of the depth tracks were defined relative to the visible swelling of the dorsal hindbrain formed by the LTTD. Accordingly, the central track was located in the center of the swelling while the two other tracks were located 150  $\mu$ m rostral and caudal to this position, respectively. Response magnitudes were normalized to the maximal field potential amplitude within a given track.

### *Close-to-natural stimuli*

To mimic naturalistic stimuli for IR-sensitive trigeminal nerve fibers, an electrical stimulus paradigm was applied that consisted of a train of single pulses and attempted to simulate a horizontal IR object motion across the pit organ. Accordingly, this stimulus would imitate the neuronal activity of trigeminal afferents induced by the heat contrast of a moving object. The design of the stimulus took into account the approximate discharge profile of IR-sensitive primary afferents (Bullock & Diecke, 1956; de Cock Buning et al., 1981; Goris & Nomoto, 1967). In addition, the dynamic parameters of the pulse train for the electrical stimulation of trigeminal nerve fibers were based on a mouse running at a speed of  $\sim 275$  mm/s (Beavers, 1976; Djawdan & Garland, 1988) and the dimension of the pit region innervated by each N.V2s sub-branch, which is  $\sim 250$   $\mu$ m in juvenile rattlesnakes (Kohl et al., 2014). Accordingly, a stimulus pulse train of 300 ms duration was constructed with a pulse rate that increased and decreased stepwise from 40 Hz to 80 Hz and back to 40 Hz (Pfanzelt et al., 2008). The stimulus train was applied sequentially to three horizontal neighboring membrane-innervating nerve branches (N.V2s in Fig. 1d) with a delay of 100 ms between each nerve branch. The sequence of stimulus train occurred either in rostro-caudal or caudo-rostral direction with respect to the position of the pit organ within the head (i.e. 1-2-3 or 3-2-1 in Fig. 1d).

### *Infrared stimulation of the pit organ*

To compare the temporal structure of LTTD responses evoked by electrical pulse train stimulation with those elicited by natural stimuli and to unveil responses of RC neurons to the latter the pit organs were kept intact during the isolation of the preparation. This allowed a natural stimulation of the thermoreceptors with a 1.3 W IR emitter (Steady State IR Source, Model EK-5270, Laser Components GmbH, Olching, Germany). Access to the sensory organ for IR stimulation was provided by mounting the pit organ with the trigeminal nerve attached onto a platform of petroleum jelly (Vaseline Weiss Ph.Eur., Bombastus-Werke, Freital, Germany) with the opening of the pit membrane protruding from the surface of the Ringer's solution in the chamber. The IR emitter was attached to the arm of a modified x-y-plotter (custom-built, Petra Haase Computertechnik, Neuss, Germany) at a distance of two centimeters above the recording chamber. The IR emitter was moved across the pit organ at a speed of 175 - 250 mm/s. The movement of the IR emitter occurred either in temporo-nasal (t-n) or naso-temporal (n-t) direction. This spatial arrangement of IR motion stimuli matched the activation pattern of electrical pulse train stimuli of multiple nerve branches described above. The temporal sequence and magnitude of activated excitatory response components in LTTD

and RC neurons were used to evaluate a directional sensitivity. For each neuron, the mean spike count during emitter-based IR object motion plus 300 ms post-motion activity was used to calculate a signed directionality index (SDI)(Wagner et al., 1994). 300 ms post-motion activity was included to account for differences in strength and onset of secondary inhibitory response components. The SDI was defined hereby as:

$$SDI = \begin{cases} 100 * \left(1 - \frac{SC_{n-t}}{SC_{t-n}}\right) & \text{for } SC_{n-t} < SC_{t-n} \\ 100 * \left(\frac{SC_{t-n}}{SC_{n-t}} - 1\right) & \text{for } SC_{n-t} > SC_{t-n} \end{cases}$$

with  $SC_{n-t}$  and  $SC_{t-n}$  as the mean spike count towards emitter movement in n-t and t-n direction, respectively. SDI values thus indicate the relative difference in discharge rate for opposite emitter movement directions. SDI values can range from -100 to 100 with values of -100 and 100 indicating that a neuron only responded to n-t or t-n movements, respectively. A SDI of 0 indicates no difference in spike count for opposite stimulus movement directions.

### Statistics

All values were indicated as mean  $\pm$  SEM, if not stated otherwise. Statistics and linear curve fitting were performed using a commercial software package (Matlab, R2014b, The MathWorks Inc., Natick Massachusetts, USA). Statistical differences in parameters were estimated using the Mann-Whitney  $U$  test (unpaired parameters) or the Wilcoxon signed-rank non-parametric tests (paired parameters).

## Results

### *Evoked trigeminal nerve activity and conduction velocity*

Electrical single pulse stimulation of the N.V2s or N.V2d ( $n = 10$ ) close to the pit organ elicited compound action potentials in the respective nerve branches with a characteristic waveform (Fig. 1e,f). Simultaneous recordings of the same nerve branch at two different positions relative to the stimulus electrode (Rec1 and Rec2 in Fig. 1e,g) allowed determining the basic parameters for electrical activation of spikes in trigeminal afferents. Plotting the amplitude of the evoked negativity peak as a function of stimulus intensity (see representative example in Fig. 1f,g) yielded the average current threshold for activating IR-sensitive trigeminal afferents ( $4.1 \pm 0.8 \mu\text{A}$ ;  $n = 10$ ). The linear increase of the peak response amplitude with current intensity (black and red curve in Fig. 1g) suggests a gradual recruitment of increasing numbers of fibers over a relatively large current range

once stimulus threshold has been reached. Dual recordings of evoked compound spike activity of trigeminal nerve afferents at two different locations from the stimulus site allowed estimating the conduction velocity of these fibers and the recruitment time for electrical activation. Independent of stimulus magnitude, the delay  $\Delta t$  between the peak negativities, measured simultaneously at the two recording sites (Fig. 1f), was intensity-invariant and amounted in the typical example to 0.5-0.6 ms (orange trace in Fig. 1g). Plotting the latency of the two negativity peaks as a function of the distance  $\Delta s$  between stimulus and recording electrodes (Fig. 1h) yielded an average recruitment time (intersection with the y-axis) for trigeminal afferents of  $1.0 \pm 0.1$  ms and a conduction velocity (inverse slope) of  $4.2 \pm 0.6$  m/s ( $n = 10$ ) at the recording temperature of  $14.0 \pm 0.2^\circ\text{C}$ .

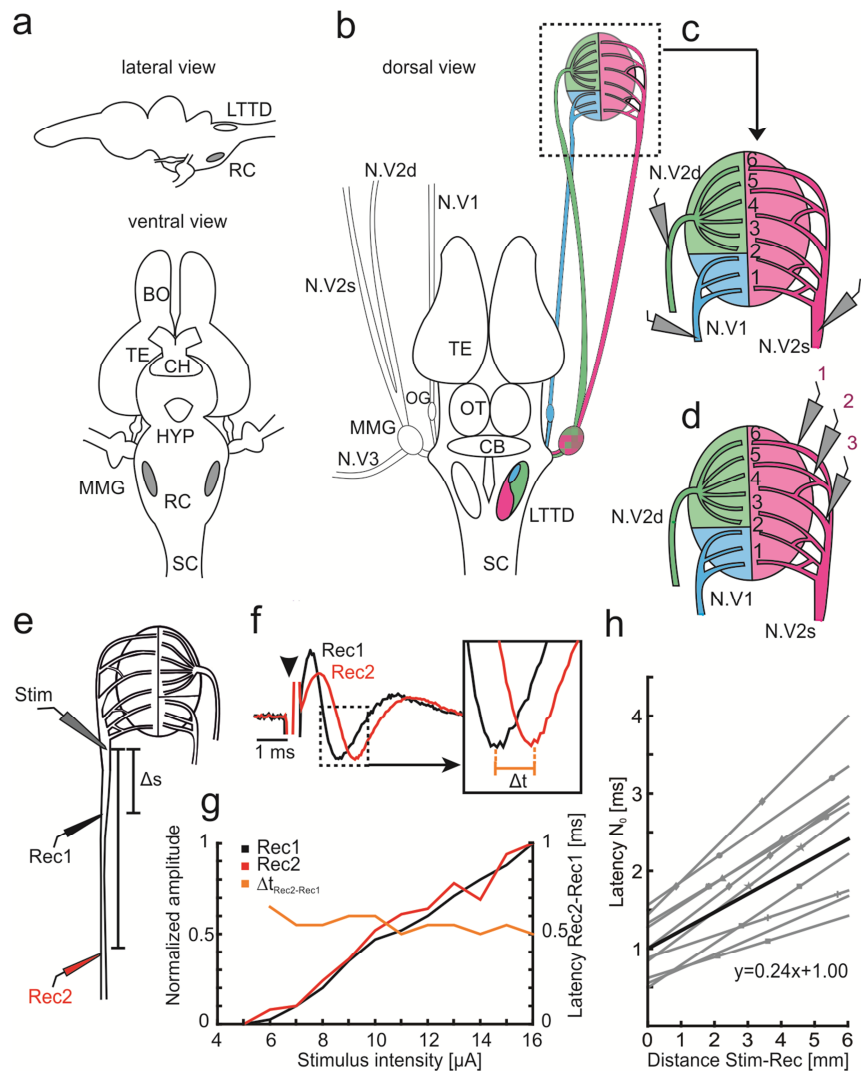


**Fig. 1: Isolated rattlesnake whole brain and pit organ for probing IR signal processing in the LTTD. (a) Lateral, ventral and (b) dorsal scheme of the isolated rattlesnake brain. (b-d) Schematic brain with color-coded trigeminal nerve innervation of the pit organ by the ophthalmic branch (N.V1, blue), the deep (N.V2d, green) and superficial maxillary branch (N.V2s, magenta); the topographic nerve projection within the LTTD is indicated by corresponding colors; higher magnification of the peripheral nerve supply indicates selective stimulation (gray electrodes) of the three main branches (c) or of individual sub-branches of the N.V2s (d). (e) Schematic depicting the arrangement of stimulus (stim) and recording electrodes (Rec1, Rec2) for determining the conduction velocity and recruitment time of IR-sensitive trigeminal afferents. (f) Representative example of compound action potentials in the trigeminal nerve, monitored at Rec1 (black trace) and Rec2 (red trace) after single pulse stimulation at 3xT (arrow head in f); the inset depicts the two responses and respective delay ( $\Delta t$ ) at an extended time scale. (g) dependency of normalized compound action potential amplitudes (black and red curves) and time difference (orange curve) of responses at Rec1 and Rec2 ( $\Delta t$  in f) on stimulus intensity. (h) Dependency of the latency of afferent compound action potentials at Rec1 and Rec2 ( $n = 10$ ) on the respective distances from the stimulus electrode; gray lines are individual linear regressions of the different pairs; the black line is the mean linear regression, used to calculate recruitment time (intersection with the y-axis) and conduction velocity (inverse of the slope) of trigeminal afferents. BO, olfactory bulb; CB, cerebellum; CH, optic chiasm; HYP, hypophysis; LTTD, nucleus of the lateral descending trigeminal tract; MMG, trigeminal ganglion; OG, ophthalmic ganglion; OT, optic tectum; RC, nucleus reticularis caloris; SC spinal cord; TE, telencephalon.**

### *Field potential recordings in the LTTD*

Systematic recordings of field potentials at three levels along the rostro-caudal extent of the LTTD (Fig. 2a-d) following separate electrical stimulation of N.V1, N.V2d and N.V2s (Fig. 2e,i,m) were used to reveal a putatively differential, nerve branch-specific regional afferent activation of central neurons. The different depth profiles of the field potentials evoked by the three nerve branches, shown in a representative example in Fig. 2, suggested the presence of a rostro-caudal and dorso-ventral topography of nerve branch-specific synaptic inputs to LTTD neurons. The rostral part of the LTTD (Fig. 2b) was particularly dominated by synaptic inputs following stimulation of N.V2d (Fig. 2j), even though an activation of N.V1 and N.V2s also caused a noticeable, yet differential activation of field potentials in this area (Fig. 2f,n). Neurons in the central part of the LTTD (Fig. 2c) predominantly received synaptic inputs following stimulation of N.V2s (Fig. 2o), with minor contributions from N.V1 and N.V2d (Fig. 2g,k). The caudal part of the LTTD (Fig. 2d) was dominated by synaptic inputs following stimulation of N.V2s (Fig. 2p) even though stimulation of N.V1 reliably evoked field potentials in this area, although of lesser amplitude (Fig. 2h). Independent of the rostro-caudal position of the recording electrodes, field potentials were generally larger in central and ventral areas of the LTTD (e.g. Fig. 2j,p) with an additional nerve branch-specific activation of longer-latency components, indicating a nerve branch- and/or region-specific activation of polysynaptic responses. Bath application of NBQX, a glutamatergic AMPA receptor antagonist (Fig. 2q-s) blocked all synaptic responses, except for a small initial component (green arrow in Fig. 2s) that likely reflects the presynaptic spike discharge of afferent fibers with an onset of  $\sim 3$  ms ( $2.9 \pm 0.1$  ms,  $n = 5$ ). This latency is compatible with the delay expected from the known afferent conduction velocity, stimulus recruitment time and distance between stimulus and recording site (see above for values). The complete block of all postsynaptic responses suggests that trigeminal afferent-evoked glutamatergic activation of LTTD neurons is largely mediated by AMPA receptors.

The obvious predominance of N.V2s-evoked field potentials across the LTTD likely corresponds to the larger size of the innervated peripheral area of this nerve branch, which extends throughout half of the sensory epithelium of the pit organ (see nerve branches in magenta in Figs. 1b, 2m). In addition, the differential distribution of field potentials within the LTTD, activated from the three nerve branches, complies with their respective anatomical termination pattern within this hindbrain area (Kohl et al., 2014). The matching anatomical and physiological topography of IR signal representations within the LTTD therefore suggests a central sensory topography of afferent synaptic inputs that was used here to guide intracellular recordings.

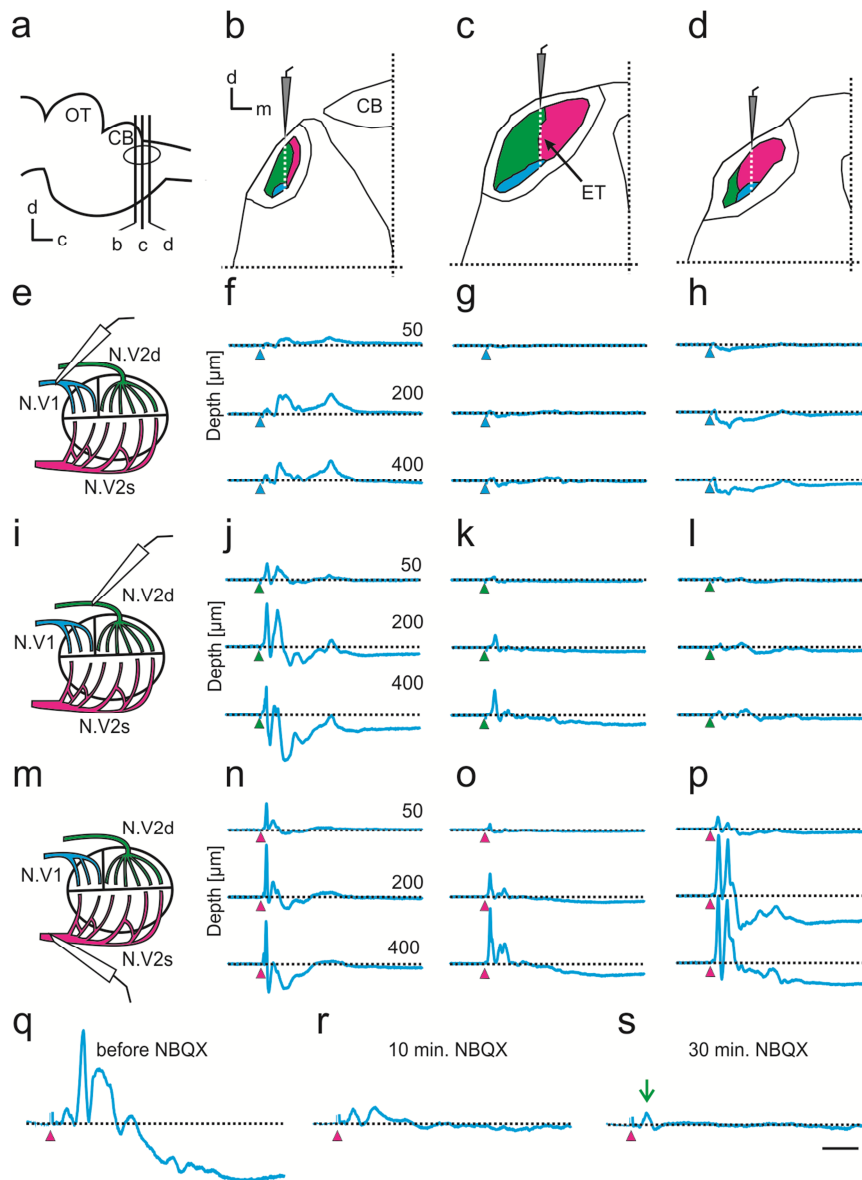


**Fig. 2: Topography of trigeminal nerve branch-evoked field potentials in the LTTD.** (a-d) Schematic cross-sections of the dorsal hindbrain at three rostro-caudal levels (b-d) illustrating the location of the LTTD (colored area; from Kohl et al., 2014), the differential termination areas of afferents from the N.V1 (blue), N.V2d (green) and N.V2s (magenta) and the electrode tracks (ET) for field potential recordings; the locations of the cross-sections are indicated in the parasagittal section in a. (e-p) Field potentials recorded along dorso-ventral electrode tracks through the rostral (f,j,n), intermediate (g,k,o) and caudal (h,l,p) LTTD, depicted in b-d; Field potentials are exemplarily plotted for a depth of 50, 200 and 400  $\mu\text{m}$  below the dorsal surface, respectively, following electrical stimulation of the N.V1 (e-h), N.V2d (i-l) and N.V2s (m-p); colored arrow heads mark stimulus onset. (q-s) Field potentials in the caudal LTTD at a depth of 200  $\mu\text{m}$  following electrical stimulation of the N.V2s, before (q), 10 min (r) and 30 min (s) after bath application of the glutamatergic AMPA receptor antagonist NBQX (10  $\mu\text{M}$ ); colored arrow heads mark stimulus onset. CB, cerebellum; LTTD, nucleus of the lateral descending trigeminal tract; OT, optic tectum. Scale in s: 25 ms, applies also for q,r.

### *Excitatory and inhibitory synaptic responses in LTTD neurons*

The response pattern of LTTD neurons was evaluated by intra- and juxtacellular recordings following single electrical pulse stimulation of up to three individual, anatomically adjacent N.V2s sub-branches. This allowed probing the convergence of synaptic inputs in LTTD neurons from separate peripheral origins (Fig. 1d). The resting membrane potential of the recorded neurons ( $n = 21$ ) spanned a wide range (between  $-39$  and  $-83$  mV), with the smallest values obtained during juxtacellular recordings. Generally, cells with a low resting membrane potential were stabilized by hyperpolarization at about  $-55$  mV. The dynamics of afferent inputs was characterized by separately activating synaptic responses from multiple N.V2s sub-branches with gradually increasing current pulses. At very low stimulus intensities, immediately above threshold ( $\sim 4.5$   $\mu$ A), the responses consisted of short-latency EPSPs with synchronized onsets over successive stimulus trails (Fig. 3a<sub>1</sub> and inset). With increasing strength of the current pulses, these EPSPs triggered single (Fig. 3a<sub>2</sub>) or multiple action potentials with delays of up to  $\sim 30$  ms (Fig. 3a<sub>3,b</sub>), indicative of additional polysynaptic excitatory components. The onset of the first spike matched that of the EPSPs and was independent of the peripheral origin from a particular N.V2s sub-branch. The latency of the excitatory inputs from up to three sub-branches in a given neuron ranged from  $5.4 - 7.6$  ms ( $6.4 \pm 0.1$  ms;  $n = 32$ ). In order to evaluate the number of intercalated synapses between the stimulated afferent fiber and the recorded LTTD neuron, we first estimated the latency of presynaptic trigeminal afferent responses in the LTTD based on the known recruitment time, conduction velocity and distance between stimulus and recording site (see above for values). The difference ( $\sim 1$  ms) between the calculated delay of  $3.9$  ms and the corresponding extracellular field potential component ( $2.9$  ms) derives from the relatively more distal stimulation of the N.V2s sub-branches ( $\sim 4$  mm). Assuming a delay of  $1.8-2.0$  ms for the synaptic transmission as in isolated amphibian brain preparations at  $14^\circ\text{C}$  (Straka et al., 1997), the calculated latency of  $5.9$  ms for trigeminal nerve-evoked responses thus corresponds to the measured onset of the short-latency EPSPs and spikes in LTTD neurons, confirming a monosynaptic origin.

In a smaller number of neurons, electrical pulse stimulation of N.V2s sub-branches evoked either a single, monosynaptic spike followed by a prolonged hyperpolarization of varying magnitude (Fig. 3c) or a distinct longer-latency IPSP without preceding monosynaptic excitatory component ( $n = 8$ ; Fig. 3d and inset). The delayed IPSPs had an average latency of  $15.1 \pm 0.5$  ms ( $n = 8$ ) and therefore were at least of disynaptic origin. However, independent of the presence or absence of a preceding monosynaptic excitation, inhibitory postsynaptic components became only visible at the highest employed stimulus intensity ( $3\times T$ ). Spontaneously active neurons ( $n = 7$ ) allowed estimating the temporal extent of the delayed inhibition on the firing rate (Fig. 3f). While all neurons exhibited a

stimulus-driven silencing of the resting discharge, the duration of the latter post-stimulus inhibition varied from 60 - 310 ms ( $137 \pm 20$  ms; red area in Fig. 3f<sub>2</sub>), depending on the stimulated N.V2s sub-branch ( $n = 15$ ). Nerve branches that evoked a pronounced monosynaptic excitation with multiple spikes upon electrical pulse stimulation (e.g. Fig. 3a<sub>3</sub>,b) also caused significantly longer periods of post-excitatory inhibition in the recorded neurons (group 1,  $n = 4$  in Fig. 3e) compared to nerve branches which activated only single monosynaptic spikes or purely inhibitory responses in the form of IPSPs (e.g. Fig. 3c,d; group 2,  $n = 11$  in Fig. 3e; Mann-Whitney  $U$  test,  $p = 0.0029$ ). This effect might be related to the fact that a more effective monosynaptic excitation also more effectively recruited local interneurons through which the feed-forward inhibition is likely mediated (Biesdorf et al., 2008). Nonetheless, common to all recorded LTTD neurons was the presence of a prolonged period of post-stimulus inhibition of spike activity as illustrated in the representative example in Fig. 3f<sub>3</sub>.

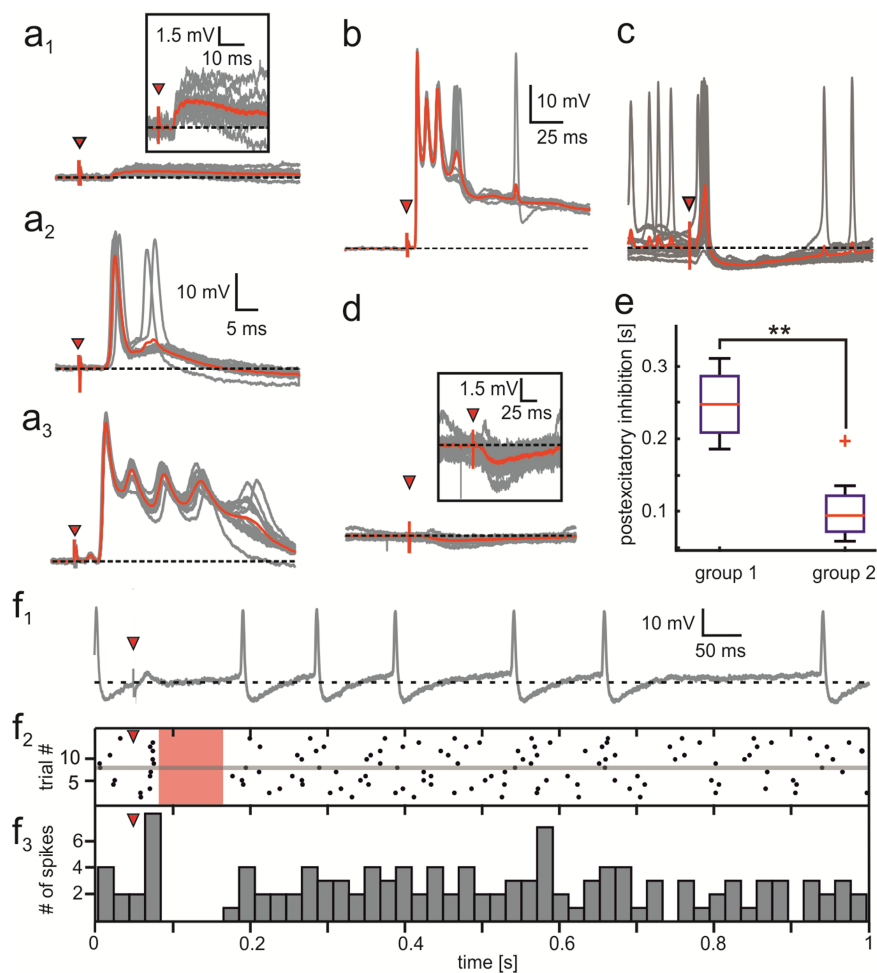


**Fig. 3: Spectrum of trigeminal afferent-evoked synaptic input patterns in LTTD neurons.** (a) Superimposed single sweeps (gray) and averages of synaptic responses (15 trials each, red) in a LTTD neuron following current pulse stimulation of the N.V2s1; with increasing stimulus intensity, responses changed from short-latency EPSPs (a1, T) to single (a2, 1.1xT) and multiple action potentials (a3, 1.4xT). (b-d) Single sweeps (gray) and averages of synaptic responses (15 trials each, red) in three LTTD neurons following current pulse stimulation (3xT) of N.V2s1 (b), N.V2s2 (c), and N.V2s3 (d); synaptic responses consisted either of a short-latency, sustained excitation with multiple spikes (b), short-latency single spikes followed by inhibitory components (c) or longer-latency IPSPs without preceding excitatory components (d); boxed insets in a1 and d show EPSPs and IPSPs at extended amplitude and time scales, respectively. (e) Extent of post-stimulus silencing of spontaneous activity following current pulse stimulation of individual N.V2s sub-branches that led to multiple (group 1) or single or no short-latency spike activity (group 2) in recorded neurons; \*\*,  $p < 0.01$ , Mann-Whitney U test. (f) Single sweep of a synaptic response in a LTTD neuron (f1) evoked by electrical pulse stimulation of the N.V2s4; the spike event plot for multiple trials ( $n = 15$ ; f2) and corresponding post-spike histogram (bin width: 20 ms; f3) reveal a robust inhibitory period (light red area) following the initial synchronized spike discharge. Red triangles in a-d,f indicate electrical pulses. Calibration bar in a2 applies also for a1,3; calibration bars in b applies also for c,d.

### *Convergence of synaptic inputs from multiple N.V2s sub-branches*

The recording of synaptic responses following separate single electrical pulse stimulation of two or three sub-branches of N.V2s (i.e. N.V2s<sub>1-3</sub>, N.V2s<sub>2-4</sub> or N.V2s<sub>4,5</sub>; see Fig. 4a,c,e) allowed characterizing the convergence of signals from spatially adjacent areas of the pit membrane in LTTD neurons ( $n = 19$ ). The predominant response in almost all neurons was an excitation with monosynaptic onset that triggered single or multiple action potentials. In general, the majority of these neurons ( $n = 13$ ) exhibited additional synaptic responses from adjacent sub-branches that, however, differed in their dynamics as depicted in the three typical examples shown in Fig. 4b,d,f. Only few LTTD neurons ( $n = 6$ ) were encountered in which each of the adjacent sub-branches evoked an excitation with similar spike discharge dynamics. In most LTTD neurons, synaptic responses from neighboring sub-branches, e.g. N.V2s<sub>1-3</sub> (Fig. 4b,d,f) consisted of a long-latency inhibition, with or without preceding monosynaptic excitation from one sub-branch (green in Fig. 4a,b<sub>1</sub>) and excitatory responses from the two other sub-branches (magenta and blue in Fig. 4a,b<sub>2,3</sub>). However, the relative weighting of excitatory and inhibitory components differed between inputs from different sub-branches as well as between different neurons (see responses in Fig. 4d<sub>1-3</sub>,f<sub>1-3</sub>). Even though the relative contributions of excitatory and inhibitory responses varied with respect to amplitude and duration, most recorded neurons received a dominant excitation from at least one of the two or three tested N.V2s sub-branches (e.g. Fig. 4b<sub>3</sub>,d<sub>2</sub>,f<sub>1</sub>).

Excitatory and inhibitory inputs in different LTTD neurons could originate from any one of the sub-branches. Thus, the recorded LTTD neurons could be differentiated into three groups. In neurons of the first group (~37%; red sector in Fig. 4g), excitatory inputs derived from a more caudal and inhibitory inputs from a more rostral area of the pit membrane. In these neurons, the synaptic inputs from interjacent sub-branches gradually shifted from a dominating excitation (red sectors in Fig. 4h<sub>1-3</sub>) to a dominating inhibition (blue sector in Fig. 4h<sub>1-3</sub>). In a similarly large group of neurons

(~37%), this pattern was inverted and consisted of an excitation that originated from more rostral sub-branches (dark blue sector in Fig. 4g) with a corresponding transition to a more caudal origin of inhibitory inputs (see red and blue sectors in Fig. 4i<sub>1-3</sub>). In the remaining ~26% of the neurons, the excitation had no predominant rostro-caudal origin (grey sector in Fig. 4g). The sub-branch-dependent transition from excitatory to inhibitory inputs in the first two groups of neurons was also

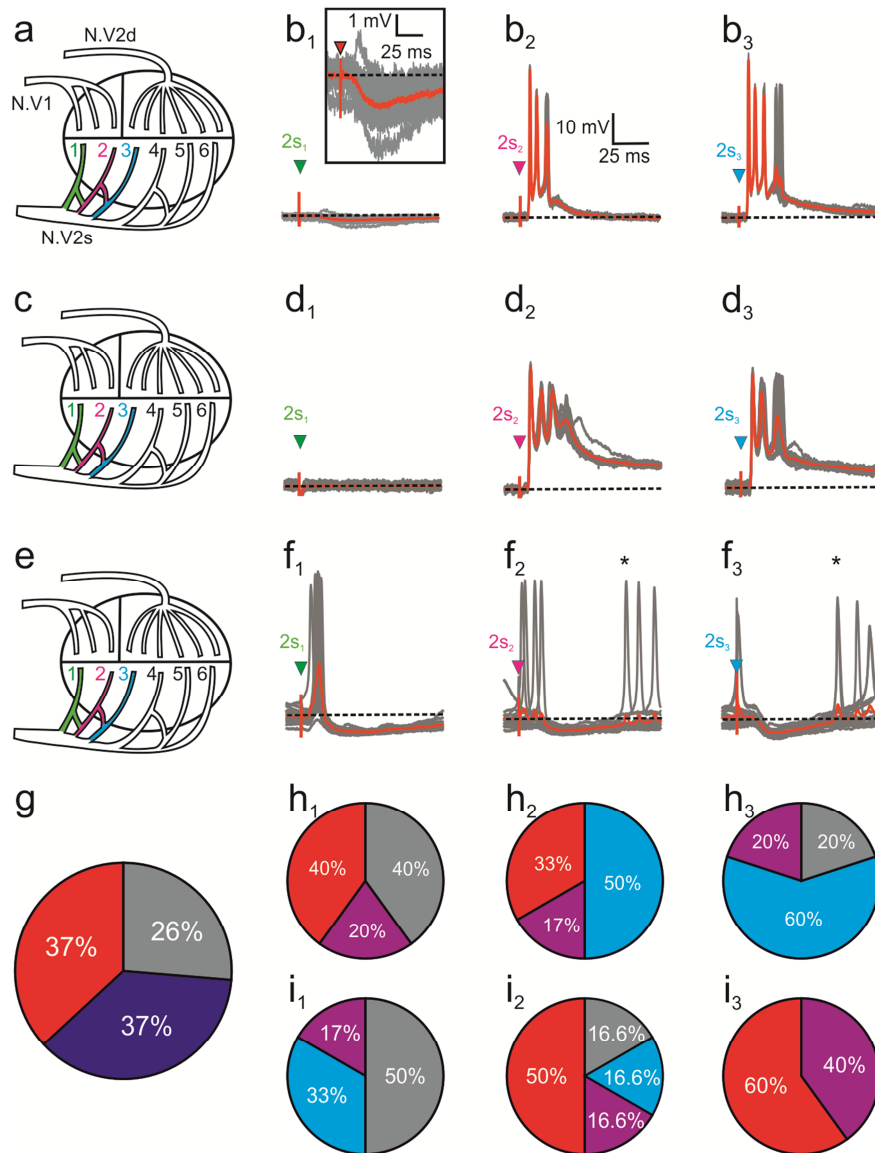


**Fig. 4: Convergence pattern of synaptic responses from adjacent N.V2s sub-branches in LTTD neurons. (a-f)** Schematics of trigeminal afferent pit organ innervation, illustrating separate single pulse stimulation of N.V2s1-3 (a,c,e) and superimposed single sweeps (gray) and averages of synaptic responses from the three sub-branches (15 trials each, red) in each of the three LTTD neurons (b1-3, d1-3, f1-3); note the different convergent pattern of the three inputs in each of the neurons; boxed inset in b1 shows synaptic responses at extended amplitude and time scales, respectively. (g) Distribution of neurons (n = 19) classified by the temporal or nasal pit membrane origin of convergent sub-branch specific excitatory and inhibitory inputs. (h,i) Distribution of strong excitation (red sectors), weak excitation (purple sectors) and inhibition (blue sectors) in inputs from temporal (h1, i1), intermediate (h2, i2) and nasal regions of the pit membrane (h3, i3); the distribution is separately plotted for neurons with a dominating excitation from temporal (h1-3) or nasal regions of the pit membrane (i1-3); gray sectors indicate the absence of a response. Green, red, blue triangles in b,d,f indicate electrical pulses applied to the respective color-coded N.V2s1-3 indicated in a,c,e. Scale bar in b<sub>2</sub> refers to all spike plots.

accompanied by an alteration in the extent of the delayed inhibition. This impression was quantified in spontaneously active neurons, where the duration of inhibition was determined as the time interval between the stimulus and the onset of the first spike after the silent period (\* in Fig. 4f<sub>2,3</sub>). This analysis demonstrated that dominant inhibitory inputs persisted on average for ~150 ms ( $151 \pm 33$  ms;  $n = 8$ ), while weaker inhibitory responses from adjacent sub-branches lasted ~110 ms ( $112 \pm 28$  ms;  $n = 8$ ). The topography of convergent excitatory and inhibitory inputs suggests a representation of sensory signals in individual LTTD neurons that depends on an enhancement of peripheral synaptic inputs from adjacent areas of the pit membrane, functionally similar to center-surround interactions in the visual system (Cook & McReynolds, 1998; Enroth-Cugell & Lennie, 1975). Moreover, a sequential activation of afferent inputs from adjacent sub-branches, as those that occur during moving IR objects might form the basis for encoding and differentiation of infrared motion directions within the LTTD.

#### *Response patterns of LTTD neurons following electrical pulse train stimulation of multiple N.V2s sub-branches*

In this set of experiments, we mimicked natural neuronal activity of trigeminal afferent fibers during a moving IR stimulus. This was done by successively stimulating three adjacent sub-branches of the N.V2s with a pulse train (Fig. 5a,c,d; see material and methods). The simulation of afferent activity evoked by a moving IR object was achieved through a

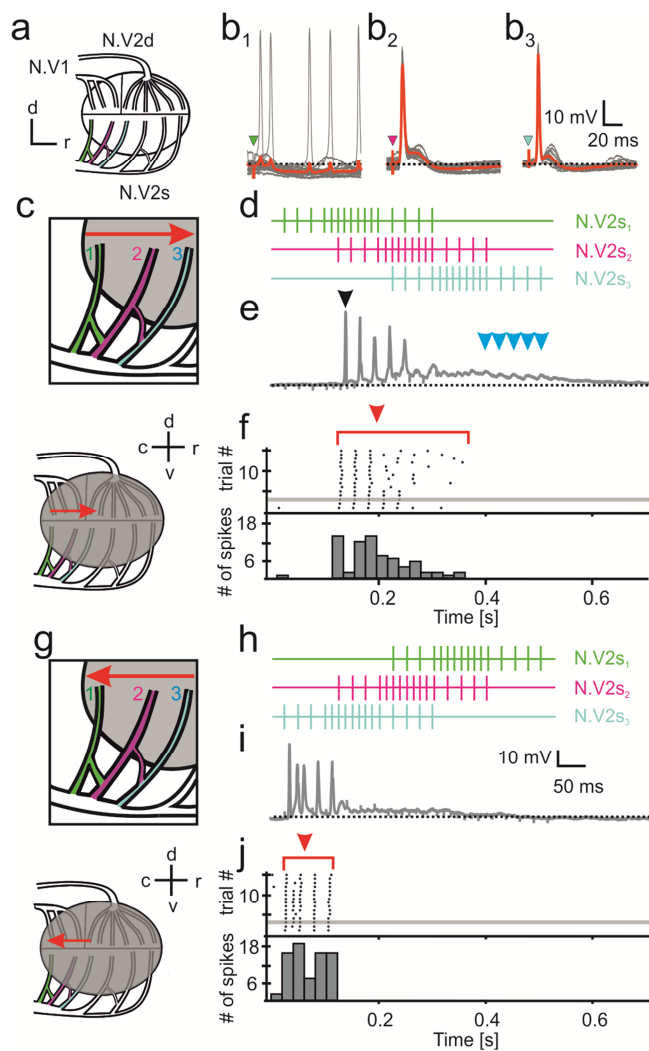


**Fig. 5: Differential response dynamics following sequence-specific activation of adjacent N.V2s sub-branches. (a,b)** Schematics of trigeminal afferent pit organ innervation, illustrating separate single pulse stimulation of N.V2s1-3 (color-coded in a) and superimposed single sweeps (gray) and averages of synaptic responses (15 trials each, red) from the three sub-branches in a LTTD neuron. (c-j) Schematics of the pit membrane (lower schemes in c,g) and magnified view of color-coded N.V2s1-3 (upper schemes in c,g) indicating the caudo-rostral (red arrow in c) and rostro-caudal sequence of stimulated sub-branches (red arrow in g), the overlap of the electrical pulse trains applied to the three sub-branches (color-coded in d,h) and a single sweep of evoked compound responses for each of the two N.V2s1-3 stimulus sequences (e,i); blue arrow heads in e indicate N.V2s3 stimulus pulse-evoked EPSPs; raster plot of evoked spikes (upper plot in f,j) and corresponding post-spike histogram (bin width: 20 ms; lower plot in f,j) over 15 consecutive trials of pulse train stimuli. Calibration bar in i also applies to e.

temporal delay of 100 ms between the onset of the individual stimulus trains applied consecutively to each of the adjacent N.V2s sub-branches (see color-coded pulse trains in Fig. 5d,h). Depending on the sequence of the electrically stimulated sub-branches (Fig. 5c,d,g,h) the afferent responses mimicked a moving IR object in the real world in naso-temporal (n-t, Fig. 5c) or in temporo-nasal (t-n) direction (Fig. 5g). Due to the pit organ optics, the IR motion direction becomes inverted, such that object motion in e.g. t-n direction consecutively activates pit membrane areas and thus corresponding nerve branches in rostro-caudal direction with respect to the orientation of the IR organ in the head. In contrast to the responses of LTTD neurons to single electrical pulses that were separately applied to individual sub-branches (e.g. Fig. 5b<sub>1-3</sub>), temporally overlapping pulse trains to N.V2s<sub>1-3</sub> elicited complex neuronal response patterns in intracellularly recorded LTTD neurons ( $n = 6$ ). Moreover, the timing of the spike discharge and the overall response dynamics depended on the sequence and interaction between different excitatory and inhibitory components (Fig. 5e,i). In a typical LTTD neuron (Fig. 5), overlapping sequential electrical pulse train stimulation in the order N.V2s<sub>1</sub> (green in Fig. 5d), N.V2s<sub>2</sub> (magenta in Fig. 5d), N.V2s<sub>3</sub> (blue in Fig. 5d), i.e. simulating a moving IR object in n-t direction, provoked a delayed spike discharge (black arrow head in Fig. 5e) beginning only with the onset of the N.V2s<sub>2</sub> stimulus pulses (magenta in Fig. 5d). Thereafter, the generation of spikes was limited to the first 5-7 pulses of the N.V2s<sub>2</sub> stimulus

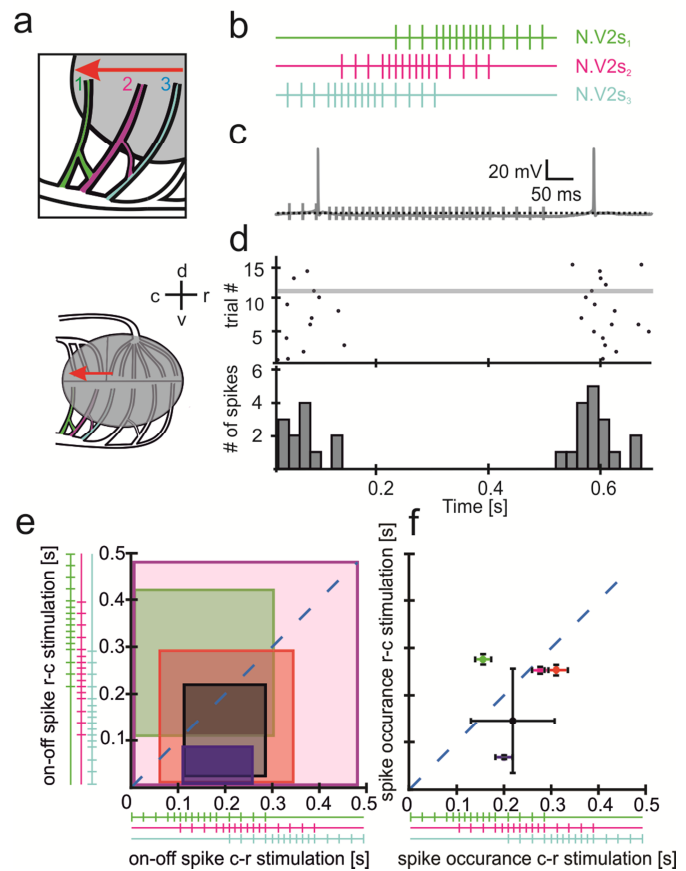


**Fig. 6: Response dynamics following sequence-specific activation of adjacent N.V2s sub-branches.** (a-d) Schematics of the pit membrane (lower scheme in a) and magnified view of color-coded N.V2s<sub>1-3</sub> (upper scheme in a) indicating the rostro-caudal sequence of stimulated sub-branches (red arrow in a), the overlap of the electrical pulse trains applied to the three sub-branches (color-coded in b) and a single sweep of an evoked compound response for this stimulus sequence (c); raster plot of spikes (upper plot in d) and accumulated spike numbers (bin width: 20 ms; lower plot in d) over 15 consecutive trials of pulse train stimuli; note that the spontaneously active LTTD neuron was entirely silenced during the consecutive pulse train stimulation of N.V2s<sub>1-3</sub>. (e,f) correlation between the temporal extent of evoked spike activity (e) and the average  $\pm$  SEM occurrence of evoked action potentials (f) following pulse train stimulation in caudo-rostral (x-axis in e,f) and rostro-caudal direction (y-axis in e,f) for LTTD neurons ( $n = 5$ ); color-coded rectangular areas in e and circles  $\pm$  SEM in f; dashed lines in e,f indicate symmetrical activity patterns for the two opposing stimulus sequences, respectively.

train and extended briefly into the beginning N.V2s<sub>3</sub> pulses (blue in Fig. 5d). The latter stimuli however failed to faithfully trigger action potentials until the end of the pulse train, likely due to a delayed inhibition, activated by the N.V2s<sub>3</sub> sub-branch. Thus, the compound response terminated with a sequence of EPSPs at the end of the N.V2s<sub>3</sub> stimulus train (blue arrow heads in Fig. 5e). This pattern corresponded to the dynamics expected from responses following separate single pulse stimulation of the three sub-branches (Fig. 5b<sub>1-3</sub>). In particular, the delayed activation of action potentials (black arrow head in Fig. 5e) derived from the pronounced inhibition from the N.V2s<sub>1</sub> sub-branch (Fig. 5b<sub>1</sub>) that preceded the synchronized excitation from N.V2s<sub>2</sub> and N.V2s<sub>3</sub> sub-branches (Fig. 5b<sub>2,3</sub>). Inverse application of the stimulus pulse train to the three sub-branches, i.e., in the order N.V2s<sub>3</sub> (blue in Fig. 5h), N.V2s<sub>2</sub> (magenta in Fig. 5h), N.V2s<sub>1</sub> (green in Fig. 5h), yielded a different synaptic compound response and discharge pattern (Fig. 5i,j). The pulse train stimulation faithfully triggered action potentials, which however were restricted to the first 5 pulses applied to the N.V2s<sub>3</sub> sub-branch (Fig. 5i,j). Thus, despite the activation of monosynaptic excitatory responses by single pulses to the second sub-branch, i.e. N.V2s<sub>2</sub>, the discharge was not continued, likely due to delayed inhibitory inputs from N.V2s<sub>3</sub> and N.V2s<sub>2</sub> sub-branches following the monosynaptic excitation (see Fig. 5b<sub>2,3</sub>). The failure to evoke robust excitatory responses was extended with the pronounced inhibitory responses following the onset of the train stimulation of the N.V2s<sub>1</sub> sub-branch (Fig. 5i,j), limiting the overall activation of spikes during a simulation of t-n IR object motion to the few first pulses.

Similar directional differences in spike timing during pulse train stimulation of multiple sub-branches were encountered in LTTD neurons that received different combinations of excitatory and inhibitory inputs from N.V2s<sub>4</sub> and N.V2s<sub>5</sub> (not illustrated). This indicates that the dependency of the spike discharge dynamics on the sequence of successively stimulated sub-branches is not limited to N.V2s<sub>1-3</sub> but could be generalized to all tested sub-branches. The very similar pattern in most neurons was complemented by a particular variation of the pattern in a single neuron. This spontaneously active neuron was completely silenced throughout the overlapping pulse train stimulation of N.V2s<sub>1-3</sub> (Fig. 6a-d), independent of the order of the activated sub-branches. This suggests that longer-latency inhibitory inputs dominated the inputs from the pit organ. However, despite the presence of such a neuron, the majority of recorded LTTD neurons (5 out of 6 neurons) exhibited a clear asymmetry of the evoked spike discharge during pulse train stimulation in rostro-caudal and caudo-rostral direction. The directional specific activity pattern was quantified by analyzing the overall spike discharge duration and average occurrence of evoked action potentials for oppositely directed stimulus sequences (red lines and arrow heads in Fig. 5f,j). Plotting the obtained spike time parameters of the evoked discharge for the five LTTD neurons during caudo-

rostral (x-axis) and during rostro-caudal directed stimulus presentation (y-axis) indicated an asymmetry in the temporal extent of evoked spike firing (colored boxes in Fig. 6e) and in the timing of the average occurrence of action potentials within the stimulus train (colored symbols and  $\pm$  STD bars in Fig. 6f) in four out of the five neurons. This suggests that temporal parameters of the spike discharge depend on the sequence of activated afferent inputs from adjacent pit membrane regions and thus consequently on the direction of IR object motion.

#### *Response patterns of LTTD and RC neurons following activation with moving IR stimuli*

The direction-specific responsiveness of LTTD neurons following electrical stimulation of individual N.V2s sub-branches was tested in a set of in vitro experiments that employed naturally moving IR stimuli. In these experiments, we employed isolated rattlesnake preparations (see material and methods), in which the trigeminal nerve on one side remained connected peripherally to the intact pit organ (Fig. 1b). The exposure of the pit membrane at the surface of the Ringer solution in the chamber allowed applying natural IR motion stimuli under in vivo-like conditions. This was achieved by a bi-directional movement of a circular IR emitter, with a diameter of 6 mm at a distance of 2 cm, across the receptive field of the pit organ at velocities of 175 - 250 mm/s. Based on the pinhole-camera optics of the pit organ that cause image inversion, an IR object motion in t-n direction stimulates the sensory epithelium in rostro-caudal direction (Fig. 7a).

At variance with the previous sets of experiments, most intra- and juxtacellularly recorded neurons from the LTTD ( $n = 19$  out of 22) exhibited a robust resting spike activity (mean  $\pm$  SEM:  $7.8 \pm 0.6$  spikes/s). This likely derived from the intact trigeminal sensory nerve endings within the pit membrane that provided tonic excitatory inputs to LTTD neurons. As during separate electrical stimulation of multiple N.V2s sub-branches, most LTTD neurons ( $n = 19$ ) revealed a variety of mixed excitatory and inhibitory response components during motion of the IR-emitter across the receptive field of the pit organ (Fig. 7b,c,d). The remaining neurons ( $n = 3$ ) expressed only weak alterations of the overall spike discharge during IR stimulation, which in addition were rather variable over successive trials. Therefore, these neurons were excluded from further analysis of directional sensitivity and only included in the estimation of the mean spontaneous spike discharge.

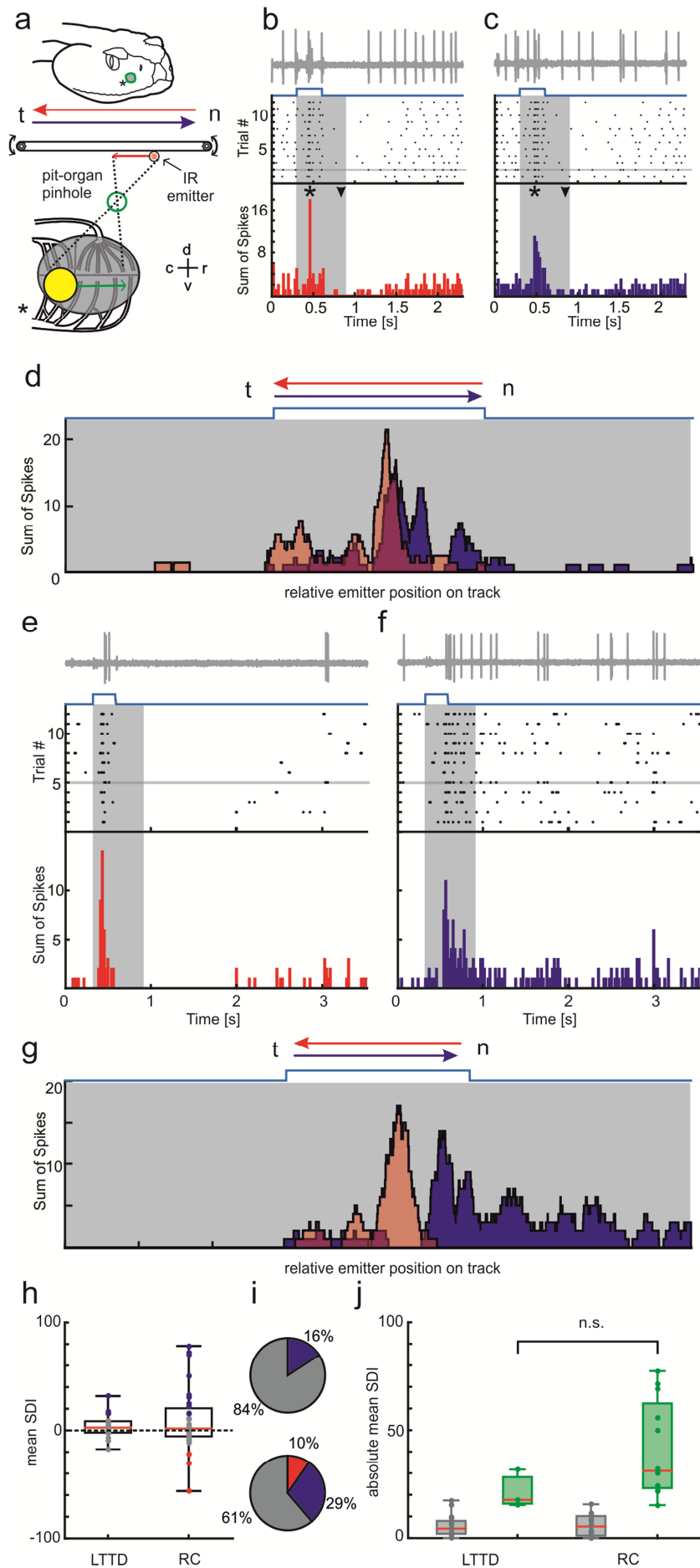


**Fig. 7: Discharge dynamics of LTTD and RC neurons during IR object motion.** (a) Schematics depicting the anatomical location of the pit organ (green area) on the snake's upper jaw, bi-directional movements of a point-like IR emitter (red and blue arrows), pinhole optics of the pit organ (green circle), pit membrane (gray area) and IR stimulus projection onto the epithelium (filled yellow circle); note the natural orientation of the stimulated pit in the head before dissection (\* in head and pit membrane schematics). (b,c) Single sweeps of spike activity of a representative LTTD neuron (gray traces, top) during motion stimulation (blue traces) of the IR emitter in n-t (b) and t-n (c) direction (red and blue arrow in a, respectively), raster plots of evoked spikes (black dots) and accumulated spike numbers (bin width: 20 ms; bottom plot) over 12 consecutive trials. (d) Accumulated spike numbers over 12 consecutive trials of IR emitter motion in n-t (red, plotted from right to left) and t-n (blue, plotted from left to right) direction from the neuron depicted in b/c. (e,f) Single sweeps of spike activity of a representative RC neuron (gray traces, top) during motion stimulation (blue traces) of the IR emitter in n-t (e) and t-n (f) direction (red and blue arrow in a, respectively), raster plots of evoked spikes (black dots) and accumulated spike numbers (bin width: 20 ms; bottom plot) over 12 consecutive trials. (g) Accumulated spike numbers over 12 consecutive trials of IR emitter motion in n-t (red, plotted from right to left) and t-n (blue, plotted from left to right) direction from the neuron depicted in e/f. (h) Boxplots of SDI values calculated from responses of LTTD (left, median: 2.63, n=19) and RC neurons (right, median: 1.72, n=31), respectively. Individual values are plotted and color coded (gray: SDIs from neurons with nonsignificant differences in spike count for opposite stimulus motion directions; red and blue: SDIs from neurons with significantly higher spike count for n-t and t-n stimulus motion, respectively). (i) Pie charts summarizing the percentage of recorded LTTD (upper plot) and RC (bottom plot) neurons with nonsignificant (gray) and significant (red, blue) differences in spike count for opposite stimulus motion directions. (j) Comparison of absolute SDI values of LTTD (left pair of boxplots) and RC (right pair of boxplots) neurons with nonsignificant (gray) and significant (green) differences in spike count for opposite stimulus motion directions (LTTD median: nonsignificant 4.39, n=16; significant: 17.65, n=3. RC median: nonsignificant 5.51, n=19; significant: 31.51, n=12).

All recorded LTTD neurons exhibited a short but distinct augmentation of the spontaneous firing rate during movement of the IR emitter across the receptive field of the pit organ (\* in bottom plot of Fig. 7b,c) independent of stimulus motion direction. However, the magnitude as well as the duration of the brief burst of spikes was rather variable and differed between individual neurons. The excitatory response was preceded by a transient inhibition of the spontaneous discharge in few neurons ( $n = 3$ , not shown) but was followed by a longer, even though temporally variable inhibition of the discharge, in all recorded neurons (arrow heads in bottom plot of Fig 7b,c). This latter inhibition started immediately after the brief spike burst and lasted in some neurons well beyond the end of the IR stimulus motion (e.g. Fig. 7b). As observed for electrically activated responses in LTTD neurons (Fig. 4), the extent of the inhibition usually coincided with the magnitude of the transient excitation (Fig. 7b,c), even though this correlation was less distinct. Nonetheless, the pronounced inhibition following the IR motion-induced burst discharge in LTTD neurons suggests the presence of a mechanism that provides a contrast enhancement of IR signals.

In another set of experiments, the same stimulus paradigm that was used to activate LTTD neurons was applied while recording from neurons in the RC. Similar to the LTTD, neurons recorded from the RC displayed mixed excitatory and inhibitory response components (Fig. 7e,f). However, while individual LTTD neurons exhibited a qualitatively rather constant activity sequence of primary excitation followed by secondary inhibition, which only differed in the shape and strength of individual components, neurons recorded in the RC were more diverse in their responses to IR emitter stimulation. ~50% ( $n=15$ ) of the RC neurons we recorded from were spontaneously active. Other than for LTTD neurons, spontaneous activity in the RC was rather irregular and bursty, i.e. consisted of bursts of two to three spikes that occurred in unsteady sequence. The second half of

recorded RC neurons ( $n=16$ ) did not show spontaneous discharges, indicating rather high input resistances of RC neurons that provide a potent filter for fluctuations in thermal background radiation. Still stable, yet strictly phasic responses to IR emitter stimulation were obtained from such units. However, stimulus motion direction impacted the strength of such phasic responses. Spontaneously active RC neurons revealed more variable excitatory and inhibitory response components that differed between neurons, but also between stimulus movement directions for individual neurons (Fig. 7e-g). A more detailed description of RC response characteristics will be provided in chapter 3.

Comparison of amplitudes and dynamics of excitatory and inhibitory response components during bi-directional IR emitter motion, i.e. t-n *versus* n-t movements, revealed direction-specific differences in the spatiotemporal activation of neuronal discharge in LTTD (Fig. 7b-d) and RC neurons (Fig. 7e-g), respectively. To quantify such direction-specific differences we characterized the burst shape and peak frequencies of IR afferent inputs during bi-directional motion stimulation (Fig. 7d,g) and compared the mean spike count from the beginning of IR motion stimulation in n-t and t-n direction until 300 ms post-stimulus motion time (gray area in Figs. 7b,c,e,f).

Compatible with the findings in the previous sets of experiments, the population of recorded LTTD neurons exhibited no directional bias for responses elicited by IR motion in n-t *versus* t-n direction (Fig. 7h, left boxplot, median=2.63;  $n=19$ ). The same was true for the population of recorded RC neurons (Fig. 7h, right boxplot, median=1.72;  $n=31$ ). However, classification according to motion direction-related differences in spike count, represented in the respective mean SDI values of individual neurons over all stimulus repetitions, yielded groups of LTTD and RC neurons with a preference for IR emitter motion in n-t (SDI < 0, LTTD:  $n = 7$ ; RC:  $n=14$ ) and t-n direction (SDI > 0, LTTD:  $n = 11$ ; RC:  $n=17$ ), respectively. One LTTD neuron exhibited equal spike counts (SDI=0) for opposite stimulus motion directions. To estimate the impact of SDI values on the activity of the respective neurons, we tested whether differences in spike count for stimulus presentations with opposite motion direction were significant over all repetitions in individual neurons (Wilcoxon signed-rank test,  $p<0.05$ ). 16 % ( $n=3$ ) of the recorded LTTD neurons showed such significant differences in spike count. All of these exhibited higher sensitivity towards stimulus motion in t-n direction (Figs. 7h,j; blue markers in Fig. 7h LTTD; blue area in upper pie chart in Fig. 7i). For recordings from the RC, the percentage of neurons with significant differences in spike count for t-n *versus* n-t stimulus motion directions increased to 39 % ( $n=12$ ), indicating convergence of multiple weakly directionally tuned LTTD neurons on individual units in the RC. A majority of the significantly directionally tuned neurons in the RC were more sensitive towards t-n motion ( $n=9$ , blue markers in Fig. 7h RC; blue area in bottom pie chart in Fig. 7i). Only three out of twelve significantly directionally

tuned RC neurons exhibited higher sensitivity towards n-t motion of a stimulus (red markers in Fig. 7h RC; red area in bottom pie chart in Fig. 7i). The absolute SDI values of LTTD neurons with no significant directional tuning lay between 0 and 17.39 (Fig. 7j gray boxplot LTTD, median=4.39). Neurons with significant differences in spike count for reversed stimulus motion directions had SDI values between 15.28 and 31.71 (Fig. 7j green boxplot LTTD, median=17.65). For RC neurons these differences increased and SDI values lay between 0 and 15.85 (Fig. 7j gray boxplot RC, median=5.51) for neurons with non-significant differences in spike count towards bi-directional stimulus motion and between 15.46 and 78.26 (Fig. 7j green boxplot RC, median=31.51) for neurons with significant differences in spike count towards bi-directional stimulus motion. The difference in the extent of directional tuning of LTTD and RC neurons did not become significant (Fig. 7j, green boxplots; Mann-Whitney U test,  $p=0.1363$ ). However, this is most likely due to the small sample size of LTTD neurons ( $n=3$ ) available for statistics.

## Discussion

Pit organ trigeminal afferent fibers and transmitted neuronal activity are topographically represented at the first central nucleus in the hindbrain. Evoked synaptic responses in LTTD neurons consist of sequences of mixed primary excitatory and secondary inhibitory components whose individual strength varies when activated through spatially adjacent pit membrane innervating trigeminal sub-branches. This sub-branch specific excitatory and inhibitory response pattern complies with strong spatiotemporal contrast enhancement in single LTTD neurons. The stimulus location dependent asymmetric impact of excitatory and inhibitory inputs on individual neurons in the LTTD additionally provides a basis for the directional sensitivity of single RC neurons that has been demonstrated in this study for the first time.

### *Synaptic processing of IR signals in LTTD neurons*

A major organizational principle of IR image processing is the topographical representation of sensory signals from the pit organ epithelium along the rostro-caudal and medio-lateral extent of the LTTD (Fig. 2). The distinct spatial pattern of electrically activated synaptic responses within the morphological limits of the LTTD directly complies with the observed region-specific termination of pit organ-innervating trigeminal afferents (Kohl et al., 2014). Thus, IR signals form a central sensory map comparable to visual signals within the tectum (Dräger & Hubel, 1976; Hartline, 1984; Hartline et al., 1978; Heric & Kruger, 1965), rather than a motor map as for example vestibular signals along the rostro-caudal extent of the hindbrain (Chagnaud et al., 2017). A major hallmark feature of the

region-specific central IR object representation is a complex response dynamics that derives from variable combinations of excitatory and inhibitory components in accordance with results from previous extracellular recordings (Stanford & Hartline, 1984). The complexity of the synaptic responses suggests that stimulation of regionally restricted epithelial areas activates microcircuit modules that cause the monosynaptic afferent excitation of LTTD neurons to be dynamically modified and temporally limited by a superimposed longer-latency inhibition (Fig. 3).

The truncation of afferent excitation in central LTTD neurons by a delayed inhibition from the same sensory area reinforces a transient central excitatory representation of IR signals, similar to the dynamic enhancement of phasic vestibular signals by local inhibitory circuits (Biesdorf et al., 2008). Common to both sensory systems is the likely mediation of the delayed inhibition by a disynaptic side-loop, through local populations of GABA and/or glycinergic interneurons. The systematic variability of the inhibition from adjacent trigeminal sub-branches causes asymmetric, stimulus site-dependent patterns of excitatory and delayed inhibitory inputs in LTTD neurons. Although single neurons in the LTTD only show weak directional tuning, convergence of output from multiple LTTD neurons likely mediates the extraction of spatiotemporal features of moving IR objects in the RC.

The sequential excitatory/inhibitory synaptic responses in LTTD neurons could theoretically also derive from a rather dynamic afferent fiber discharge (de Cock Buning et al., 1981; Goris & Nomoto, 1967). However, the highly dynamic afferent spike activity in the latter studies resulted from an illumination of the pit organ with very long or even permanent stimuli of high IR intensity. Our recordings of afferent fibers (not shown) yielded no evidence for the presence of a phasic spike pattern that might cause the observed sequence of excitation and inhibition in central LTTD neurons. Rather, afferent fibers exhibited a tonic firing pattern during IR pulses and a relatively linear correlation between stimulus magnitude and spike rate. This therefore suggests that the excitatory/inhibitory synaptic responses in LTTD neurons upon stimulation of afferent fibers derive from interactions within central synaptic circuits.

The activation of variable sequences of excitatory and inhibitory synaptic response components in the present study not only complies with but also further extends previous findings obtained from extracellular recordings (Stanford & Hartline, 1984). In accordance with emerging suggestions, the receptive field of LTTD neurons is characterized by an excitation that is spatially and temporally flanked by an inhibition. This spatiotemporal specific synaptic arrangement is well suited for a contrast enhancement of IR object representations in the LTTD. Likely through the convergence of multiple LTTD units onto individual RC neurons, stimulus location dependent, asymmetric LTTD response characteristics mediate the detection of IR image motion direction in the RC (Fig. 7).

### *IR contrast enhancement in LTTD neurons*

Trigeminal IR-sensitive afferent fibers transmit heat flux-related signals, which reflect the temperature contrast between the IR-background and emerging objects (Bullock & Diecke, 1956; Goris & Nomoto, 1967; Terashima et al., 1968). This is comparable to the spike discharge pattern of retinal ganglion cells, which also reflects stimulus contrast-related interactions between ON- and OFF bipolar cell responses (Kuffler, 1953; Rodieck, 1965). The encoding of IR contrast differences is further enhanced in the LTTD by local inhibitory circuitries. Interactions between excitatory and inhibitory response components in distinct neurons shape their activity and thereby increase the contrast between an emerging stimulus and the background on a single cell level. Such a spatiotemporal sharpening of sensory signals at early central processing stages by inhibitory components is typical and widely described in other sensory systems (Adolphs, 1993; Burkhardt & Fahey, 1998; Sachdev & Catania, 2002; Schiller, 1992; Stanford & Hartline, 1980; Suga, 1995).

The similarity between the IR and other sensory systems in central signal processing also includes encoding and differentiation of motion direction. Such a feature has been classically described for the auditory (Kuo & Wu, 2012; Wagner et al., 1994; Wagner & Takahashi, 1992), somatosensory (Lichtenstein et al., 1990; Wilent & Contreras, 2005) and visual system (Ariel & Daw, 1982; Barlow et al., 1964; Barlow & Hill, 1963). As described for the retinal output, individual ganglion cells respond strongly to a visual motion stimulus in a “preferred” direction, but decrease their activity in the “null” direction (Ariel & Daw, 1982; Barlow et al., 1964; Barlow & Hill, 1963). The mechanism of this directional selectivity in the retina derives from an asymmetric inhibition within adjacent sensory compartments (Barlow & Levick, 1965; Briggman et al., 2011). Such a computation has been demonstrated as the origin of responses in LTTD neurons evoked from adjacent epithelial areas of the pit organ. In fact, the asymmetry of excitatory and inhibitory response components in the latter neurons derives from the spatiotemporal sequence of peripherally activated inputs. Accordingly, the overall directional IR motion sensitivity is not generally accomplished by single cells in the LTTD, but rather encoded at the population level. It is therefore reasonable to assume that convergence of directionally specific LTTD neuronal output reinforces directional IR motion sensitivity of individual neurons in the RC.

### *Influence of the pit organ pinhole camera optics on directional tuning of LTTD responses*

While the results presented in the first part of this study were obtained from electrical stimulations of the IR sensory periphery and therefore unaltered by the pit organs’ pinhole-camera optics, IR emitter stimulation was impacted by the intact pit organs’ point spread function (psf).

Previous studies have already demonstrated that the power density spectrum calculated from the activity of IR sensitive trigeminal nerves, exhibits directional tuning due to the pit organs' psf (Kohl et al., 2012). The directional tuning of response characteristics in the LTTD and subsequently the RC is therefore most likely composed of effects from both, the camera-optics of the IR sensory periphery and the asymmetric interplay of excitatory and inhibitory response components derived from the LTTD circuitry. This prediction is also well represented in our data. While previous whole nerve recordings from N.V2s revealed varying sensitivity towards an IR stimulus presented in different horizontal angles in front of a snake (Kohl et al., 2012), the stimulus that was used in the mentioned study was not moving but stationary. It elicited higher response frequencies in primary afferents when presented in the nasal part of the pit organ's receptive field as compared to stimulation of more temporal areas. This is in compliance with our finding of a majority of LTTD and RC neurons exhibiting higher spike count towards t-n moving stimuli. Stronger primary input from more nasal parts of the membrane should initially also elicit higher spike count or, to be more precise, higher instantaneous frequencies in the LTTD. However, in compliance with the dependence of secondary inhibition upon the strength of primary excitation (Fig. 3e), such strong excitatory responses would also elicit stronger secondary inhibition, quickly silencing the neural activity (e.g. Fig. 7b,e). Contrary, the stimuli presented in t-n direction probably initially elicited a milder primary excitation within the LTTD that subsequently also led to weaker secondary inhibition and ongoing excitability of the recorded neurons. Still, such mild secondary inhibitory effects might have prevented peak excitation and subsequent strong and longer lasting secondary inhibition that would have been caused by the moving stimulus upon reaching more nasal parts of the receptive field. Accordingly, the overall spike count towards stimuli moving in t-n direction was higher than for such moving in n-t direction (e.g. Fig. 7c,f). Again, this effect is less distinct in single LTTD neurons (Fig.7 b-d) and rather coded in its neuron population, while it is clearly displayed in recordings from individual RC neurons (Fig. 7 e-g). While the described response characteristics are found in a majority of our recordings, there are still some neurons that display opposite directional tuning, i.e. highest spike count towards n-t moving stimuli. This most likely underlines the importance of the spatial asymmetry with which the LTTD inhibitory micro circuitry influences the activity of ascending neurons that project towards the RC. In addition to the evidence from the electrical stimulation protocols in this study, which allowed the recording of neural responses unaltered by pit organ morphology, the impact of the inhibitory LTTD micro circuitry on directional tuning upon natural stimulation of the pit organ should be demonstrable by means of pharmacological treatment. Thereby, inhibitory responses could be blocked and the pure effects of the pit organ psf on LTTD activity would be unveiled.

### *IR sensitive hindbrain nuclei as directionally tuned edge movement detectors*

In IR-sensitive rattlesnakes, the somatosensory trigeminal nucleus of the vertebrate hindbrain was transformed into a highly specialized sensory system that shares several processing characteristics with other sensory systems. The somatosensory periphery has been specialized into an optic apparatus and a sensory epithelium, which is sensitive to IR and allows the generation of images that represent the thermal signature of objects in the environment. Although the spatial resolution of the pinhole-camera is considerably lower than that of the eye, the pit organ nonetheless provides an image-like representation of the IR environment (Bakken et al., 2012; Bakken & Krochmal, 2007; Otto, 1972; Sichert et al., 2006). The presence of spatially aligned topographic representations of both systems in the optic tectum (Hartline et al., 1978) suggests that visual and IR signals are combined in specific sets of neurons and potentially complement each other dynamically to generate a single image of the visual/IR environment. However, given the large difference of the image resolution, it is unlikely that IR information about the spatial location of an object is simply integrated with visual signals in the form of e.g. an additional “color”. Instead, IR signals potentially facilitate an edge detection mechanism for moving stimuli. In this case, the prominent lateral inhibition within the LTTD micro circuitry, observed in the current study might not only enhance the contrast of stationary objects in front of a background with different temperature but also facilitate the detection of moving IR objects with distinct thermal signatures in the RC.

The mechanism for such motion detection is likely based on the specific sequences of activated excitation and inhibition already at the level of the first central nucleus. The relative synaptic weight of excitatory and inhibitory inputs depends on the chronology of activated adjacent epithelial areas of the pit membrane. Accordingly, warm objects moving within the receptive field of the pit organ, cause transient patterns of excitation and inhibition in LTTD neurons, which in their sequential appearance vary for different stimulus movement directions. Through the convergence of LTTD output, stimulus motion dependent differences in response patterns are intensified and implemented on a single cell level in the RC (Figs. 7 b,c,e,f). Based on the topographic representation of the sensory epithelium in the LTTD (Kohl et al., 2014), distinct sets of neurons in the LTTD encode different trajectories of IR objects. As soon as the IR object enters the receptive field of a particular neuron, the activity will rise immediately while the subsequent delayed inhibition suppresses this initial excitation quickly. During IR stimulus motion, this causes a wave of transient activity that propagates through adjacent compartments of the LTTD, thus implementing an edge-detection mechanism. The preceding and trailing inhibition thereby facilitates the contrast enhancement. From a spatiotemporal point of view, the LTTD acts as a filter that maps altering positions of IR objects in space and time as soon as they enter the receptive field, with certain sub-populations of

neurons being additionally tuned to particular stimulus motion directions. The integration of this information eventually takes place on a single cell level in the RC.

Mechanisms for the extraction and processing of spatiotemporal information from sensory inputs need to be optimized according to both the input modality and the according spatiotemporal detail the sensory periphery can provide. The pit organ of rattlesnakes supplies a simple visual input to the somatosensory system. However, despite this simplicity, the first central IR-sensitive nucleus extracts precise spatiotemporal information from this low-resolution input. Presumably through output convergence, the motion sensitive contrast coding in LTTD neurons combined with strong post-excitatory inhibition implements an event-based motion detection mechanism in the RC, therefore emphasizing changes in the IR environment rather than overall thermal profiles. Such an event-based computation is highly suitable for the efficient localization and tracking of objects in the environment in computational vision applications (Serrano-Gotarredona & Linares-Barranco, 2013; Weikersdorfer et al., 2013) and recently developed into a new paradigm for resource efficient vision-processing in robotics (Conradt et al., 2009; Delbruck & Lang, 2013). Our data therefore demonstrate the considerable flexibility and tuning-capability of early sensory processing circuits in a relatively simple biological system. The rattlesnake trigeminal hindbrain nuclei are a good example for such tuning towards the optimal usage of provided sensory information and the evolution of available circuitry that is shaped by neural plasticity and adapts according to modality dependent correlations in sensory inputs.

## References

- Adolphs, R. (1993). Bilateral inhibition generates neuronal responses tuned to interaural level differences in the auditory brainstem of the barn owl. *Journal of Neuroscience*, *13*(9), 3647–3668.
- Amemiya, F., Ushiki, T., Goris, R. C., Atobe, Y., & Kusunoki, T. (1996). Ultrastructure of the crotaline snake infrared pit receptors: SEM confirmation of TEM findings. *The Anatomical Record*, *246*(1), 135–146.
- Ariel, M., & Daw, N. W. (1982). Pharmacological analysis of directionally sensitive rabbit retinal ganglion cells. *Journal of Physiology*, *324*, 161–185.
- Bakken, G. S., Colayori, S. E., & Duong, T. (2012). Analytical methods for the geometric optics of thermal vision illustrated with four species of pitvipers. *Journal of Experimental Biology*, *215*, 2621–2629.
- Bakken, G. S., & Krochmal, A. R. (2007). The imaging properties and sensitivity of the facial pits of pitvipers as determined by optical and heat-transfer analysis. *Journal of Experimental Biology*, *210*(Pt 16), 2801–2810.
- Barlow, H. B., & Hill, R. M. (1963). Selective sensitivity to direction of movement in ganglion cells of the rabbit retina. *Science*, *139*(3553), 412–414.
- Barlow, H. B., Hill, R. M., & Levick, W. R. (1964). Retinal ganglion cells responding selectively to direction and speed of image motion in the rabbit. *Journal of Physiology*, *173*(3), 377–407.
- Barlow, H. B., & Levick, W. R. (1965). The mechanism of directionally selective units in rabbit's retina. *Journal of Physiology*, *178*, 477–504.
- Beavers, R. A. (1976). Food habits of the western diamondback rattlesnake, *Crotalus atrox*, in Texas (Viperidae). *The Southwestern Naturalist*, *20*(4), 503–515.
- Biesdorf, S., Malinvaud, D., Reichenberger, I., Pfanzelt, S., & Straka, H. (2008). Differential inhibitory control of semicircular canal nerve afferent-evoked inputs in second-order vestibular neurons by glycinergic and GABAergic circuits. *Journal of Neurophysiology*, *99*, 1758–1769.
- Briggman, K. L., Helmstaedter, M., & Denk, W. (2011). Wiring specificity in the direction-selectivity circuit of the retina. *Nature*, *471*(7337), 183–188.
- Bullock, T. H., & Diecke, F. P. (1956). Properties of an infra-red receptor. *Journal of Physiology*, *134*(1), 47–87.
- Bullock, T. H., & Fox, W. (1957). The anatomy of the infra-red sense organ in the facial pit of pit

- vipers. *Journal of Microscopical Science*, 98, 219–234.
- Burkhardt, D. A., & Fahey, P. K. (1998). Contrast enhancement and distributed encoding by bipolar cells in the retina. *Journal of Neurophysiology*, 80(3), 1070–1081.
- Chagnaud, B. P., Engelmann, J., Fritzsche, B., Glover, J. C., & Straka, H. (2017). Sensing external and self-motion with hair cells: A comparison of the lateral line and vestibular systems from a developmental and evolutionary perspective. *Brain, Behavior and Evolution*, 90(2), 98–116.
- Chen, Q., Deng, H., Brauth, S. E., Ding, L., & Tang, Y. (2012). Reduced performance of prey targeting in pit vipers with contralaterally occluded infrared and visual senses. *PLoS ONE*, 7(5), 1–8.
- Conradt, J., Cook, M., Berner, R., Lichtsteiner, P., Douglas, R. J., & Delbruck, T. (2009). A pencil balancing robot using a pair of AER dynamic vision sensors. *2009 IEEE International Symposium on Circuits and Systems*, 781–784.
- Cook, P. B., & McReynolds, J. S. (1998). Lateral inhibition in the inner retina is important for spatial tuning of ganglion cells. *Nature Neuroscience*, 1(8), 714–719.
- de Cock Buning, T., Terashima, S. I., & Goris, R. C. (1981). Crotaline pit organs analyzed as warm receptors. *Cellular and Molecular Neurobiology*, 1(1), 69–85.
- Delbruck, T., & Lang, M. (2013). Robotic goalie with 3 ms reaction time at 4% CPU load using event-based dynamic vision sensor. *Frontiers in Neuroscience*, (7 NOV), 1–7.
- Desalvo, J. A., & Hartline, P. H. (1978). Spatial properties of primary infrared sensory neurons in Crotalidae. *Brain Research*, 142, 338–342.
- Djawdan, M., & Garland, T. J. (1988). Maximal running speeds of bipedal and quadrupedal rodents. *Journal of Mammalogy*, 69(4), 765–772.
- Dräger, U., & Hubel, D. H. (1976). Topography of visual and somatosensory projections to mouse superior colliculus. *Journal of Neurophysiology*, 91–101.
- Enroth-Cugell, C., & Lennie, P. (1975). The control of retinal ganglion cell discharge by receptive field surrounds. *Journal of Physiology*, 257, 551–578.
- Gilland, E., & Baker, R. (2005). Evolutionary patterns of cranial nerve efferent nuclei in vertebrates. *Brain, Behavior and Evolution*, 66(4), 234–254.
- Goris, R. C., Kadota, T., & Kishida, R. (1989). Innervation of snake pit organ membranes mapped by receptor terminal succinate dehydrogenase activity. *Current Herpetology in East Asia*, 8–16.
- Goris, R. C., & Nomoto, M. (1967). Infrared reception in oriental crotaline snakes. *Comparative*

*Biochemistry and Physiology*, 23, 879–892.

- Gracheva, E. O., Ingolia, N. T., Kelly, Y. M., Cordero-Morales, J. F., Hollopeter, G., Chesler, A. T., ... Julius, D. (2010). Molecular basis of infrared detection by snakes. *Nature*, 464(7291), 1006–1011.
- Hartline, P. H. (1984). The optic tectum of reptiles: Neurophysiological studies. In H. Vanegas (Ed.), *Comparative Neurology of the Optic Tectum* (pp. 601–618).
- Hartline, P. H., Kass, L., & Loop, M. S. (1978). Merging of modalities in the optic tectum: infrared and visual integration in rattlesnakes. *Science*, 199(4334), 1225–1229.
- Haverly, J. E., & Kardong, K. V. (1996). Sensory deprivation effects on the predatory behavior of the rattlesnake, *Crotalus viridis*. *Copeia*, (2), 419–428.
- Heric, T. M., & Kruger, L. (1965). Organization of the visual projection upon the optic tectum of a reptile (Alligator Mississippiensis). *Journal of Comparative Neurology*, 124(1), 101–111.
- Kardong, K. V., & MacKessy, S. P. (1991). The strike behaviour of a congenitally blind rattlesnake. *Journal of Herpetology*, 25(2), 208–211.
- Kass, L., Loop, M. S., & Hartline, P. H. (1978). Anatomical and physiological localization of visual and infrared cell layers in tectum of pit vipers. *J Comp Neurol*, 182(4 Pt 2), 811–820.
- Kishida, R., Terashima, S. I., Goris, R. C., & Toyokazu, K. (1982). Infrared sensory neurons in the trigeminal ganglia of crotaline snakes : Transganglionic HRP transport. *Brain Research*, 241, 3–10.
- Kohl, T., Bothe, M. S., Luksch, H., Straka, H., & Westhoff, G. (2014). Organotopic organization of the primary infrared sensitive nucleus (LTDD) in the western diamondback rattlesnake (*Crotalus atrox*). *Journal of Comparative Neurology*, 522(18), 3943–3959.
- Kohl, T., Colayori, S. E., Westhoff, G., Bakken, G. S., & Young, B. A. (2012). Directional sensitivity in the thermal response of the facial pit in western diamondback rattlesnakes (*Crotalus atrox*). *The Journal of Experimental Biology*, 215(Pt 15), 2630–2636.
- Kuffler, S. W. (1953). Discharge Patterns and Functional Organization of Mammalian Retina. *Journal of Neurophysiology*, 16(1), 37–68.
- Kuo, R. I., & Wu, G. K. (2012). The generation of direction selectivity in the auditory system. *Neuron*, 73(5), 1016–1027.
- Lichtenstein, S. H., Carvell, G. E., & Simons, D. J. (1990). Responses of rat trigeminal ganglion neurons to movements of vibrissae in different directions. *Somatosensory & Motor Research*, 7(1), 47–

65.

- Lynn, W. G. (1931). The structure and function of the facial pit of the pit vipers. *The American Journal of Anatomy*, 49(1), 97–139.
- Meszler, R. M., Auker, C. R., & Carpenter, D. O. (1981). Fine structure and organization of the infrared receptor relay, the lateral descending nucleus of the trigeminal nerve in pit vipers. *Journal of Comparative Neurology*, 196, 571–584.
- Moiseenkova, V., Bell, B., Motamedi, M., Wozniak, E., & Christensen, B. (2003). Wide-band spectral tuning of heat receptors in the pit organ of the copperhead snake (Crotalinae). *American Journal of Physiology, Regulatory, Integrative and Comparative Physiology*, 284(2), R598–R606.
- Newman, E. A., Gruberg, E. R., & Hartline, P. H. (1980). The infrared trigemino-tectal pathway in the rattlesnake and in the python. *Journal of Comparative Neurology*, 191(3), 465–477.
- Noble, G. K., & Schmidt, A. (1937). The structure and function of the facial and labial pits of snakes. *Proceedings of the American Philosophical Society*, 77(3), 263–288.
- Nowak, L., Bregestovski, P., Ascher, P., Herbet, A., & Prochiantz, A. (1984). Magnesium gates glutamate-activated channels in mouse central neurones. *Nature*, 307(February), 462–465.
- Otto, J. (1972). Das Grubenorgan, ein biologisches System zur Abbildung von Infrarotstrahlern. *Biological Cybernetics*, 10(2), 103–106.
- Pfanzelt, S., Rossert, C., Rohregger, M., Glasauer, S., Moore, L. E., & Straka, H. (2008). Differential dynamic processing of afferent signals in frog tonic and phasic second-order vestibular neurons. *Journal of Neuroscience*, 28(41), 10349–10362.
- Rodieck, R. W. (1965). Quantitative analysis of cat retinal ganglion cell response to visual stimuli. *Vision Research*, 5, 583–601.
- Roelke, C. E., & Childress, M. J. (2007). Defensive and infrared reception responses of true vipers, pitvipers, azemiops and colubrids. *Journal of Zoology*, 273(4), 421–425.
- Sachdev, R. N. S., & Catania, K. C. (2002). Receptive fields and response properties of neurons in the star-nosed mole's somatosensory fovea. *Journal of Neurophysiology*, (87), 2602–2611.
- Schiller, P. H. (1992). The ON and OFF channels of the visual system. *Science*, 15(3), 86–92.
- Schroeder, D. M., & Loop, M. S. (1976). Trigeminal projections in snakes possessing infrared sensitivity. *Journal of Comparative Neurology*, 169(1), 1–11.
- Serrano-Gotarredona, T., & Linares-Barranco, B. (2013). A 128 × 128 1.5% contrast sensitivity 0.9%

- FPN 3  $\mu$ s latency 4 mW asynchronous frame-free dynamic vision sensor using transimpedance preamplifiers. *IEEE Journal of Solid-State Circuits*, 48(3), 827–838.
- Sichert, A., Friedel, P., & van Hemmen, L. (2006). Snake's perspective on heat: Reconstruction of input using an imperfect detection system. *Physical Review Letters*, 97(6), 068105.
- Stanford, L. R., & Hartline, P. H. (1980). Spatial sharpening by second-order trigeminal neurons in crocotaline infrared system. *Brain Research*, 185(1), 115–123.
- Stanford, L. R., & Hartline, P. H. (1984). Spatial and temporal integration in primary trigeminal nucleus of rattlesnake infrared system. *Journal of Neurophysiology*, 51(5), 1077–1090.
- Straka, H., Biesdorf, S., & Dieringer, N. (1997). Canal-specific excitation and inhibition of frog second-order vestibular neurons. *Journal of Neurophysiology*, 78(3), 1363–1372.
- Suga, N. (1995). Sharpening of frequency tuning by inhibition in the central auditory system: tribute to Yasuji Katsuki. *Neuroscience Research*, 21(4), 287–299.
- Terashima, S. I., & Goris, R. C. (1977). Infrared bulbar units in crocotaline snakes. *Proceedings of the Japan Academy. Ser. B: Physical and Biological Sciences*, 53(7), 292–296.
- Terashima, S. I., Goris, R. C., & Katsuki, Y. (1968). Generator potential of crocotaline snake infrared receptor. *Journal of Neurophysiology*, 31(5), 682–688.
- Terashima, S. I., Goris, R. C., & Katsuki, Y. (1970). Structure of warm fiber terminals in the pit membrane of vipers. *Journal of Ultrastructure Research*, 31(5–6), 494–506.
- Terashima, S. I., & Liang, Y. F. (1991). Temperature neurons in the crocotaline trigeminal ganglia. *Journal of Neurophysiology*, 66(2), 623–634.
- van Dyke, J. U., & Grace, M. S. (2010). The role of thermal contrast in infrared-based defensive targeting by the copperhead, *Agkistrodon contortrix*. *Animal Behaviour*, 79(5), 993–999.
- Wagner, H., & Takahashi, T. (1992). Influence of temporal cues on acoustic motion-direction sensitivity of auditory neurons in the owl. *Journal of Neurophysiology*, 68(6), 2063–2076.
- Wagner, H., Trinath, T., & Kautz, D. (1994). Influence of stimulus level on acoustic motion-detection sensitivity in barn owl midbrain neurons. *Journal of Neurophysiology*, 71(5), 1907–1916.
- Weikersdorfer, D., Hoffmann, R., & Conradt, J. (2013). Simultaneous localization and mapping for event-based vision systems. *International Conference on Computer Vision Systems*, 133–142.
- Westhoff, G. (2014). Giftschiangen und Krustenechsen. In *Sachkunde Gefährliche Reptilien* (pp. 32–42). VDA/DGHT Sachkunde GbR.

- Westhoff, G., Morsch, M., & Ebert, J. (2006). Infrared detection in the rattlesnake *Crotalus atrox* – from behavioural studies to midbrain recordings. In *Proceedings of the 13th Congress of the Societas Europaea Herpetologica* (pp. 225–228).
- Wilent, W. B., & Contreras, D. (2005). Dynamics of excitation and inhibition underlying stimulus selectivity in rat somatosensory cortex. *Nature Neuroscience*, 8(10), 1364–1370.

## Chapter 3

### **Infrared object motion-processing in the rattlesnake hindbrain depends on rate- as well as spike time encoding mechanisms**

Maximilian S. Bothe<sup>1,2\*</sup>, Harald Luksch<sup>1</sup>, Hans Straka<sup>3</sup>, and Tobias Kohl<sup>1</sup>

<sup>1</sup> Chair of Zoology, Technical University Munich, Liesel-Beckmann-Str. 4, 85354 Freising-Weihenstephan, Germany

<sup>2</sup> Graduate School of Systemic Neurosciences, Ludwig-Maximilians-University Munich, Großhaderner Str. 2, 82152 Planegg

<sup>3</sup> Department Biology II, Ludwig-Maximilians-University Munich, Großhaderner Str. 2, 82152 Planegg

\*First-author

#### Contributions of Maximilian S. Bothe:

- Participated in the development of study concept and design
- Acquisition of data
- Statistical analysis
- Preparation of all figures
- Writing of the manuscript
- Analysis of data
- Review and discussion of the manuscript

#### Contributions of other authors:

- Study concept and design: T.K., H.S.
- Review and discussion of data analysis and figures: T.K., H.L.
- Review and discussion of the manuscript: T.K., H.L.
- Administrative, technical and material support: H.L., H.S., T.K.

## **Infrared object motion-processing in the rattlesnake hindbrain depends on rate- as well as spike time encoding mechanisms**

### **Abstract**

Using an in vitro whole brain preparation of the western diamondback rattlesnake, *Crotalus atrox*, we here investigated response characteristics of individual neurons in the hindbrain nucleus reticularis caloris (RC) towards a moving infrared (IR) stimulus of varying velocity. We could not find a tuning of directionally sensitive RC neurons towards specific stimulus motion velocities. Instead, a velocity-independent opposite directional tuning of RC neurons with respect to spike count and interspike intervals (ISI) was found. A majority of RC neurons that showed significant differences in spike count upon opposite stimulus motion directions, exhibited more spikes, (i.e. higher sensitivity) towards temporal-nasal (t-n) than towards naso-temporal (n-t) stimulus motion. Contrary, the majority of neurons with significant differences in ISI displayed shorter ISI times and therefore higher instantaneous frequencies (i.e. signal gain) towards n-t moving stimuli. Such directionally tuned parallel processing of multiple characteristics of ecologically relevant stimuli within one neuron population might be an important feature in the extraction of IR input properties in the hindbrain that are relevant for the eventual integration of IR with visual input in the optic tectum (OT).

## Introduction

Rattlesnakes are somatosensory specialists. They use their bilateral loreal pit organs to detect thermal contrast in the infrared (IR) radiation profile of their environment (Bullock & Diecke, 1956; Goris & Nomoto, 1967). The pit organ is used in a variety of behaviors such as thermoregulation (Krochmal & Bakken, 2003) and hunting (Haverly & Kardong, 1996; Kardong & MacKessy, 1991). Through each pit cavity spans a thin sensory membrane which is innervated by the ophthalmic (N.V1) and deep (N.V2d) and superficial (N.V2s) maxillary trigeminal nerve branches (Bullock & Fox, 1957; Kohl et al., 2014; Lynn, 1931). The rather wide opening of the pit organ attributes low resolution pinhole camera optics to the IR recipient periphery (Otto, 1972; Sichert et al., 2006). Despite the low resolution of the resulting image on the pit membrane, the IR environment is still represented in an image like fashion (Bakken & Krochmal, 2007). Primary afferents from each of the pit organ innervating trigeminal nerves innervate distinct areas of the pit membrane (Kohl et al., 2014; Lynn, 1931). From the periphery, the primary afferents project to the ipsilateral hindbrain where they topographically innervate the nucleus of the lateral descending trigeminal tract (LTTD) (Kohl et al., 2014). LTTD neurons exhibit a combination of primary excitatory and secondary inhibitory response components whose relative strength depends on the temporal sequence of activation of adjacent receptive areas on the pit membrane (chapter 2). LTTD output is conveyed to another ipsilateral nucleus of the rattlesnake hindbrain, called nucleus reticularis caloris (RC) (Gruberg et al., 1979; Newman et al., 1980). While the directional sequence of stimulus transition at the periphery and the corresponding asynchronous strength of excitatory and inhibitory response components only cause a rather weak directional tuning of individual neurons in the LTTD, neurons in the RC clearly exhibit such directional tuning (chapter 2). From the RC, neurons project to the contralateral lobe of the optic tectum (OT) (Newman et al., 1980) where input coding the IR environment is aligned with visual input and topographically represented in the somatosensory recipient layers (Hartline et al., 1978; Kass et al., 1978). So far, further studies on physiological properties of the RC are missing. However, its position within the IR system as a nucleus connecting the hindbrain IR processing circuitry with the tectal IR map makes it a promising target of further studies. It is of special interest to unveil the relevant parameters extracted from IR input in the RC to prepare integration of the low resolution IR input with the highly resolved visual input in the OT.

Here we used an in vitro whole brain preparation of the western diamondback rattlesnake, *Crotalus atrox*, to unveil response characteristics of RC neurons towards an IR stimulus moving horizontally in front of the pit organ at varying velocities. While we could not find a dependence of RC directional tuning on stimulus velocity, an opposite directional tuning of neurons with respect to

sensitivity and signal gain was demonstrated. Sensitivity was hereby represented in the rate code of neural responses, while signal gain was represented in the temporal code.

## **Material and Methods**

### *Animals and experimental preparation*

Experiments were performed on isolated brain preparations of 7 juvenile western diamondback rattlesnakes (*Crotalus atrox*). Snakes of either sex and a body weight of 33-48 g were obtained from the in house animal breeding facility at the Chair of Zoology at the Technical University of Munich. Snakes were kept at a temperature of 22-30°C at a 12h/12h light/dark cycle. Animals were fed weekly with pre-killed mice and water was provided *ad libitum*. Care and maintenance of the animals followed the established guidelines for venomous snakes (Westhoff, 2014). Electrophysiological experiments were performed in-vitro on isolated, semi-intact preparations and complied with the "Principles of animal care", publication No. 86-23, 212 revised 1985 of the National Institute of Health. Permission for the experiments was granted by the respective governmental institution at the Regierung von Oberbayern (55.2-1-54-2532.6-9-12).

For all experiments, animals were initially anesthetized with isoflurane in an induction chamber. After the tail-pinch reflex ceased, snakes were secured with u-shaped pins to the Sylgard® (Dow Corning, Wiesbaden, Germany) floor of a large petri dish. Intramuscular injection of a combination of Ketamine hydrochloride (40 mg/kg; Ketamine 100 mg/ml, Ketavet, Zoetis Deutschland GmbH, Berlin, Germany) and Xylazine hydrochloride (20 mg/kg; Rompun 2%, Bayer Vital GmbH, Leverkusen, Germany) ensured deep anesthesia for the subsequent surgical procedure. The body was opened ventrally at the level of the heart and snakes were perfused transcordially with 30-50 ml of ice-cold snake Ringer solution (in mM: 96.5 NaCl, 31.5 NaHCO<sub>3</sub>, 4 CaCl<sub>2</sub>, 2.6 KCl, 2 MgCl<sub>2</sub>, and 20 D-glucose, pH 7.4). Thereafter, the animals were decapitated and the lower jaws including muscle and connective tissue were removed. The bilateral pit organs in the upper jaw and the innervating trigeminal nerve branches on both sides were maintained intact. The skull was then carefully opened ventrally to isolate the entire brain with the trigeminal nerve branches and the pit organs on both sides attached (Fig. 1a). To mechanically stabilize the trigeminal ganglia, the bone surrounding them was kept intact. After completion of the isolation procedure, preparations were stored in ice-cold Ringer solution. For all experiments, the preparations were placed in a recording chamber (2 x 3 cm) with a volume of ~6 ml and fixed with insect pins to the Sylgard® floor. Preparations were continuously superfused with oxygenated snake Ringer solution, however, with

lower magnesium and calcium concentrations (in mM: 0.4 MgCl<sub>2</sub>, CaCl<sub>2</sub>: 2mM). Magnesium was hereby lowered for facilitated activation of NMDA receptors (Nowak et al., 1984), while the lowered calcium concentration provided a temporally more stable resting discharge. Throughout the experiments, the temperature of the Ringer solution in the chamber was electronically controlled and maintained at  $14.0 \pm 0.2^{\circ}\text{C}$ . For the presentation of a natural IR stimulus, a platform of petroleum jelly (Vaseline Weiss Ph.Eur., Bombastus-Werke, Freital, Germany) was built beneath the pit organ to lift it up until the pit opening protruded from the ringer solution. Ringer was afterwards carefully sucked out of the pit cavity by means of a small piece of paper tissue. Whole brain preparations were used for up to 4 days and kept overnight at  $4^{\circ}\text{C}$  in oxygenated Ringer solution with standard magnesium and calcium concentration. No noticeable differences in response parameters were encountered during the daily recording sessions over this period.

#### *IR emitter stimulus presentation and recordings of neurons in the RC*

A 1.3 W IR emitter (Steady State IR Source, Model EK-5270, Laser Components GmbH, Olching, Germany) was used as a stimulus source. The emitter was attached to a custom built x-y-plotter (Petra Haase Computertechnik, Neuss, Germany) in a height of 2 cm above the recording chamber. At this distance the maximal radiance intensity delivered to the in vitro pit membrane was calculated to be around  $94 \text{ mW}/\text{cm}^2$ . The Emitter was presented to the pit organ at varying velocities between 0.05 m/s and 0.25 m/s. Velocity was kept constant within a three minute recording session. The movement of the emitter occurred in alternating temporo-nasal (t-n) and naso-temporal (n-t) direction during each session. After each stimulus presentation, emitter movement was automatically paused for five or seven seconds to ensure neural responses were independent and unaltered from previous stimulus presentations. No differences were found between recordings with five and seven second stimulus pauses, respectively

For extra- and juxtacellular recordings in the RC, glass microelectrodes were pulled with a micropipette puller (P-87 Micropipette Puller, Sutter Instrument, Novato California, USA) and filled with 3M potassium acetate and 2 M potassium chloride in a ratio of 9:1 to reach a final resistance between 50 and 60 M $\Omega$ . Electrodes were positioned above the RC by means of a 3-axis piezo-stepper (Triple Axis Micromanipulator, Sensapex, Oulu, Finland) and subsequently stepwise forwarded through the nucleus. Activity of RC neurons was recorded (BA-03X, npi electronic GmbH, Tamm, Germany; DAM80, WPI, Sarasota Florida, USA) and digitized (NI USB-6211, National Instruments, Austin Texas, USA) with a sampling rate of 20 kHz using a custom built Matlab-script (Matlab2014a, The MathWorks Inc., Natick Massachusetts, USA). To reduce low-frequency noise introduced by the

x-y-plotter and high frequency interference, data was band-pass filtered with lower and upper cutoff frequencies of 300 Hz and 13 kHz, respectively.

For each neuron, the mean spike count and inversed interspike interval (i.e. instantaneous frequency) during emitter-based IR object motion plus 300 ms post-motion activity were used to calculate signed directionality indices ( $SC_{SDI}$  and  $IF_{SDI}$ , respectively) (Wagner et al., 1994). 300 ms post-motion activity was included to account for differences in strength and onset of secondary inhibitory response components.  $SC_{SDI}$  and  $IF_{SDI}$  were defined hereby as:

$$(1) \quad SC_{SDI} = \begin{cases} 100 * \left(1 - \frac{SC_{n-t}}{SC_{t-n}}\right) & \text{for } SC_{n-t} < SC_{t-n} \\ 100 * \left(\frac{SC_{t-n}}{SC_{n-t}} - 1\right) & \text{for } SC_{n-t} > SC_{t-n} \end{cases}$$

$$(2) \quad IF_{SDI} = \begin{cases} 100 * \left(1 - \frac{IF_{n-t}}{IF_{t-n}}\right) & \text{for } IF_{n-t} < IF_{t-n} \\ 100 * \left(\frac{IF_{t-n}}{IF_{n-t}} - 1\right) & \text{for } IF_{n-t} > IF_{t-n} \end{cases}$$

with  $SC_{n-t}$  and  $IF_{n-t}$  as the mean spike count and instantaneous frequency towards emitter movement in n-t direction and  $SC_{t-n}$  and  $IF_{t-n}$  as the mean spike count and instantaneous frequency towards emitter movement in t-n direction, respectively.  $SC_{SDI}$  values thus indicate the relative difference in discharge rate (i.e. total spikes) for opposite emitter movement directions, while  $IF_{SDI}$  values display relative differences in the instantaneous frequency (i.e. temporal distribution or intensity profile of spike discharge). SDI values can range from -100 to 100 with values of -100 and 100 indicating that a neuron only responded to n-t or t-n movements, respectively. A SDI of 0 indicates no difference in SC or IF for opposite stimulus movement directions.

### *Statistics*

Differences in spike count and mean interspike intervals for opposite stimulus motion directions were checked for significance using the Wilcoxon signed-rank test over all applied stimulus repetitions of a recording. For the purpose of illustration, mean interspike intervals are displayed as their inversed value, i.e. “instantaneous frequency” (1/mean interspike interval). Calculations were performed using a commercial software package (Matlab, R2014b, The MathWorks Inc., Natick Massachusetts, USA).

## Results

### *Background activity and response characteristics of RC neurons towards a moving IR emitter*

In this study, a total of 152 recordings were obtained from 38 RC neurons which were stable enough to perform stimulus presentation with varying velocities. Ten neurons only showed activity upon stimulus presentation, while the other 28 neurons also exhibited background activity in absence of an IR stimulus (e.g. Fig. 1c-f). However, this activity was rather variable. It consisted of bursts of two or three spikes that occurred in irregular sequences (Fig. 1c,e). The frequency of

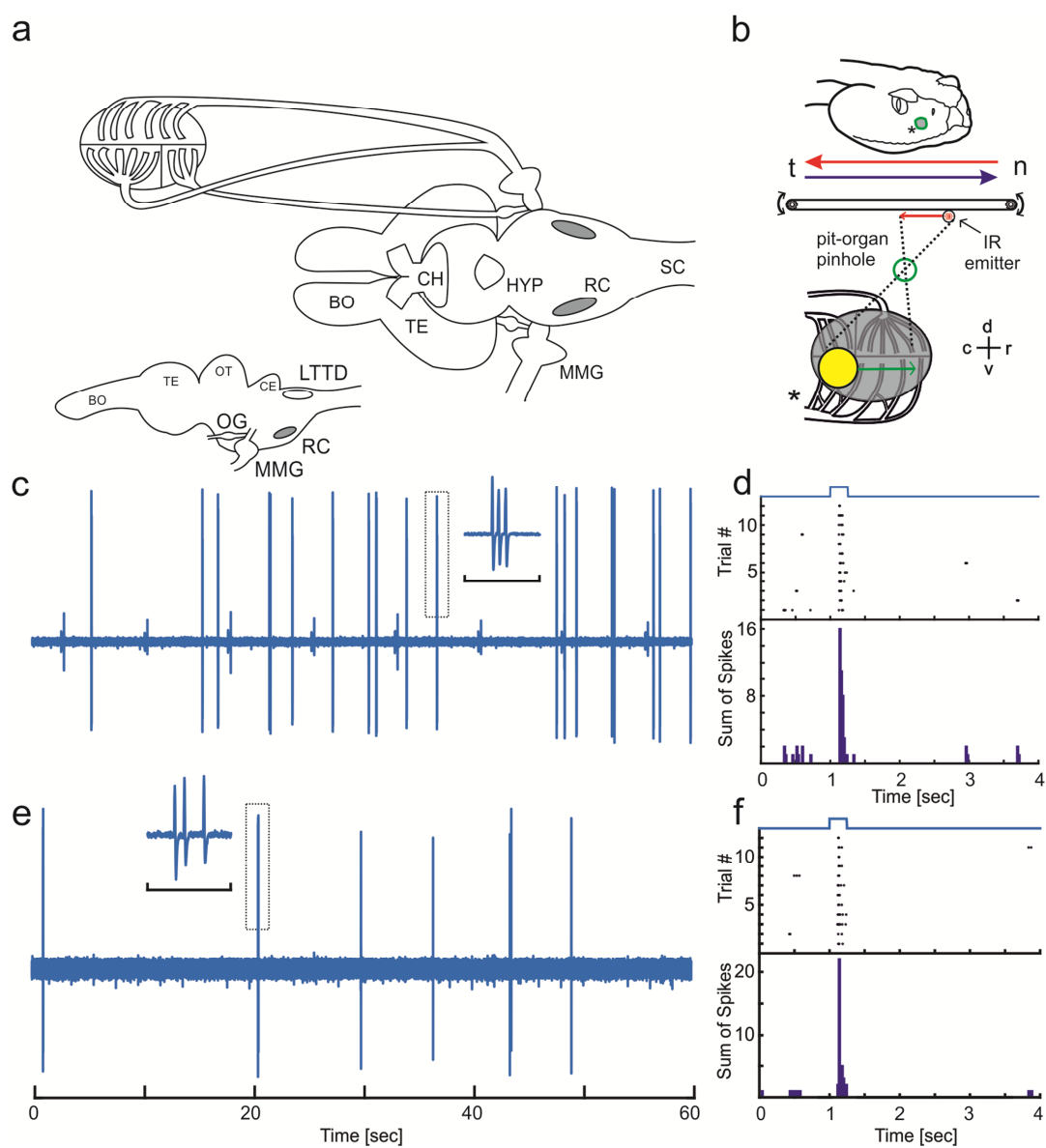


**Fig. 1: Experimental setup and spontaneous activity of RC neurons. (a) Upper scheme: Ventral view of the in vitro preparation as positioned in the recording chamber. The pit organ surrounding the membrane was kept attached to maintain pinhole camera optics (see b). Lower inset: lateral view of the brain. RC highlighted in gray. (b) Schematics depicting the location of the pit organ in the snakes' upper jaw, bi-directional movements of a point-like IR emitter (red and blue arrows), pinhole camera optics of the pit organ (green circle), pit membrane (gray area) and IR stimulus projection onto the membrane (filled yellow circle); note the natural orientation of the stimulated pit in the head before dissection (\* in head and pit membrane schematics). (c-f) Exemplary recordings of spontaneously active neurons in the RC with higher (c) and lower (e) mean background activity and corresponding responses towards IR emitter stimulation (d,f). Note the burst-like nature of spontaneous discharges (insets in c, e; timescale: 100 ms) and the independence of response strength on spontaneous discharge. Abbreviations: BO: olfactory bulb; CE: cerebellum; CH: optic chiasm; HYP: hypophysis; LTTD: nucleus of the lateral descending trigeminal tract; MMG: maxillo-mandibular ganglion; OG: ophthalmic ganglion; OT: optic tectum; RC: nucleus reticularis caloris; SC: spinal cord; TE: telencephalon.**

background activity was no indicator for the strength and stability of a neuron's response to a presented stimulus. Neurons that exhibited no or weak background activity could still be as responsive to stimulus presentation as those with higher background activity (Fig. 1d,f). Despite this, the response magnitude of RC neurons to the stimulus still varied, with some neurons exhibiting stronger responses than others (Fig. 2a,b). To quantify the difference in response characteristics over the applied stimulus velocity range, the mean spike count and instantaneous frequency of individual neurons was calculated over all repetitions of a stimulus presentation (Fig. 2c,e, gray traces). This was done for each velocity used to stimulate a neuron. For each neuron, responses from both stimulus motion directions (i.e. n-t and t-n movement) were pooled and their mean was calculated. To get a better estimation of the velocity dependence of spike count and instantaneous frequency, only those neurons (n=15) were included in the analysis, of which at least one complete recording was obtained from the low (0.04-0.09 m/s), intermediate (0.12-0.17 m/s) and fast (0.2-0.25 m/s) velocity ranges, respectively. The response characteristics of individual neurons over the applied velocity range were consistent, i.e. spike count decreased with increasing stimulus velocities (Fig. 2a<sub>1-3</sub>,b<sub>1-3</sub>,c,d), while the instantaneous frequency increased (Fig. 2e,f). However, while some neurons showed a continuous rise in instantaneous frequency, others reached a peak instantaneous frequency already at intermediate stimulus velocities with a subsequent decrease at faster velocities. To compensate for the variability in base response strength between individual neurons (Fig. 2c,e), the data obtained from each neuron was normalized to its mean spike count and instantaneous frequency, respectively, over all recorded velocities (Fig. 2d,f). The mean instantaneous frequencies of individual neurons over all velocities hereby varied between 15.39 Hz and 72.20 Hz. Spike counts were between 2.89 and 14.70.

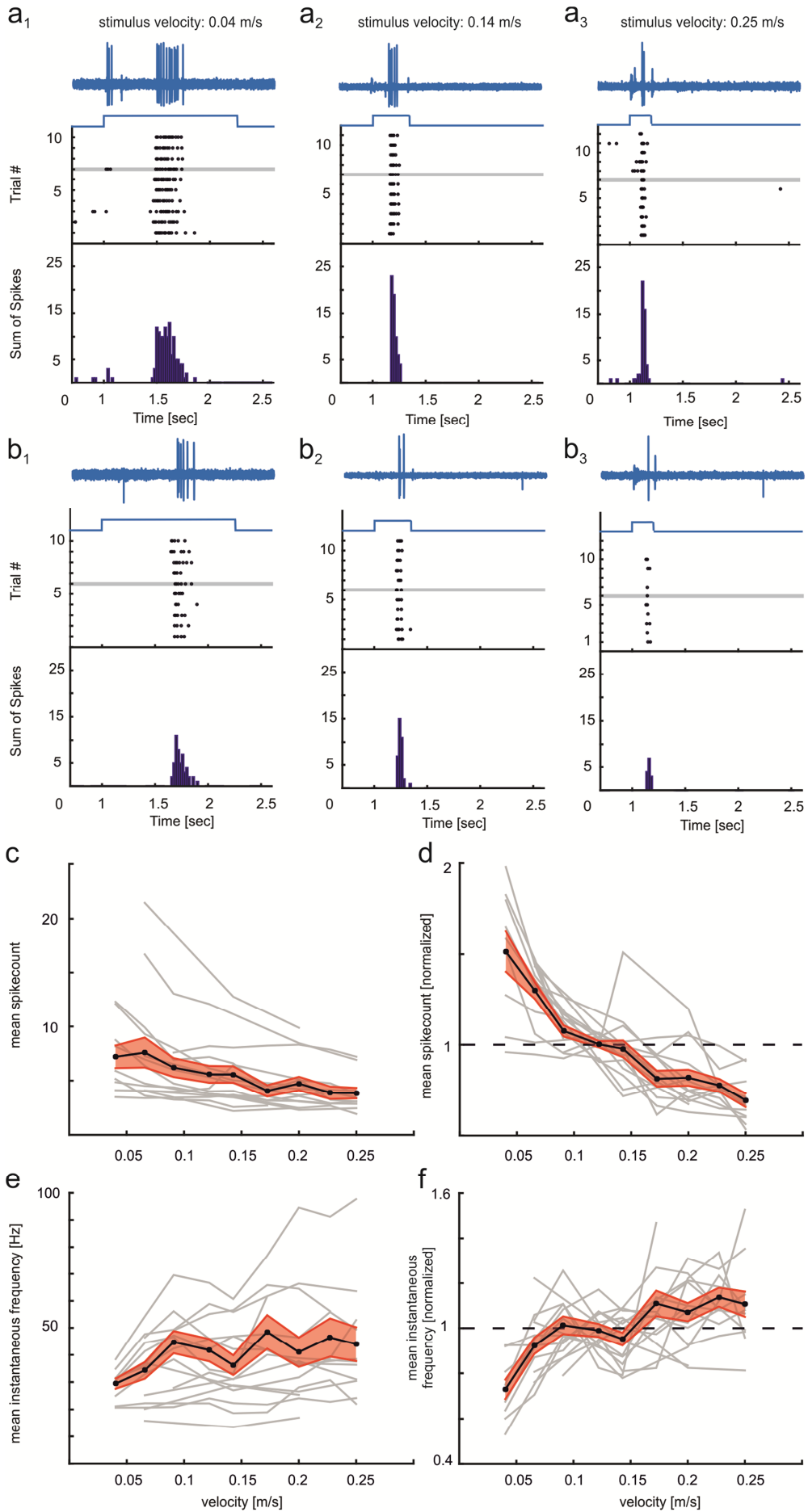


**Fig. 2: Differences in spike count and interspike intervals towards increasing stimulus velocities. The responsiveness towards the moving IR stimulus varied between neurons. (a,b) Exemplary neurons that exhibited strong (a) or weak (b) responses towards the IR stimulus presented at increasing velocities ( $a_1, b_1$ : 0.04 m/s,  $a_2, b_2$ : 0.14 m/s,  $a_3, b_3$ : 0.25 m/s). (c-f) Mean spike counts (c,d) and instantaneous frequencies (e,f) over all stimulus repetitions per stimulus velocity, as measured for individual neurons ( $n=15$ , gray lines). Black curves represent the respective mean of all neurons. Corresponding S.E.M. is indicated by the light red colored area. To account for the differences in base response strength between neurons, data from each neuron was normalized towards the mean spike count (d) or instantaneous frequency (f) over all presented stimulus velocities (i.e. towards the “mean responsiveness” of a neuron in the presented velocity range).**

### *Directional tuning of RC neurons is independent of motion velocity*

To reveal changes in spatiotemporal response characteristics of RC neurons upon different stimulus motion directions and velocities, two signed directionality indices were calculated (see Material and Methods). Classically, SDI values are calculated from the numbers of spikes towards stimuli that are presented with opposite motion direction. However, although spike count did differ for opposite stimulus motion directions in many of the recorded neurons (e.g. Fig. 3a<sub>1,2</sub>), others did not exhibit such differences. Despite this, neurons that did not exhibit differences in spike count for opposite stimulus motion directions often still displayed clear differences in the temporal characteristics of their responses (see exemplary recordings and PSTHs in Fig. 3d<sub>1,2</sub>). Therefore, in addition to the classic SDI based on spike counts (referred to as “SC<sub>SDI</sub>”), we also calculated SDI values based on the mean instantaneous frequency (i.e. inversed mean interspike interval) of neurons towards stimulus presentation with opposite motion direction (referred to as “IF<sub>SDI</sub>”). SC<sub>SDI</sub> was defined as a measure for a neuron’s rate code and thus for its sensitivity towards n-t and t-n stimulus movements. Complementary, IF<sub>SDI</sub> was taken as a measure of the temporal code and therefore reflected differences in signal gain, i.e. the intensity of a signal’s representation in a given RC neuron upon opposite stimulus motion directions. Positive SC/IF<sub>SDI</sub> values indicate higher spike count and instantaneous frequencies towards t-n motion of a stimulus, negative values display tuning towards n-t movement (see material and methods).

In accordance with the RC recordings described in chapter 2, about 30 % of RC neurons again exhibited significant differences in spike counts, i.e. sensitivity (represented in their SC<sub>SDI</sub>), towards bi-directional stimulus motion on the horizontal axis. However, the investigated velocity range in the former study was comparably small. We here tested whether individual neurons were tuned towards certain velocities, when comparing measurements from a broader velocity range between 0.04m/s and 0.25m/s. Therefore, we checked whether their SC<sub>SDI</sub> and IF<sub>SDI</sub> approached a peak value for one particular stimulus velocity. From our recordings we could not find such a trend. Rather, neurons showed varying SDI values that meandered around the respective neuron’s mean SC<sub>SDI</sub> and IF<sub>SDI</sub> over all measured velocities (not shown). However, if neurons showed significant differences in

spike count (represented in  $SC_{SDI}$ ) or instantaneous frequency (represented in  $IF_{SDI}$ ), the sign of the respective SDIs was constant over all velocities for most neurons, indicating a general directional tuning of individual neurons in the RC. Only in two neurons the sign of a significant  $SC_{SDI}$  value changed for one of the measured velocities.

#### *RC neurons exhibit opposite directional tuning with respect to sensitivity and signal gain*

$SC_{SDI}$  and  $IF_{SDI}$  values were quantified by grouping them according to significance and sign (Fig. 3b,c,e,f). SDI values were considered significant if the parameters they were calculated from displayed significant differences for opposite stimulus motion directions over all applied stimulus repetitions (Wilcoxon-signed-rank test,  $p < 0.05$ ). Unfortunately, we were not able to record complete data sets over the whole velocity range (i.e. 9 different stimulus velocities between 0.04 m/s and 0.25 m/s) for every neuron. This was because acquiring a complete velocity profile from a neuron required a long stimulus paradigm, which could not always be obtained due to a loss of recording quality. While the acquired data does indicate that directional sensitivity of RC neurons is independent from stimulus velocity in the applied range, we cannot exclude that some of the recorded neurons might have been tuned to a different movement axis (e.g. vertical movements or departing and approaching stimuli). Since the data did not indicate a velocity dependence of directional tuning for horizontally moving stimuli, data from different stimulus velocities were pooled for the analysis. However, to account for potential differences in the axis of directional tuning, all analyzed neurons were equally weighted by including only data from a velocity range of which complete response profiles were acquired. Thereby, the impact of a neuron that did not show significant tuning towards the presented stimulus was the same as the impact of neurons that did show significant differences. Accordingly, the data set that was used for the analysis included data from 17 neurons, each of which was presented with a stimulus moving on the horizontal axis at three different velocities of 0.14 m/s, 0.2 m/s and 0.25 m/s, which resulted in a total of 51 analyzed recordings.

Data were analyzed both with focus on  $SC_{SDI}$  values (Fig. 3b,c; as measure for sensitivity tuning) and with focus on  $IF_{SDI}$  values (Fig. 3e,f; as measure for gain tuning). First, absolute  $SC_{SDI}$  values of measurements with non-significant and significant differences in spike count for bi-directional stimulus presentation were grouped and their distribution was plotted (Fig. 3b). This allowed for an analysis of the general strength of directional tuning, independent from the preferred direction of stimulus motion. Non-significant  $SC_{SDI}$  values varied between 0 and 21.95 with a median

at 5.98 (Fig. 3b, gray boxplot). Significant  $SC_{SDI}$  values varied between 15.46 and 64.18 with a median at 27.08 (Fig. 3b, green boxplot). On average, as could be expected, measurements with significant differences in spike count for opposite stimulus motion directions displayed much higher  $SC_{SDI}$  values as those with non-significant differences. The distribution differences between both groups were also highly significant (Mann-Whitney-U test,  $p < 0.001$ ). To analyze the directional preferences of neurons towards the presented stimulus,  $SC_{SDI}$  values from all measurements were plotted again, including their sign (Fig. 3c, boxplot). 59 % ( $n=30$ ) of all measurements displayed non-significant  $SC_{SDI}$  values (Fig. 3c, gray markers in boxplot, gray area in pie chart). Despite the distribution of  $SC_{SDI}$  values from all measurements therefore did not display a preferred stimulus motion direction (median  $SC_{SDI}$ : 3.0; min.  $SC_{SDI}$ : -56.25; max.  $SC_{SDI}$ : 64.18), a majority of significant  $SC_{SDI}$  values (41 %,  $n=21$ ; Fig. 3c, colored markers in boxplot; colored areas in pie chart) had a positive sign (29 %,  $n=15$ ; Fig. 3c, colored markers in boxplot's positive area; blue area in pie chart), indicating a higher spike count during stimulus presentation in t-n direction. Only 12 % ( $n=6$ ) of the measurements displayed negative significant  $SC_{SDI}$  values and were therefore tuned towards n-t stimulus movement with respect to spike count (Fig. 3c, colored markers in boxplot's negative area; red area in pie chart). While 14 measurements did only display significant  $SC_{SDI}$  values (Fig. 3c, boxplot, green markers), another seven measurements simultaneously revealed significant differences in the instantaneous frequency and therefore significant  $IF_{SDI}$  values for bi-directional stimulus presentation (Fig. 3c, boxplot, cyan and magenta markers). In five of those the sign of  $SC_{SDI}$  and  $IF_{SDI}$  was reversed (Fig. 3c, boxplot cyan markers), while for the other two it was equal (Fig. 3c, boxplot, magenta markers).

The above explained analysis was repeated with focus on  $IF_{SDI}$  values (Fig. 3e,f). As for  $SC_{SDI}$  values, to display the distribution of significant and non-significant  $IF_{SDI}$  values, their absolute values were grouped and plotted (Fig. 3e: gray: non-significant  $IF_{SDI}$  values, median=11.64, min=0.65, max=46.53; green: significant  $IF_{SDI}$  values, median=43.00, min=7.47, max=67.94, Mann-Whitney-U test,  $p < 0.001$ ). Overall, fewer neurons showed significant differences in instantaneous frequencies towards bi-directional stimulus presentation. Eleven measurements displayed significant differences in instantaneous frequency for opposite stimulus motion directions but no difference in spike count (Fig. 3f, boxplot, green markers). These measurements were again pooled with those that displayed significant differences in both spike count as well as instantaneous frequency with opposite ( $n=5$ , Fig. 3f cyan markers) or equal ( $n=2$ , Fig. 3f, magenta markers) sign of  $IF_{SDI}$  and  $SC_{SDI}$ , respectively. Interestingly, a majority of 25 % of measurements displayed significantly higher gain of neural responses towards n-t moving stimuli ( $n=13$ , Fig. 3f, colored markers in boxplot's negative area, red area in pie chart), compared to only 10 % of measurements with higher gain towards t-n movement of a stimulus ( $n=5$ , Fig. 3f, colored markers in boxplot's positive area, blue area in pie chart).

Therefore, the distribution of positive and negative signs of  $IF_{SDI}$  values was reversed when compared to that of  $SC_{SDI}$  values, i.e. in a majority of measurements, neurons exhibited higher spike counts towards t-n moving stimuli, while higher instantaneous frequencies were obtained from stimulus presentation in n-t direction.

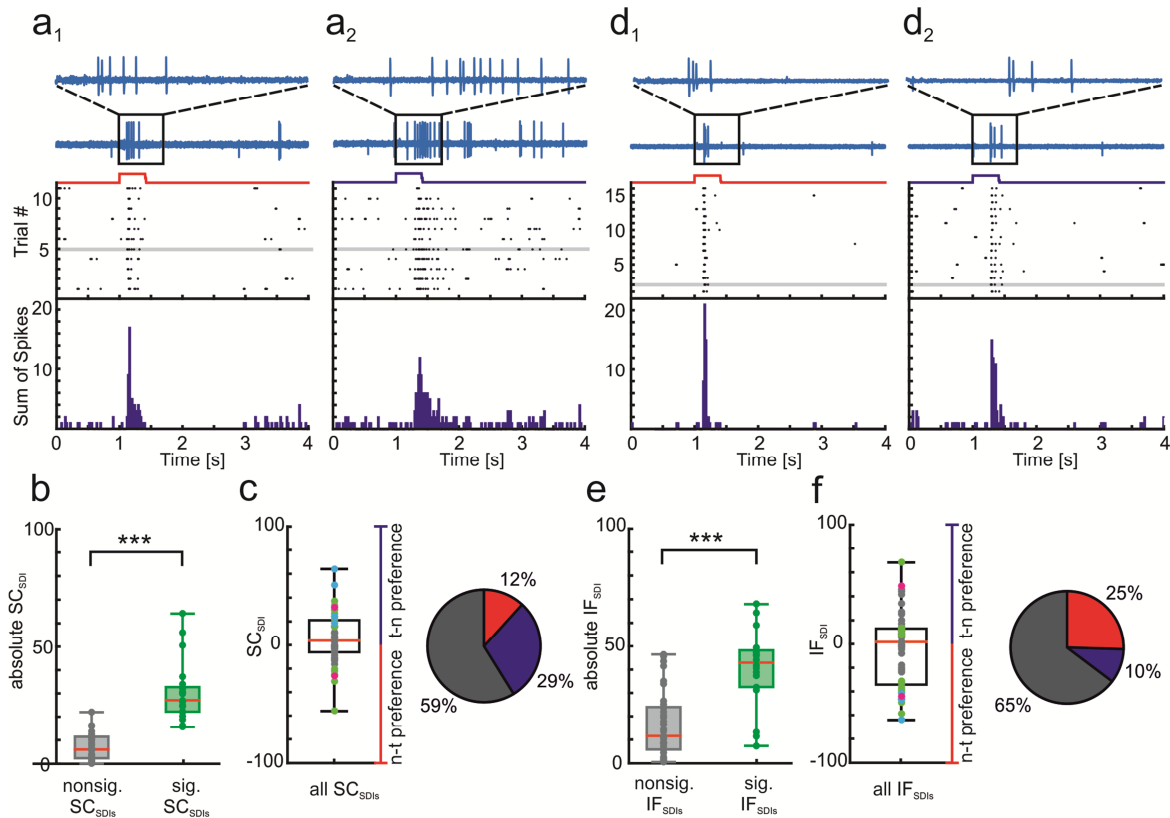


**Fig. 3: Directional tuning of rate code (a-c) and temporal code (d-f) in RC neurons. Exemplary recordings acquired from two different neurons depicting directional tuning towards t-n emitter movement with respect to spike count (a) and towards n-t emitter movement with respect to mean instantaneous frequency (d). Red trace in a<sub>1</sub>, d<sub>1</sub> indicates n-t emitter movement. Blue trace in a<sub>2</sub>, d<sub>2</sub> indicates t-n emitter movement. (b,e) Distribution of absolute mean  $SC_{SDI}$  and  $IF_{SDI}$  values, for measurements that displayed non-significant (gray) and significant (green) differences in spike count (b) and interspike intervals (e), respectively (Mann-Whitney-U test,  $p < 0.001$ ). (c,f) Pooled  $SC_{SDI}$  (c) and  $IF_{SDI}$  (f) values of 51 recordings from 17 RC neurons presented with an emitter stimulus moving at three different velocities on the horizontal axis. Pie charts in (c) and (f) indicate the distribution between negative (red, n-t tuned;  $n=6$  in c;  $n=13$  in f) and positive (blue, t-n tuned;  $n=15$  in c;  $n=5$  in f)  $SC/IF_{SDI}$  values. Gray area of pie chart: Measurements with non-significant differences in  $SC/IF_{SDI}$  for bi-directional stimulus presentation.**

The analysis presented in Fig. 3 shows the influence the LTTD-RC network circuitry has on the processing of moving IR input. However, to put into perspective what the results from individual measurements at different velocities mean on a single neuron level, neurons were categorized according to their directional tuning (Fig. 4). Neurons with no significant differences in spike count or instantaneous frequency for any of the presented stimulus velocities were grouped as type 1, while neurons with significant differences in spike count or instantaneous frequency for at least one of the three presented stimulus velocities were grouped as type 2 neurons. Next, the mean  $SC_{SDI}$  and  $IF_{SDI}$  for each neuron was calculated, with all SDIs (significant and non-significant) of a neuron included.

Differences between absolute values of mean  $SC_{SDI}$  of type1 and type 2 neurons were highly significant (Fig. 4a; Mann-Whitney-U-Test,  $p < 0.001$ ). Of 17 neurons 41 % ( $n=7$ , Fig. 4b gray area) showed no  $SC_{SDI}$  tuning towards the horizontal motion axis. 41 % ( $n=7$ , Fig. 4b, blue area) exhibited significant tuning towards t-n motion of the stimulus, while 18 % ( $n=3$ , Fig. 4b, red area) were tuned towards n-t stimulus motion with respect to spike count. Despite showing a wider distribution, absolute values of mean  $IF_{SDI}$  still differed significantly between type 1 and type 2 neurons (Fig. 4c; Mann-Whitney-U-Test,  $p=0.019$ ). While 41 % ( $n=7$ , Fig. 4d gray area) of neurons did again not show any significant tuning towards the horizontal motion axis, 24 % ( $n=4$ , Fig. 4d, blue area) exhibited significantly higher instantaneous frequencies towards t-n stimulus motion, while 35 % ( $n=6$ , Fig. 4d, red area) were tuned towards n-t motion of a stimulus. Therefore, the directional tuning of the temporal code (represented in  $IF_{SDI}$ ) was reversed with respect to the rate code (represented in  $SC_{SDI}$ ). In compliance with the previously described independency of  $SC_{SDI}$  and  $IF_{SDI}$  towards stimulus velocity, these results are due to the SDIs of individual neurons being rather stable within the applied velocity range, meandering around a neuron's respective mean SDI over all velocities. Accordingly, the mean  $SC_{SDI}$  and  $IF_{SDI}$  of type 1 and type 2 neurons also differed significantly (Fig. 4a,c).

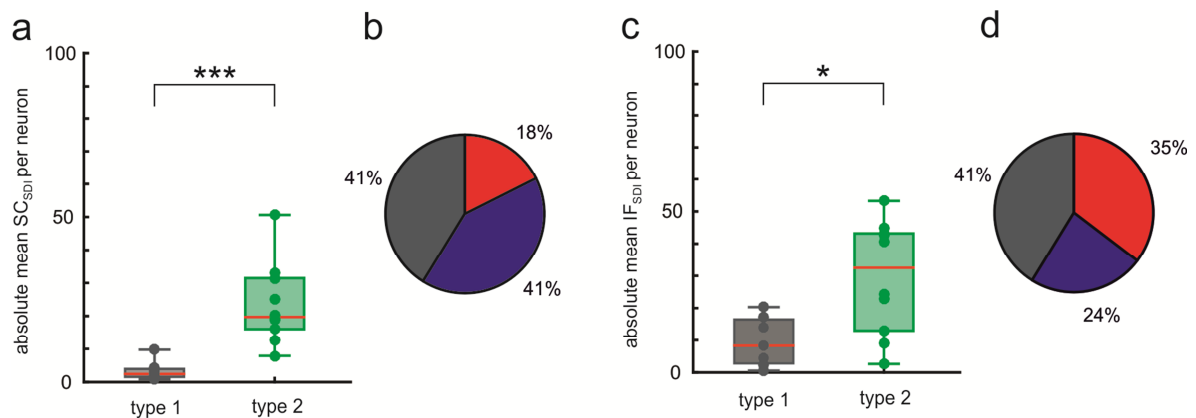


**Fig. 4:** Directional tuning of individual RC neurons with respect to spike count (a,b) and instantaneous frequency (c,d), respectively. (a,c) Comparison of absolute mean  $SC_{SDI}$  (a) and  $IF_{SDI}$  (c) of neurons with no significant differences in spike count and instantaneous frequency within the applied stimulus velocity range (type 1), with the absolute mean  $SC_{SDI}$  and  $IF_{SDI}$  of neurons that displayed significant differences in SC or IF towards at least one stimulus velocity (type 2). (a) Absolute mean  $SC_{SDI}$  of type 1 neurons varied between 0.87 and 9.76 with a median of 2.43, while that of type 2 neurons lay between 7.92 and 50.68 with a median at 19.71.  $SC_{SDI}$  value from both groups differed significantly (Mann-Whitney-U-Test,  $p < 0.001$ ). (b) 41 % of neurons (gray area) did not show significant differences in SC towards opposite motion direction on the horizontal axis. Another 41 % (blue area) were tuned towards t-n movements (positive  $SC_{SDI}$ ), while 18 % (red area) were tuned towards n-t movement (negative  $SC_{SDI}$ ). (c) Absolute mean  $IF_{SDI}$  of type 1 neurons varied between 0.56 and 20.30 with a median of 8.29, while that of type 2 neurons lay between 2.63 and 53.28 with a median at 32.49.  $IF_{SDI}$  from both groups differed significantly (Mann-Whitney-U-Test,  $p=0.019$ ). (d) While 41 % (gray area) of neurons did again not show any significant differences in IF towards opposite stimulus motion on the horizontal axis, 24 % (blue area) were tuned towards t-n movement (positive  $IF_{SDI}$ ) and 35 % (red area) were tuned towards n-t movement (negative  $IF_{SDI}$ ). Note the reversed distribution of  $IF_{SDI}$  values with respect to  $SC_{SDI}$  values.

## Discussion

In rattlesnakes, primary processing of IR sensory trigeminal input takes place in the LTTD (Molenaar, 1974; Schroeder & Loop, 1976; Terashima & Goris, 1977). The nucleus is topographically innervated by the ophthalmic and the deep and superficial maxillary branches of the N.V (Kohl et al., 2014). In the LTTD, spatiotemporal contrast of IR input is enhanced by an interplay of primary excitatory and secondary inhibitory response components (Stanford & Hartline, 1980, 1984) (chapter2). When presented with moving stimuli, the strength of these components varies depending on motion direction. Within the LTTD, this asymmetry in excitation and inhibition only causes weak directional tuning of individual neurons. However, from the LTTD neurons project to the RC where directional tuning of individual neurons has been demonstrated (chapter 2). Stimulus velocity had no influence on the directional tuning of RC neurons in this study. In contrast, when comparing the directional tuning of spike count (as measure of a neuron's sensitivity towards a stimulus, represented in  $SC_{SDI}$ ) and instantaneous frequency (as a measure for stimulus gain within a neuron, represented in  $IF_{SDI}$ ), we found that both parameters displayed maximum strength to opposite stimulus motion directions. A majority of RC neurons with significant  $SC_{SDI}$  were more sensitive towards stimulus motion in t-n direction, while the majority of neurons with significant  $IF_{SDI}$  exhibited higher instantaneous frequencies towards n-t stimulus motion.

### *Background activity and response characteristics of RC neurons towards moving IR stimuli*

In contrast to the LTTD, neurons in the RC do not exhibit regular background activity (Fig. 1). In our in vitro preparation, RC background activity rather consisted of sporadic bursts of two to three spikes or was even completely missing. Those neurons with the highest background activity revealed the same basic response components as demonstrated for LTTD neurons, i.e. primary excitation followed by secondary inhibition (e.g. Fig. 3a). However, the variability in the strength of both components was higher in the RC. While we cannot exclude inhibition from an RC intrinsic circuitry, it seems more likely that this finding is due to an integration of LTTD responses. Accordingly, decreased background activity of LTTD neurons would result in a temporally defined decrease of LTTD input to the RC, thereby reducing the spike probability of RC neurons. However, stable responses were recorded towards IR emitter stimulation of the pit organ independent from the background activity level in RC neurons. This indicates a functional role of the RC as filter for thermal background fluctuations and peripheral neural noise as well as further reinforcement of thermal contrast coding in this nucleus as already described for the LTTD. The range of mean instantaneous

frequencies and spike counts was rather broad. This might be due to the experimental setup and standard stimulus used in this study. We only presented the stimulus in t-n and n-t motion direction and some neurons might rather be tuned towards ventro-dorsal (v-d) or dorso-ventral (d-v) moving stimuli. Also, the RC neuron populations' broad dynamic range might facilitate the processing of variable thermal cues from different behavioral contexts rattlesnakes are confronted with in their natural habitat (e.g. thermoregulation vs. prey strikes). While the mean spike count towards a moving stimulus decreased with increasing stimulus velocity, the mean instantaneous frequency increased. This is probably due to the physics of the applied emitter stimulus. Unlike a laser stimulus, the cone of radiance emitted from our IR source leads to a distinct intensity distribution. The radiant exitance of our emitter at 0° polar angle in a distance of 2 cm from the pit organ is specified with 94 mW/cm<sup>2</sup>. Radiant exitance decreases with increasing polar angle. At a polar angle of +/-20°, radiant exitance drops to 43 mW/cm<sup>2</sup>. IR sensitive trigeminal afferents are highly sensitive to thermal contrast at the pit membrane and have been shown to encode temperature differences as small as 0.003 °C (Bullock & Diecke, 1956). Thermal contrast, i.e. the change of heat flux over a receptive area, is hereby coded in the firing frequency of primary afferent fibers (de Cock Buning et al., 1981; Goris & Nomoto, 1967), which subsequently determines response characteristics of neurons in the LTTD (Stanford & Hartline, 1980, 1984) and RC. Although we cannot reconstruct the exact thermal profile our emitter superimposed on the pit membrane through the point-spread-function (psf) of the pit organ pinhole, it is still reasonable that the observed effects can be explained through the transient character in which different zones of the emitter's temperature profile temporally impact the pit membrane upon varying stimulus velocities. At slow velocities, the heat intensity profile of the emitter will also pass the receptive area of a recorded RC neuron slower, i.e. the change in heat flux over the membrane per time is lower as for faster emitter velocities. Therefore, although the overall time during which the emitter imposes changes in heat flux over the receptive area is higher for slower velocities (eliciting more spikes in total over a longer period of time), the peak change in heat flux will be higher for faster moving stimuli (inducing higher instantaneous frequencies), due to the faster transition of the emitter's intensity profile. Depending on stimulus intensity, the peak it can induce in heat flux should be reached at variable velocities. Accordingly, the trend of increasing instantaneous frequency with increasing velocity should be reversed at the point where peak intensity of the emitter's radiance profile impacts the membrane too shortly to induce sufficient temperature changes. This is supported by our data that shows a decreased slope of mean instantaneous frequencies in the second half of the presented stimulus velocity range (Fig. 2d). However, while some neurons already exhibited a decrease of instantaneous frequencies towards the highest stimulus velocity we applied, others had not reached peak

frequency, complying with variable sensitivities of individual RC neurons towards IR input. In addition to the described physical effects, the interplay of excitatory and inhibitory response components in the LTTD (chapter 2) will further influence RC activity. Given the high level of integration of information already present in primary afferents and the LTTD, respectively, a detailed study of global RC activity by means of multi-electrode arrays might be beneficial to decipher coding of specific parameters from stimuli of varying intensity and speed.

#### *Opposite directional tuning of RC response characteristics with respect to sensitivity and signal gain*

Directional sensitivity based on asymmetric inhibition from spatially adjacent receptive areas as demonstrated in the LTTD is reminiscent of directional processing in the retina (Barlow & Levick, 1965). Here, we checked whether further similarities between processing of IR information in the brainstem of rattlesnakes and visual processing in the retina exist. A moving IR stimulus was therefore applied with varying velocities to the pit organ attached in vitro preparation in n-t and t-n direction, respectively. We could however not find a velocity tuning of the directional sensitivity of RC neurons. While  $SC_{SDI}$  and  $IF_{SDI}$  values of individual neurons did vary, they did not exhibit clear peaks towards particular velocities. Rather, the general directional tuning of RC neurons was constant over all tested velocities and all significant  $SC_{SDI}$  and  $IF_{SDI}$  values generally kept the same sign in individual neurons with only very few exceptions.

While we could not find a velocity tuning of individual RC neuron's  $SC_{SDI}$  or  $IF_{SDI}$ , both parameters revealed opposite directional tuning with respect to sensitivity and signal gain (i.e. rate code and temporal code). While the majority of neurons with significant differences in spike count for opposite stimulus motion directions was tuned towards t-n moving stimuli, neurons with significant differences in instantaneous frequencies achieved higher signal gain from stimuli moving in n-t direction. This is in compliance with effects implemented from both the pinhole camera optics of the IR sensory periphery (Bakken & Krochmal, 2007; Kohl et al., 2012), as well as spatially asymmetric interplay of excitatory and inhibitory response components in the LTTD (chapter 2). The presented data might impose interesting consequences for signal processing in its ecologically relevant context. Many rattlesnakes are ambush predators. Typically, they wait for prey animals that pass by to immediately strike towards them as soon as they are in striking range. According to the presented results here, the thermal profile of a potential prey entering a rattlesnake's receptive field from the side, i.e. in t-n direction, could be recognized with higher sensitivity. The higher spike count that is elicited in the RC during stimulus motion in t-n direction might serve as a priming mechanism

and raise general attention towards the respective area in the tectal IR map. This might be based on altering the internal background or resting state of the tectal IR circuitry through higher yet temporally wider distributed quantized emitter release caused by the population of RC neurons that is  $SC_{SDI}$  tuned towards t-n stimulus motion. After detection of the prey and potential alignment of the head (Kardong & Bels, 1998), a subsequent strike could benefit from higher signal gain towards a departing, i.e. n-t moving, stimulus. The higher instantaneous frequencies cause a more pronounced and, due to stronger secondary inhibition, temporally more defined representation of the stimulus in individual RC neurons, which eventually project to and probably converge on the tectal IR map. In compliance with the phasic character of LTTD, RC and tectal (Kaldenbach et al., 2016) responses towards IR stimuli, this might play a role in edge-detection and tracking of the IR profiles of moving prey animals. During hunting, elicitation of successful strikes is a time-critical process. This is especially true since rattlesnakes do not actively chase their prey but rely on successful envenomation upon the first strike. It is therefore reasonable to assume that once a snake displays predatory behavior, triggering the stereotype strike pattern does not involve complex higher order “decision-making” but is rather reflexive behavior elicited within the midbrain sensorimotor circuitry. It has previously been described in toads and frogs that basic behavioral patterns like approach/avoidance or snap/orientation and the choice between such patterns are directly controlled from within the tectal sensorimotor circuitry (Didday, 1976; Ewert, 1967; Ingle, 1970). Similarly reflexive mechanisms in rattlesnakes might ultimately rely on the higher signal gain towards n-t moving stimuli which could help to reach threshold excitation for strike elicitation and the higher sensitivity towards t-n moving stimuli that might trigger orientation towards a stimulus. An edge detection mechanism by transient excitatory representation of IR stimuli entering a particular receptive field is also supported by the tendency of rattlesnakes to aim their strikes to the anterior region of a prey animal (Kardong & Bels, 1998; Kardong & MacKessy, 1991). This behavior has even been reported in a congenitally blind snake, which needed to rely on IR cues only for strike preparation (Kardong & MacKessy, 1991). However, using mechanisms for edge detection and -tracking as described above, such behavioral capabilities could be explained. While both effects, i.e. higher overall spike count towards t-n moving stimuli and higher signal gain towards n-t moving stimuli, are surely noise-flawed when observed within individual neurons, convergence of multiple similarly tuned neurons, for example in the OT, would likely emphasize their relevance. To decipher the implications of the here reported response properties of single RC neurons and their eventual converged influence on spatiotemporal processing within the tectal IR map, future approaches should investigate global RC and OT activity towards IR stimuli by means of multi electrode recordings in both areas of the brain.

## References:

- Bakken, G. S., & Krochmal, A. R. (2007). The imaging properties and sensitivity of the facial pits of pitvipers as determined by optical and heat-transfer analysis. *Journal of Experimental Biology*, 210(Pt 16), 2801–2810.
- Barlow, H. B., & Levick, W. R. (1965). The mechanism of directionally selective units in rabbit's retina. *Journal of Physiology*, 178, 477–504.
- Bullock, T. H., & Diecke, F. P. (1956). Properties of an infra-red receptor. *Journal of Physiology*, 134(1), 47–87.
- Bullock, T. H., & Fox, W. (1957). The anatomy of the infra-red sense organ in the facial pit of pit vipers. *Journal of Microscopical Science*, 98, 219–234.
- de Cock Buning, T., Terashima, S. I., & Goris, R. C. (1981). Crotaline pit organs analyzed as warm receptors. *Cellular and Molecular Neurobiology*, 1(1), 69–85.
- Didday, L. (1976). A Model of Visuomotor in the Frog Optic Tectum Mechanisms. *Mathematical Biosciences*, 30, 169–180.
- Ewert, J. (1967). Electric stimulation of the retinal projection field in the midbrain of the terrestrial toad (*Bufo bufo* L.). *Pflügers Archiv*, 295(1), 90–98.
- Goris, R. C., & Nomoto, M. (1967). Infrared reception in oriental crotaline snakes. *Comparative Biochemistry and Physiology*, 23, 879–892.
- Gruberg, E. R., Kicliter, E., Newman, E. A., Kass, L., & Hartline, P. H. (1979). Connections of the Tectum of the Rattlesnake *Crotalus viridis* : An HRP Study. *Journal of Comparative Neurology*, 188, 31–41.
- Hartline, P. H., Kass, L., & Loop, M. S. (1978). Merging of modalities in the optic tectum: infrared and visual integration in rattlesnakes. *Science*, 199(4334), 1225–1229.
- Haverly, J. E., & Kardong, K. V. (1996). Sensory deprivation effects on the predatory behavior of the rattlesnake, *Crotalus viridis*. *Copeia*, (2), 419–428.
- Ingle, D. (1970). Visuomotor Functions of the Frog Optic Tectum. *Brain Behavior and Evolution*, 3, 57–71.
- Kaldenbach, F., Bleckmann, H., & Kohl, T. (2016). Responses of infrared-sensitive tectal units of the pit viper *Crotalus atrox* to moving objects. *Journal of Comparative Physiology A: Neuroethology, Sensory, Neural, and Behavioral Physiology*, 202(6), 389–398.
- Kardong, K. V., & Bels, V. L. (1998). Rattlesnake strike behavior: kinematics. *Journal of Experimental Biology*, 201, 837–850.
- Kardong, K. V., & MacKessy, S. P. (1991). The strike behaviour of a congenitally blind rattlesnake. *Journal of Herpetology*, 25(2), 208–211.
- Kass, L., Loop, M. S., & Hartline, P. H. (1978). Anatomical and physiological localization of visual and infrared cell layers in tectum of pit vipers. *J Comp Neurol*, 182(4 Pt 2), 811–820.
- Kohl, T., Bothe, M. S., Luksch, H., Straka, H., & Westhoff, G. (2014). Organotopic organization of the primary infrared sensitive nucleus (LTTD) in the western diamondback rattlesnake (*Crotalus atrox*). *Journal of Comparative Neurology*, 522(18), 3943–3959.

- Kohl, T., Colayori, S. E., Westhoff, G., Bakken, G. S., & Young, B. A. (2012). Directional sensitivity in the thermal response of the facial pit in western diamondback rattlesnakes (*Crotalus atrox*). *The Journal of Experimental Biology*, *215*(Pt 15), 2630–2636.
- Krochmal, A. R., & Bakken, G. S. (2003). Thermoregulation is the pits: use of thermal radiation for retreat site selection by rattlesnakes. *J Exp Biol*, *206*(Pt 15), 2539–2545.
- Lynn, W. G. (1931). The structure and function of the facial pit of the pit vipers. *The American Journal of Anatomy*, *49*(1), 97–139.
- Molenaar, G. J. (1974). An additional trigeminal system in certain snakes possessing infrared receptors. *Brain Research*, *78*, 340–344.
- Newman, E. A., Gruberg, E. R., & Hartline, P. H. (1980). The infrared trigemino-tectal pathway in the rattlesnake and in the python. *Journal of Comparative Neurology*, *191*(3), 465–477.
- Nowak, L., Bregestovski, P., Ascher, P., Herbet, A., & Prochiantz, A. (1984). Magnesium gates glutamate-activated channels in mouse central neurones. *Nature*, *307*(February), 462–465.
- Otto, J. (1972). Das Grubenorgan, ein biologisches System zur Abbildung von Infrarotstrahlern. *Biological Cybernetics*, *10*(2), 103–106.
- Schroeder, D. M., & Loop, M. S. (1976). Trigeminal projections in snakes possessing infrared sensitivity. *Journal of Comparative Neurology*, *169*(1), 1–11.
- Sichert, A., Friedel, P., & van Hemmen, L. (2006). Snake's perspective on heat: Reconstruction of input using an imperfect detection system. *Physical Review Letters*, *97*(6), 068105.
- Stanford, L. R., & Hartline, P. H. (1980). Spatial sharpening by second-order trigeminal neurons in crotaline infrared system. *Brain Research*, *185*(1), 115–123.
- Stanford, L. R., & Hartline, P. H. (1984). Spatial and temporal integration in primary trigeminal nucleus of rattlesnake infrared system. *Journal of Neurophysiology*, *51*(5), 1077–1090.
- Terashima, S. I., & Goris, R. C. (1977). Infrared bulbar units in crotaline snakes. *Proceedings of the Japan Academy. Ser. B: Physical and Biological Sciences*, *53*(7), 292–296.
- Wagner, H., Trinath, T., & Kautz, D. (1994). Influence of stimulus level on acoustic motion-detection sensitivity in barn owl midbrain neurons. *Journal of Neurophysiology*, *71*(5), 1907–1916.
- Westhoff, G. (2014). Giftschlangen und Krustenechsen. In *Sachkunde Gefährliche Reptilien* (pp. 32–42). VDA/DGHT Sachkunde GbR.

## Discussion

The data presented in this thesis reveals basic principles of IR sensory processing in the rattlesnake brainstem. The results provide insight into the four main questions the experimental design aimed to answer:

1) Is the IR environment topographically represented in the LTTD?

The anatomical study presented in chapter 1 of this thesis (Kohl et al., 2014) reveals a clearly topographic innervation of the LTTD by primary afferent axon terminals from the three main membrane innervating trigeminal nerve branches (N.V1, N.V2d and N.V.2s). Preliminary data from staining of individual sub-branches that innervate the three main areas of the membrane indicate that the principle of organotopic representation of primary input is also held up for these sub areas (see section one of the upcoming discussion).

2) What are the consequences of spatiotemporal sharpening in the LTTD for more complex, i.e. more natural, IR input?

Electrophysiological data presented in chapter 2 shows the spatiotemporal properties of primary excitatory and delayed inhibitory response components in the LTTD. The delayed inhibition could be demonstrated to be of at least disynaptic origin and therefore probably derived from an inhibitory interneuron population. Complete silencing of LTTD neurons after initial excitation provides strong contrast enhancement for IR sensory input. Consequently, the neural activity elicited by a moving IR stimulus that enters a receptive field is silenced quickly, likely implementing edge detection functionality to the LTTD circuitry. Electric and IR stimulation of adjacent membrane areas revealed an asymmetric strength of inhibition that depended on the peripheral stimulation side. Accordingly, a moving IR stimulus provoked varying excitatory-inhibitory response patterns in individual recorded LTTD neurons that depended on the stimulus' motion direction.

- 3) Does lateral inhibition provide a basis for directional sensitivity of LTTD neurons as it is known from the retina?

The stimulation side dependent asymmetric influence of inhibitory response components on LTTD neurons provides a physiological basis for directional sensitivity in the IR processing brainstem circuitry of rattlesnakes. Still, directional sensitivity was rather weak on a single cell level in the LTTD and therefore likely encoded in the population activity of LTTD neurons. Accordingly, the found directional sensitivity of single RC neurons could be attributed to the converged input from multiple LTTD neurons on individual neurons in the RC.

- 4) What is the function of the RC in hindbrain processing of IR input?

Based on the results presented in chapter 3, two basic functions can be attributed to the RC. Given the highly reduced spontaneous activity of RC neurons, as compared to neurons in the LTTD, a lot of peripheral noise, that is probably induced by fluctuations in thermal background as well as neural noise, is effectively filtered out before IR information reaches the optic tectum. In contrast to recordings from LTTD neurons, directional sensitivity could be demonstrated on a single cell level in the RC. This highlights the role of the RC as an integrator of primary processed IR input from the LTTD. Response characteristics of RC neurons, i.e. primary excitation followed by secondary inhibition, resembled those recorded from LTTD neurons. Whether the post-excitatory silence of RC neurons reflects the integration of inhibitory responses in the LTTD or is derived from an additional inhibitory network within the RC is yet unclear. However, the former seems more likely. In addition, an opposite directional tuning of RC neurons, with respect to the rate- and temporal code of their response towards moving IR stimuli, was demonstrated. As already discussed, this implies interesting consequences for the role of the IR processing brainstem circuitry in its ecologically relevant context (e.g. ambush hunting and strike behavior). Altogether, the RC data presented in this thesis demonstrate the functional role of the RC in hindbrain sensory processing of IR input for the first time and refutes the hypothesis of the RC functioning as a simple relay to convey IR input from the hindbrain to the OT.

In summary, the results presented in this thesis demonstrate the importance of “pre-tectal” processing in the IR recipient brainstem circuitry for the extraction of spatiotemporal properties of

IR input. The organotopic representation of IR input, together with strong secondary, spatiotemporally variable inhibition, provide the anatomical and physiological basis for a potent, event-based edge detection mechanism in the LTTD-RC brainstem circuitry. Such a mechanism is highly beneficial to precisely localize and attack moving prey. While some of the presented results indeed resemble functional principles that have classically been attributed to retinal processing, such parallels cannot be drawn generally. Rather, a discussion of the findings within the context of other somatosensory specialists will be provided in the last section of the upcoming segment.

*Anatomy and electrophysiology of the crotaline IR processing brainstem circuitry provide a neuronal basis for event-based edge detection and -tracking*

The experimental evidence provided during the course of the presented thesis demonstrates the anatomical basis of early IR sensory processing in the LTTD and its functional implications on processing of IR-input in the LTTD-RC brainstem circuitry.

Whole-nerve staining of trigeminal nerve branches N.V1, N.V2d and N.V2s that innervate the pit membrane revealed a topographic representation of the three principle membrane areas (i.e. ventral, dorso-rostral, dorso-caudal) within the LTTD. Such a topographic innervation pattern complies with a representation of distinct divisions of the IR sensory environment within particular subunits of the LTTD. This could subsequently also be verified by means of field-potential recordings (chapter 2). The data presented in the manuscript in chapter 1 only demonstrated such a topographic representation of input from the three main membrane innervating trigeminal branches. Multi-color fluorescent dye application to adjacent sub-branches of N.V2s proximal to the pit membrane did unfortunately not result in staining of primary axon terminals in the LTTD. However, previous publications have demonstrated a wide spread of individual primary afferent axons and axon terminals through the LTTD (Terashima & Liang, 1991). This raised the question whether IR space is only roughly divided in three main compartments in the LTTD

or whether the three main divisions can be further sub-divided. To answer this question, additional in vitro neurobiotin tracings (see appendix 1 for material and methods) were applied to decipher the anatomical representation of individual membrane area innervating sub-branches within the three main LTTD input areas. While double color staining was not possible with this approach, axon terminals of single N.V2s sub-branches in the LTTD could be traced (Preliminary data, Fig 1a). Tracings indeed revealed a predominant termination of axons from individual N.V2s sub-branches within distinct areas of the N.V2s main LTTD compartment. However, less dense termination patterns were also seen in areas surrounding the main innervation side. In combination with the

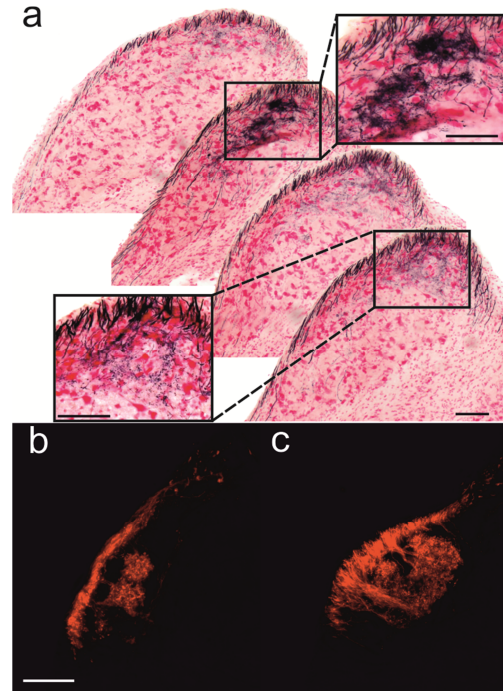


**Fig. 1: Transversal sections through the LTTD after staining of single N.V2s sub-branches with biocytin proximal to the pit membrane (a) or pressure injection of fluorescence-tagged dextran into the lttD (b,c). (a) Series of 4 adjacent sections (thickness 40  $\mu\text{m}$ ) after biocytin stain. Note the major termination side which only extends over one slice. Adjacent areas only show pale termination patterns. (b,c) LTTD after local pressure injection of fluorescence-tagged dextran into the lttD. Fibers run over the LTTD dorsally before they turn medial to terminate locally in the LTTD. Scale bars: (a) 100  $\mu\text{m}$ ; (b): 250  $\mu\text{m}$ . Scale bar in (b) also applies to (c).**

mentioned study of Terashima and Liang (1991), which provided insight to primary termination patterns through intracellular fillings of single afferents, these results demonstrate a mix of concurrent divergence and convergence of individual primary fibers onto multiple functional units of the LTTD. In addition, dextran coupled fluorescent dyes were locally injected into the superficially running lttD, which is constituted of primary afferent axons running towards the hindbrain. Such tracer application also revealed bundles of primary afferent fibers that ran into the LTTD and gave rise to spatially confined termination fields (Preliminary data, Fig. 1b,c). Consequently, IR sensory input is anatomically not only divided into three main compartments but further sub-divisions are formed by fibers from individual membrane innervating nerve branches. While it is likely that adjacent membrane areas are hereby also represented in neighboring LTTD compartments, further staining of single N.V1, N.V2d and N.V2s sub-branches are needed to provide definitive proof.

The detailed spatiotopic representation of membrane sub-divisions within the LTTD supports the idea of LTTD response components being composed of a mixture of sensitivity differences applied to TNMs by the pit organ point spread function and an asymmetric strength of primary excitatory and secondary inhibitory response components emerging from within the LTTD circuitry (chapter 2). To get further insight into the interplay of primary afferent termination fields and the intrinsic inhibitory LTTD network, further anatomical studies that quantify the density-distribution of primary termination patterns outside their respective main area of innervation would be highly interesting. This could answer the question whether the stimulus direction dependent asymmetric ratio of excitatory and inhibitory response components is mainly caused by an asymmetry in the primary innervation patterns that activate the secondary inhibitory network or whether the asymmetry is derived from the connectivity strength within the inhibitory LTTD circuitry. Such an anatomical approach should consequently be accompanied by further electrophysiological experiments that make use of multi-electrode recordings to decipher global LTTD activity towards moving stimuli. While the strong spatiotemporal contrast enhancement in single LTTD-neurons emphasizes a general edge-detection mechanism, multi-electrode recordings would help to examine the suggested edge-tracking functionality of the LTTD and/or RC neuron population. With respect to RC functionality, further studies on its anatomy and electrophysiological properties seem useful. A first step would certainly be to analyze to what extent the LTTD topography of sensory input is maintained in the RC. Further, it would be interesting to know whether its activity purely arises from converged LTTD input that is filtered by high input resistances of RC neurons. The spontaneous activity of RC neurons which is reduced and rather bursty, as compared to the more regular LTTD background activity, gives a first hint towards such a mechanism. Intracellular recordings in the RC could provide proof for this assumption. Still, although it seems rather unlikely, it should also be

checked whether a more complex intrinsic network, maybe comprised of excitatory and inhibitory components, contributes to RC functionality. Again, multi-electrode recordings from the RC neuron population would be of high interest to proof the suggested edge detection and -tracking functionality. Ultimately, such recordings would reveal the consequences of the demonstrated opposite directional tuning of rate- and temporal code in individual RC neurons for overall RC activity towards t-n and n-t moving stimuli, respectively. Finally, behavioral studies on snakes only provided with IR sensory cues should be designed to clarify to what extent the suggested functionality is represented in prey detection and strike performance of hunting snakes.

#### *Rate coding and temporal coding of sensory inputs*

It has classically been assumed that the characteristics of sensory stimuli are encoded in the firing rate of sensory neurons, i.e. in the number of spikes elicited within a defined integration window. While such rate coding is certainly an important factor in the neural representation of the sensory environment, it is unlikely to be the only measure for the vertebrate central nervous system (CNS) to encode sensory stimuli (Ferster & Spruston, 1995; Panzeri et al., 2010; Stevens & Zador, 1995) and is rather combined with additional features of spike patterns elicited by sensory input. A second important concept in this respect is temporal encoding of sensory information. Here, not only the spike count is expected to carry information that can be integrated in higher order sensory circuits, but also the distribution of spikes, i.e. the interspike intervals (ISI), within an integration window (Theunissen & Miller, 1995). A third concept that is often also referred to as temporal code is the latency code. Here, stimulus characteristics are encoded within the latency with which different sets of neurons respond to sensory inputs. Such “first-spike latencies” seem to carry information in cortical processing of auditory (Middlebrooks et al., 1998) and somatosensory (Panzeri et al., 2001) input locations. However, other concepts can as well be summarized under “temporal coding” which serve a variety of functions in sensory signal processing in the CNS, such as phase locking of spike events in the representation of amplitude modulations in the auditory cortex (Middlebrooks, 2008) or coding of interaural time differences (ITDs), which together with interaural level disparities (ILDs) allow spatial discrimination in the auditory brainstem of birds (Yang et al., 1999; Yin, 2002). Temporal codes have also been demonstrated to potentially provide potent mechanisms for sparse and precise spatiotemporal discrimination of visual inputs (van Rullen & Thorpe, 2001).

The data presented in chapter 3 of this thesis is a good example of how multiple aspects of transient spike patterns, in this case the rate of spike occurrence on the one side and their temporal distribution on the other, might emphasize different aspects of sensory input within a single neural circuit. However, in how far rate code and temporal code of the RC neural ensemble influence the higher order representations of IR stimuli, for example in the optic tectum, needs to be further investigated. Intracellular recordings for an evaluation of properties such as input resistances and membrane time constants of IR recipient neurons in the OT might be a first step towards a deeper understanding of how the IR sensory brainstem output described here influences the activity of tectal IR recipient neurons and how it is eventually integrated in the midbrain IR map.

#### *The ecological relevance of the trigeminal system in somatosensory specialists*

In addition to its function in proprioception and motor control of certain parts of the facial musculature, the trigeminal system plays a key role in the topographic processing of somatosensory stimuli received by the vertebrate head. It is involved in the processing of sensory stimuli such as pain, touch and temperature (Saper, 2000). When compared to the visual, auditory, vestibular or olfactory system, which are clearly specialized on the processing of single-modality sensory inputs, the trigeminal system with its rather broad tuning to a variety of modalities could be seen as the somatosensory “generalist” among vertebrate sensory systems. However, despite the wide bandwidth of input modalities, a key feature of trigeminal processing seems to be the high spatial precision in the somatotopic representation of sensory input (DaSilva et al., 2002; Erzurumlu et al., 2010). This becomes especially apparent when one looks at the variety of somatosensory specialists that have evolved among different lineages of vertebrates and that make use of the spatiotemporal information their trigeminal system provides them with. One of the most prominent examples are the vibrissae of rats which are somatotopically represented in so-called barrelettes already in the trigeminal brainstem nuclei (Albert & Göpfert, 2013; Arvidsson, 1982; Belford & Killackey, 1979; Erzurumlu et al., 2010). By using their vibrissae, rats gather precise information about the shape and surface structure of surrounding objects and are able to discriminate minute differences in both parameters (Carvell & Simons, 1990; Diamond et al., 2008; Krupa et al., 2001). However, the ability for such discrimination has been demonstrated to be directly correlated with the number of available vibrissae which are arranged in a specific spatial order on their snout (Diamond et al., 2008; Krupa et al., 2001). It is interesting to note that, while vibrissae of the rat are represented in the “grid-like” arrangement of barrelettes in the hindbrain, another somatosensory specialist, the star-nosed mole (*Condylura cristata*), shows an equivalent star arrangement of functional units in the

spinal trigeminal hindbrain nuclei that represent distinct arms of its sensory organ (Sawyer et al., 2014). The vibrissae of rats and star arms of star-nosed moles are predominantly used to gather tactile information through direct contact with the probed surroundings. Nonetheless, in the right environment, tactile information detected through vibrissae can also be used to receive information about more distant objects. It has been demonstrated that harbour seals (*Phoca vitulina*) use their vibrissae not only for direct object size discrimination (Grant et al., 2013) but to sense flow- and pressure gradients in water and hereby are able to detect and trail flow patterns elicited by potential prey up to half a minute ago (Dehnhardt et al., 1998, 2001; Wieskotten et al., 2010). The capability to precisely follow such flow patterns again emphasizes the necessity of a detailed spatial representation of the underlying tactile input. Among reptiles, another somatosensory specialist makes use of tactile information from a trigeminal-innervated sensory organ – the tentacle snake (*Erpeton tentaculatus*). Although these snakes rely heavily on visual cues for prey capture, they are still able to catch prey in complete darkness with only mechanical cues available (Catania et al., 2010). While studies on the representation of fibers from the tentacle-innervating trigeminal branches N.V1 and N.V2 in the trigeminal hindbrain nuclei are yet missing, the tentacles have been shown to be topographically represented in the OT (Catania et al., 2010). The previously mentioned animals all make use of trigeminal-innervated mechanosensory appendages. However, specializations have also evolved towards other sensory modalities. The monotremes, whose only extant families are the Tachyglossidae and Ornithorhynchidae, possess electroreceptors at their bills that are innervated by the fifth cranial nerve and highly sensitive towards electric stimuli as small as 20  $\mu\text{V}/\text{cm}$  (Gregory et al., 1987; Manger et al., 1996; Manger & Pettigrew, 1995; Pettigrew, 1999; Scheich et al., 1986). Platypuses (*Ornithorhynchus anatinus*) use their electroreceptors for prey capture and have been demonstrated to show reflex-like, directed orientation towards electric field stimuli in their environment (Manger & Pettigrew, 1995). Electroreceptors are arranged in a stripe-like manner on the bill of the platypus and are topographically represented in S1 (Manger et al., 1996). It is assumed that the spatial precision with which platypuses detect the source of electric fields is due to the decay of such fields over distance. Accordingly, the integration of multiple measurements from electroreceptors positioned at different spatially adjacent stripes on the bill could enable them to estimate source location (Manger et al., 1996). Within the somatosensory cortex, trigeminal electrosensory input is somatotopically represented in the same area as mechanosensory input from the bill (Manger et al., 1996). The platypus trigeminal system therefore underlines the wide applicability of trigeminal spatiotemporal processing mechanisms to topographic sensory input. The main limiting factor for the trigeminal circuitry appears to be the availability of a sensory periphery that delivers a distinct spatiotemporally ordered input. If

trigeminal sensory organs are able to provide such spatiotemporally correlated input patterns, central trigeminal processing principles seem to be rather universal. In this light it is not surprising that within the vertebrate lineage specialized trigeminal innervated sensory organs have evolved for the perception of temperature differences. While the vertebrate sense of temperature is commonly involved in the perception of body- and skin temperature and temperature changes, it is known that species from four subfamilies of vertebrates have evolved specialized sensory organs to detect temperature differences on distant surfaces (Campbell et al., 2002). These subfamilies are the vampire bats (Desmodontinae) from the family of leaf-nosed bats (Phyllostomidae), two subfamilies of boas and pythons (Boidae and Pythonidae) and the subject of this thesis – the pit-vipers (Crotalinae) as subfamily of the vipers (Viperidae). Little is known so far about the anatomy of the IR processing trigeminal tract of vampire bats. However, comparative studies of their trigeminal brainstem nuclei with those of non IR sensing leaf-nosed bats have revealed a unique nucleus in the common vampire bat (*Desmodus rotundus*) which is probably related to IR processing (Kishida et al., 1984). Their IR sense enables vampire bats to sense blood vessels under the skin of their hosts over distances up to 16 cm (Kürten & Schmidt, 1982). Again, the ability to precisely locate such vessels for incision and feeding (Greenhall, 1972; Greenhall et al., 1971) demonstrates the necessity of precise spatial processing of IR input in vampire bats. Analogous to the former mentioned specialized tactile and electric senses, the prerequisite for such a highly performant temperature sense was the evolution of a sensory periphery that provides heat sensitive receptors with a scaffold that allows for the detection of minute changes in the spatial distribution of heat flux. The surface temperature of the nose leaf of vampire bats has been demonstrated to be up to 9° C lower than body temperature (Kürten & Schmidt, 1982). Its exposed position not only provides insulation from the inner body temperature but might also serve as a thermal mass reduced scaffold for the vampire bat thermoreceptors (Kürten et al., 1984; Kürten & Schmidt, 1982). The same is true for the sensory periphery of crotaline snakes. The extremely thin pit membrane minimizes the thermal mass of the TNMs' scaffold and is insulated from surrounding tissue by the inner and outer chamber of the pit organ (see Introduction Fig. 1 d). However, while such thermal mass reduction, although not to the same degree, has been found in the other mentioned species, the pit organ as a whole makes the crotaline IR sensory system unique. This is because the pit organ embeds the IR recipient TNMs in a framework that functionally resembles a simple, yet clearly optic apparatus in form of a pinhole camera. The TNMs of primary trigeminal afferents, or “pixels” of the IR sense, exhibit a distinct spatial distribution on the membrane which has been demonstrated to be topographically represented in the LTTD. Chapter one of this thesis together with preliminary work presented above (Fig. 1) point towards a topographic representation of not only the gross innervation sides (i.e.

dorso-caudal, dorso-rostral and ventral) of the membrane but also of the subareas innervated by distinct ramifications of the three main membrane innervating trigeminal branches, N.V1, N.V2d and N.V2s. The type of primary afferent IR sensory input the crotaline trigeminal circuitry is provided with is therefore in compliance with the formerly described prerequisites for spatiotemporally precise processing of somatotopic input by the vertebrate trigeminal system. However, the modality of IR input (i.e. electromagnetic waves) and the pinhole-camera optics of the sensory periphery provide the LTTD and subsequently the RC of rattlesnakes with a low-resolution, yet image-like representation of the IR sensory environment. Therefore, parts of the trigeminal somatosensory periphery of crotaline snakes evolved into a radiance detector that not only provides information about the spatiotemporal distribution of somatosensory input, but ultimately turns the LTTD-RC brainstem network into a basic, image-processing neural circuitry. While it seems rather unlikely that this circuitry is able to provide a high resolution reconstruction of the blurred primary IR input, the data presented within this thesis make it reasonable to attribute functionality in directionally tuned edge-detection to the IR processing brainstem of rattlesnakes. Such functionality is likely based on the optics of the pit organ itself, the interplay of excitatory and inhibitory response components of the LTTD and the convergence of LTTD output on individual neurons in the RC. Future investigations of the functional implications the directionally tuned RC output (i.e. opposite tuning of rate- and temporal code) has on tectal processing of IR stimuli and the integration of IR- with visual input should give further insight into neural mechanisms that allow the correlation of multimodal input components in the OT. Behavioral studies on blindfolded snakes should complement such electrophysiological approaches for a clarification of their ecological relevance.

## References

- Albert, J. T., & Göpfert, M. C. (2013). Mechanosensation. In G. C. Galizia & P.-M. Lledo (Eds.), *Neurosciences* (2nd editio, pp. 321–335). Springer Spektrum.
- Amemiya, F., Nakano, M., Goris, R. C., Kadota, T., Atobe, Y., Funakoshi, K., ... Kishida, R. (1999). Microvasculature of Crotaline Snake Pit Organs: Possible Function as a Heat Exchange Mechanism, *115*(March 1998), 107–115.
- Amemiya, F., Ushiki, T., Goris, R. C., Atobe, Y., & Kusunoki, T. (1996). Ultrastructure of the crotaline snake infrared pit receptors: SEM confirmation of TEM findings. *The Anatomical Record*, *246*(1), 135–146.
- Arvidsson, J. (1982). Somatotopic organization of vibrissae afferents in the trigeminal sensory nuclei of the rat studied by transganglionic transport of HRP. *Journal of Comparative Neurology*, *211*(1), 84–92.
- Bajer, K., Molnár, O., Török, J., & Herczeg, G. (2010). Female European green lizards (*Lacerta viridis*) prefer males with high ultraviolet throat reflectance. *Behavioral Ecology and Sociobiology*, *64*(12), 2007–2014.
- Bakken, G. S., & Krochmal, A. R. (2007). The imaging properties and sensitivity of the facial pits of pitvipers as determined by optical and heat-transfer analysis. *Journal of Experimental Biology*, *210*(Pt 16), 2801–2810.
- Belford, G. R., & Killackey, H. P. (1979). Vibrissae representation in subcortical trigeminal centers of the neonatal rat. *Journal of Comparative Neurology*, *183*(2), 305–321.
- Berson, D. M., & Hartline, P. H. (1988). A Tecto-Rotundo-Telencephalic Pathway in the Rattlesnake: Evidence for a Forebrain Representation of the Infrared Sense. *The Journal of Neuroscience*, *8*(March), 1074–1088.
- Bowmaker, J. K., & Kunz, Y. W. (1987). Ultraviolet receptors, tetrachromatic colour vision and retinal mosaics in the brown trout (*Salmo trutta*): Age-dependent changes. *Vision Research*, *27*(12), 2101–2108.
- Bullock, T. H., & Diecke, F. P. (1956). Properties of an infra-red receptor. *Journal of Physiology*, *134*(1), 47–87.
- Bullock, T. H., & Fox, W. (1957). The anatomy of the infra-red sense organ in the facial pit of pitvipers. *Journal of Microscopical Science*, *98*, 219–234.
- Campbell, A. L., Naik, R. R., Sowards, L., & Stone, M. O. (2002). Biological infrared imaging and sensing. *Micron*, *33*(2), 211–225.
- Carvell, G. E., & Simons, D. J. (1990). Biometric analyses of vibrissal tactile discrimination in the rat. *The Journal of Neuroscience: The Official Journal of the Society for Neuroscience*, *10*(8), 2638–2648.
- Catania, K. C., Leitch, D. B., & Gauthier, D. (2010). Function of the appendages in tentacled snakes (*Erpeton tentaculatus*). *Journal of Experimental Biology*, *213*(3), 359–367.
- DaSilva, A. F., Becerra, L., Makris, N., Strassman, A. M., Gonzalez, R. G., Geatrakis, N., & Borsook, D. (2002). Somatotopic activation in the human trigeminal pain pathway. *J Neurosci*, *22*(18), 8183–8192.

- de Cock Buning, T., Terashima, S. I., & Goris, R. C. (1981). Crotaline pit organs analyzed as warm receptors. *Cellular and Molecular Neurobiology*, 1(1), 69–85.
- Dehnhardt, G., Mauck, B., & Bleckmann, H. (1998). Seal whiskers detect water movements. *Nature*, 394(July), 235–236.
- Dehnhardt, G., Mauck, B., Hanke, W., & Bleckmann, H. (2001). Hydrodynamic Trail-Following in Harbor Seals (*Phoca vitulina*). *Science*, 293(July), 102–104.
- Desalvo, J. A., & Hartline, P. H. (1978). Spatial properties of primary infrared sensory neurons in Crotalidae. *Brain Research*, 142, 338–342.
- Diamond, M. E., von Heimendahl, M., Knutsen, P. M., Kleinfeld, D., & Ahissar, E. (2008). “Where” and “what” in the whisker sensorimotor system. *Nature Reviews Neuroscience*, 9(8), 601–612.
- Dräger, U., & Hubel, D. H. (1975). Physiology of visual cells in mouse superior colliculus and correlation with somatosensory and auditory input. *Nature*, 253(5488), 203–204.
- Dräger, U., & Hubel, D. H. (1976). Topography of visual and somatosensory projections to mouse superior colliculus. *Journal of Neurophysiology*, 39(1), 91–101.
- Erzurumlu, R. S., Murakami, Y., & Rijli, F. M. (2010). Mapping the face in the somatosensory brainstem. *Nature Reviews Neuroscience*.
- Feldman, D. E., & Knudsen, E. I. (1997). An anatomical basis for visual calibration of the auditory space map in the barn owl’s midbrain. *The Journal of Neuroscience*, 17(17), 6820–6837.
- Ferster, D., & Spruston, N. (1995). Cracking the Neuronal Code. *Science*, 270(5237), 756–757.
- Goris, R. C. (2011). Infrared Organs of Snakes: An Integral Part of Vision. *Journal of Herpetology*, 45(1), 2–14.
- Goris, R. C., Atobe, Y., Nakano, M., Funakoshi, K., & Terada, K. (2007). Blood flow in snake infrared organs: response-induced changes in individual vessels. *Microcirculation*, 14(2), 99–110.
- Goris, R. C., Kadota, T., & Kishida, R. (1989). Innervation of Snake Pit Organ Membranes Mapped by Receptor Terminal Succinate Dehydrogenase Activity. *Current Herpetology in East Asia*, 8–16.
- Goris, R. C., & Nomoto, M. (1967). Infrared reception in oriental crotaline snakes. *Comparative Biochemistry and Physiology*, 23, 879–892.
- Gracheva, E. O., Cordero-Morales, J. F., González-Carcacia, J. A., Ingolia, N. T., Manno, C., Aranguren, C. I., ... Julius, D. (2011). Ganglion-specific splicing of TRPV1 underlies infrared sensation in vampire bats. *Nature*, 476(7358), 88–92.
- Gracheva, E. O., Ingolia, N. T., Kelly, Y. M., Cordero-Morales, J. F., Hollopeter, G., Chesler, A. T., ... Julius, D. (2010). Molecular basis of infrared detection by snakes. *Nature*, 464(7291), 1006–1011.
- Grant, R., Wieskotten, S., Wengst, N., Prescott, T., & Dehnhardt, G. (2013). Vibrissal touch sensing in the harbor seal (*Phoca vitulina*): How do seals judge size? *Journal of Comparative Physiology A: Neuroethology, Sensory, Neural, and Behavioral Physiology*, 199(6), 521–533.
- Greenhall, A. M. (1972). The biting and feeding habits of the Vampire bat, *Desmodus rotundus*. *Journal of Zoology*, 168, 451–461.

- Greenhall, A. M., Schmidt, U., & Lopez-Forment, W. (1971). Attacking behavior of the Vampire Bat, *Desmodus rotundus*, under field conditions in Mexico. *Biotropica*, 3(2), 136–141.
- Gregory, J. E., Iggo, A., McIntyre, A. K., & Proske, U. (1987). Electroteceptors in the bill of the platypus. *Nature*, 326, 386–387.
- Gruberg, E. R., Kicliter, E., Newman, E. A., Kass, L., & Hartline, P. H. (1979). Connections of the Tectum of the Rattlesnake *Crotalus viridis*: An HRP Study. *Journal of Comparative Neurology*, 188, 31–41.
- Hartline, P. H., Kass, L., & Loop, M. S. (1978). Merging of modalities in the optic tectum: infrared and visual integration in rattlesnakes. *Science*, 199(4334), 1225–1229.
- Hinz, M., Klein, A., Schmitz, A., & Schmitz, H. (2018). The impact of infrared radiation in flight control in the Australian “firebeetle” *Merimna atrata*. *PLoS ONE*, 13(2), 1–19.
- Jacobs, G. H. (1996). Primate photopigments and primate color vision. *Proceedings of the National Academy of Sciences of the United States of America*, 93(2), 577–581.
- Kass, L., Loop, M. S., & Hartline, P. H. (1978). Anatomical and physiological localization of visual and infrared cell layers in tectum of pit vipers. *J Comp Neurol*, 182(4 Pt 2), 811–820.
- King, A. J., Hutchings, M. E., Moore, D. R., & Blakemore, C. (1988). Developmental plasticity in the visual and auditory representations in the mammalian superior colliculus. *Nature*.
- Kishida, R., Amemiya, F., Kusunoki, T., & Terashima, S. I. (1980). A new tectal afferent nucleus of the infrared sensory system in the medulla oblongata of crotaline snakes. *Brain Research*, 195(2), 271–279.
- Kishida, R., Goris, R. C., Terashima, S. I., & Dubbeldam, J. L. (1984). A suspected infrared-recipient nucleus in the brainstem of the vampire bat, *Desmodus rotundus*. *Brain Research*, 322, 351–355.
- Knudsen, E. I. (1982). Auditory and Visual Maps of Space in the Optic Tectum of the Owl. *The Journal of Neuroscience*, 2(9), 1177–1194.
- Knudsen, E. I., & Brainard, M. S. (1991). Visual Instruction of the Neural Map of Auditory Space in the Developing Optic Tectum. *Science*, 253(5015), 85–87.
- Kohl, T., Bothe, M. S., Luksch, H., Straka, H., & Westhoff, G. (2014). Organotopic organization of the primary infrared sensitive nucleus (LTTD) in the western diamondback rattlesnake (*Crotalus atrox*). *Journal of Comparative Neurology*, 522(18), 3943–3959.
- Krochmal, A. R., Bakken, G. S., & LaDuc, T. J. (2004). Heat in evolution’s kitchen: evolutionary perspectives on the functions and origin of the facial pit of pitvipers (Viperidae: Crotalinae). *The Journal of Experimental Biology*, 207(Pt 24), 4231–4238.
- Krupa, D. J., Matell, M. S., Brisben, A. J., Oliveira, L. M., & Nicolelis, M. A. (2001). Behavioral properties of the trigeminal somatosensory system in rats performing whisker-dependent tactile discriminations. *The Journal of Neuroscience: The Official Journal of the Society for Neuroscience*, 21(15), 5752–5763.
- Kürten, L., & Schmidt, U. (1982). Thermoperception in the common vampire bat (*Desmodus rotundus*). *Journal of Comparative Physiology* □ A, 146(2), 223–228.

- Kürten, L., Schmidt, U., & Schäfer, K. (1984). Warm and cold receptors in the nose of the vampire bat *Desmodus rotundus*. *Naturwissenschaften*, *71*(6), 327–328.
- Lee, M. S. Y., Hugall, A. F., Lawson, R., & Scanlon, J. D. (2007). Phylogeny of snakes (Serpentes): Combining morphological and molecular data in likelihood, Bayesian and parsimony analyses. *Systematics and Biodiversity*, *5*(4), 371–389.
- Losey, G. S., Cronin, T. W., Goldsmith, T. H., Hyde, D., Marshall, N. J., & McFarland, W. N. (1999). The UV visual world of fishes: A review. *Journal of Fish Biology*, *54*(5), 921–943.
- Lumpkin, E. A., & Caterina, M. J. (2007). Mechanisms of sensory transduction in the skin. *Nature*, *445*(7130), 858–865.
- Lynn, W. G. (1931). The structure and function of the facial pit of the pit vipers. *The American Journal of Anatomy*, *49*(1), 97–139.
- Manger, P. R., Calford, M. B., & Pettigrew, J. D. (1996). Properties of Electrosensory Neurons in the Cortex of the Platypus (*Ornithorhynchus anatinus*): Implications for Processing of Electrosensory Stimuli. *Proceedings of the Royal Society B: Biological Sciences*.
- Manger, P. R., & Pettigrew, J. D. (1995). Electroreception and the Feeding Behaviour of Platypus (*Ornithorhynchus anatinus*: Monotremata: Mammalia). *Philosophical Transactions of the Royal Society B: Biological Sciences*, *347*(1322), 359–381.
- Meszler, R. M. (1983). Fine Structure and Organization of the Infrared Receptor Relays : Lateral Descending Nucleus of V in Boidae and Nucleus Reticularis Caloris in the Rattlesnake. *The Journal Of Comparative Neurology*, *220*, 299–309.
- Meszler, R. M., Auken, C. R., & Carpenter, D. O. (1981). Fine structure and organization of the infrared receptor relay , the lateral descending nucleus of the trigeminal nerve in pit vipers. *Journal of Comparative Neurology*, *196*, 571–584.
- Meszler, R. M., & Webster, D. B. (1968). Histochemistry of the rattlesnake facial pit. *Copeia*, *1968*(4), 722–728.
- Middlebrooks, J. C. (2008). Auditory Cortex Phase Locking to Amplitude-Modulated Cochlear Implant Pulse Trains. *Journal of Neurophysiology*, *100*, 76–91.
- Middlebrooks, J. C., Xu, L., Eddins, A. C., & Green, D. M. (1998). Codes for Sound-Source Location in Nontopographic Auditory Cortex. *Journal of Neurophysiology*, *80*(2), 863–881.
- Moiseenkova, V., Bell, B., Motamedi, M., Wozniak, E., & Christensen, B. (2003). Wide-band spectral tuning of heat receptors in the pit organ of the copperhead snake ( *Crotalinae* ). *American Journal of Physiology, Regulatory, Integrative and Comparative Physiology*, *284*(2), R598–R606.
- Molenaar, G. J. (1992). Anatomy and Physiology of Infrared Sensitivity of Snakes. In C. Gans & P. S. Ulinski (Eds.), *Biology of the Reptilia - Sensorimotor Integration* (pp. 367–453). The University of Chicago Press.
- Newman, E. A., Gruberg, E. R., & Hartline, P. H. (1980). The infrared trigemino-tectal pathway in the rattlesnake and in the python. *Journal of Comparative Neurology*, *191*(3), 465–477.
- Newman, E. A., & Hartline, P. H. (1981). Integration of visual and infrared information in bimodal neurons in the rattlesnake optic tectum. *Science*, *213*(4509), 789–791.

- Noble, G. K., & Schmidt, A. (1937). The structure and function of the facial and labial pits of snakes. *Proceedings of the American Philosophical Society*, 77(3), 263–288.
- Otto, J. (1972). Das Grubenorgan, ein biologisches System zur Abbildung von Infrarotstrahlern. *Biological Cybernetics*, 10(2), 103–106.
- Panzeri, S., Brunel, N., Logothetis, N. K., & Kayser, C. (2010). Sensory neural codes using multiplexed temporal scales. *Trends in Neurosciences*, 33(3), 111–120.
- Panzeri, S., Petersen, R. S., Schultz, S. R., Lebedev, M. A., & Diamond, M. E. (2001). The Role of Spike Timing in the Coding of Stimulus Location in Rat Somatosensory Cortex. *Neuron*, 29, 769–777.
- Pettigrew, J. D. (1999). Electroreception in monotremes. *Journal of Experimental Biology*, 202(Pt 10), 1447–1454.
- Pyron, R. A., Burbrink, F. T., Colli, G. R., de Oca, A. N. M., Vitt, L. J., Kuczynski, C. A., & Wiens, J. J. (2011). The phylogeny of advanced snakes (Colubroidea), with discovery of a new subfamily and comparison of support methods for likelihood trees. *Molecular Phylogenetics and Evolution*, 58(2), 329–342.
- Rajchard, J. (2009). Ultraviolet (UV) light perception by birds: A review. *Veterinarni Medicina*, 54(8), 351–359.
- Saper, C. B. (2000). Brain Stem, Reflexive Behavior, and the Cranial Nerves. In E. R. Kandel, J. H. Schwartz, & T. M. Jessell (Eds.), *Principles of Neural Science* (4th ed., pp. 873–888). McGraw-Hill.
- Sawyer, E. K., Leitch, D. B., & Catania, K. C. (2014). Organization of the spinal trigeminal nucleus in star-nosed moles. *Journal of Comparative Neurology*, 522(14), 3335–3350.
- Scheich, H., Langner, G., Tidemann, C., Coles, R. B., & Guppy, A. (1986). Electroreception and electrolocation in platypus. *Nature*, 319(6052), 401–402.
- Schmitz, A., Gebhardt, M., & Schmitz, H. (2008). Microfluidic photomechanic infrared receptors in a pyrophilous flat bug. *Naturwissenschaften*, 95(5), 455–460.
- Schmitz, H., & Bleckmann, H. (1998). The photomechanic infrared receptor for the detection of forest fires in the beetle *Melanophila acuminata* (Coleoptera: Buprestidae). *Journal of Comparative Physiology - A Sensory, Neural, and Behavioral Physiology*, 182(5), 647–657.
- Schmitz, H., Schmitz, A., & Bleckmann, H. (2000). A new type of infrared organ in the Australian “fire-beetle” *Merimna atrata* (Coleoptera: Buprestidae). *Naturwissenschaften*, 87(12), 542–545.
- Schmitz, H., Schmitz, A., Trenner, S., & Bleckmann, H. (2002). A new type of insect infrared organ of low thermal mass. *Naturwissenschaften*, 89(5), 226–229.
- Sichert, A., Friedel, P., & van Hemmen, L. (2006). Snake’s perspective on heat: Reconstruction of input using an imperfect detection system. *Physical Review Letters*, 97(6), 068105.
- Smith, C. U. M. (2008a). *Biology of Sensory Systems* (2nd edition). John Wiley & Sons Ltd.
- Smith, C. U. M. (2008b). Thermosensitivity. In *Biology of Sensory Systems* (2nd edition, pp. 415–421). John Wiley & Sons Ltd.
- Stanford, L. R., & Hartline, P. H. (1980). Spatial sharpening by second-order trigeminal neurons in crotaline infrared system. *Brain Research*, 185(1), 115–123.

- Stanford, L. R., & Hartline, P. H. (1984). Spatial and temporal integration in primary trigeminal nucleus of rattlesnake infrared system. *Journal of Neurophysiology*, *51*(5), 1077–1090.
- Stevens, C. F., & Zador, A. (1995). Neural Coding: The enigma of the brain. *Current Biology*, *5*(12), 1370–1371.
- Taiz, L., Zeiger, E., Moller, I. M., & Murphy, A. (2014). *Plant Physiology and Development* (6th Editio). Sinauer.
- Terashima, S. I., & Goris, R. C. (1977). Infrared bulbar units in crotaline snakes. *Proceedings of the Japan Academy. Ser. B: Physical and Biological Sciences*, *53*(7), 292–296.
- Terashima, S. I., & Goris, R. C. (1979). Receptive areas of primary infrared afferent neurons in crotaline snakes. *Neuroscience*, *4*(8), 1137–1144.
- Terashima, S. I., Goris, R. C., & Katsuki, Y. (1968). Generator potential of crotaline snake infrared receptor. *Journal of Neurophysiology*, *31*(5), 682–688.
- Terashima, S. I., Goris, R. C., & Katsuki, Y. (1970). Structure of warm fiber terminals in the pit membrane of vipers. *Journal of Ultrastructure Research*, *31*(5–6), 494–506.
- Terashima, S. I., & Liang, Y. F. (1991). Temperature neurons in the crotaline trigeminal ganglia. *Journal of Neurophysiology*, *66*(2), 623–634.
- Theunissen, F., & Miller, J. P. (1995). Temporal encoding in nervous systems: A rigorous definition. *Journal of Computational Neuroscience*, *2*(2), 149–162.
- Triplett, J. W., Phan, A., Yamada, J., & Feldheim, D. A. (2012). Alignment of Multimodal Sensory Input in the Superior Colliculus through a Gradient-Matching Mechanism. *Journal of Neuroscience*, *32*(15), 5264–5271.
- van Dyke, J. U., & Grace, M. S. (2010). The role of thermal contrast in infrared-based defensive targeting by the copperhead, *Agkistrodon contortrix*. *Animal Behaviour*, *79*(5), 993–999.
- van Rullen, R., & Thorpe, S. J. (2001). Rate Coding Versus Temporal Order Coding: What the Retinal Ganglion Cells Tell the Visual Cortex. *Neural Computation*, *12*, 1255–1283.
- von Düring, M. (1974). The radiant heat receptor and other tissue receptors in the scales of the upper jaw of *Boa constrictor*. *Zeitschrift Für Anatomie Und Entwicklungsgeschichte*, *145*(3), 299–319.
- Warren, J. W., & Proske, U. (1968). Infrared Receptors in the Facial Pits of the Australian Python *Morelia spilotes*. *Science*, *159*(3813), 439–441.
- Whiting, M. J., Stuart-Fox, D. M., O'Connor, D., Firth, D., Bennett, N. C., & Blomberg, S. P. (2006). Ultraviolet signals ultra-aggression in a lizard. *Animal Behaviour*, *72*(2), 353–363.
- Wieskotten, S., Dehnhardt, G., Mauck, B., Miersch, L., & Hanke, W. (2010). Hydrodynamic determination of the moving direction of an artificial fin by a harbour seal (*Phoca vitulina*). *Journal of Experimental Biology*, *213*(13), 2194–2200.
- Yang, L., Monsivais, P., & Rubel, E. W. (1999). The superior olivary nucleus and its influence on nucleus laminaris: a source of inhibitory feedback for coincidence detection in the avian auditory brainstem. *The Journal of Neuroscience*, *19*(6), 2313–2325.

- Yin, T. C. T. (2002). Neural Mechanisms of Encoding Binaural Localization Cues in the Auditory Brainstem. In D. Oertel, R. R. Fay, & A. N. Popper (Eds.), *Integrative Functions in the Mammalian Auditory Pathway* (pp. 99–159). Springer, New York.
- Zischka, H., Keller, H., Kellermann, J., Eckerskorn, C., & Schuster, S. C. (2003). Proteome analysis of the thermoreceptive pit membrane of the western diamondback rattlesnake *Crotalus atrox*. *Proteomics*, 3, 78–86.

## Appendix 1

### **Material and Methods used to obtain preliminary data included in the summarizing discussion**

#### *Neurobiotin whole mount nerve staining*

Neurobiotin staining of individual ramifications of pit membrane innervating trigeminal nerves followed the staining protocol described in the material and methods section of chapter one. As a staining solution 10 % neurobiotin (NEUROBIOTIN tracer, Vectorlabs, Burlingame California, USA) in 0.1 M PB was used.

#### *Pressure injection of fluorescent dextran*

Pressure injection of red fluorescent dextran (Dextran, Texas Red™, 3000 MW, Invitrogen, Paisley, United Kingdom) was performed in vitro by means of a nanoliter injector (Nanoliter 2010, World Precision Instruments, Sarasota Florida, USA). The micropipettes for tracer injection were pulled with a micropipette puller (P-87 Micropipette Puller, Sutter Instrument, Novato California, USA). The pipette was positioned above the lateral descending trigeminal tract and subsequently forwarded about 25 µm into the tissue by means of a micromanipulator (U-31 CF, Narishige Group, Tokyo, Japan). 10 nl of tracer were injected into the tract. The micropipette was kept in position and injection was repeated two to four times within one minute. The preparation was afterwards incubated in oxygenated SNAKE ringer solution for 48 h. The tissue was subsequently fixated, cut and mounted following the protocol described in the material and methods section of chapter one.

## Published manuscripts included in this thesis

Kohl, T., **Bothe, M.S.**, Luksch, H., Straka, H., & Westhoff, G. (2014). Organotopic organization of the primary infrared sensitive nucleus (LTTD) in the western diamondback rattlesnake (*Crotalus atrox*). *Journal of Comparative Neurology*, 522(18), 3943–3959.

Online access: <https://onlinelibrary.wiley.com/doi/epdf/10.1002/cne.23644>

## Copyrights

### Introduction, Figure 1a:

Reproduced from Figure 10 'Phylogeny of snakes (Serpentes): Combining morphological and molecular data in likelihood, Bayesian and parsimony analyses' by Michael S. Y. Lee , Andrew F. Hugall , Robin Lawson & John D. Scanlon *Systematics and Biodiversity* Vol 5:4 pp. 371-389 (2007). With permission of "Taylor & Francis Group"; <http://www.tandfonline.com>; Permission reference: JB/TSAB/P18/1050

### Chapter 1:

Reprinted from Kohl, T., Bothe, M.S., Luksch, H., Straka, H., & Westhoff, G. (2014). Organotopic organization of the primary infrared sensitive nucleus (LTTD) in the western diamondback rattlesnake (*Crotalus atrox*). *Journal of Comparative Neurology*, 522(18), 3943–3959. With permission of "John Wiley and Sons"; <https://www.wiley.com>; Rightslink license number: 4347670114730

## Danksagung

Einigen Menschen, die meine Arbeit im Laufe der letzten vier Jahre begleitet haben, gilt besonderer Dank:

Professor Harald Luksch für die Möglichkeit meine Doktorarbeit an diesem faszinierenden Modellorganismus an seinem Lehrstuhl durchzuführen.

Professor Hans Straka gilt großer Dank für seine kritische und stets hilfreiche Begleitung der Doktorarbeit und für viele lehrreiche Hinweise und Diskussionen.

Im Besonderen danke ich Dr. Tobias Kohl, der mich als direkter Betreuer meiner Dissertation an die Arbeit mit einem spannenden Modellorganismus herangeführt hat, stets bereit war neue Ideen und Ansätze zu diskutieren und bei allen Fragen und Problemen mit Geduld und hilfreichem Rat zur Seite stand.

Dr. Martin Stemmler für seine Teilnahme an meinem TAC und Rat und Tat beim Umgang mit Matlab und Python.

Professor Gerhard von der Emde für das Verfassen eines externen Gutachtens zu meiner Doktorarbeit.

Allen Arbeitsgruppenleitern des TUM Lehrstuhls für Zoologie und besonders PD Dr. Uwe Firzlaff für viele hilfreiche Kommentare und Diskussionen und stets offene Türen bei etwaigen Fragen.

Yvonne Schwarz, Birgit Seibel, Gabi Schwabedissen, Christian Fink und Elmar Jocham für die geduldige Unterstützung in Labor und Werkstatt.

Meinen Mitdoktoranden Hansa, Wolfgang, Katha, Quirin, Michi und Stephen für schöne Jahre am Lehrstuhl und eine gute Gemeinschaft im Doktorandenbüro.

Schließlich danke ich meiner Familie für fortwährende Unterstützung und Rückhalt während meines gesamten Studiums.

## Eidesstattliche Versicherung/Affidavit

Hiermit versichere ich an Eides statt, dass ich die vorliegende Dissertation

**Infrared processing in the infrared pathway of the western diamondback rattlesnake, *Crotalus atrox***

selbstständig angefertigt habe, mich außer der angegebenen keiner weiteren Hilfsmittel bedient und alle Erkenntnisse, die aus dem Schrifttum ganz oder annähernd übernommen sind, als solche kenntlich gemacht und nach ihrer Herkunft unter Bezeichnung der Fundstelle einzeln nachgewiesen habe.

I hereby confirm that the dissertation

**Infrared processing in the infrared pathway of the western diamondback rattlesnake, *Crotalus atrox***

is the result of my own work and that I have only used sources or materials listed and specified in the dissertation.

München, den 26.06.2018

Maximilian Bothe

Munich, 06/26/2018

Unterschrift /signature

## Declaration of author contributions

Additional authors that contributed to the results presented in this thesis are (in alphabetical order):

- Dr. Tobias Kohl (T.K.)
- Prof. Dr. Harald Luksch (H.L.)
- Prof. Dr. Hans Straka (H.S.)
- Dr. Guido Westhoff (G.W.)

### Chapter 1:

Kohl, T., **Bothe, M.S.**, Luksch, H., Straka, H., & Westhoff, G. (2014). Organotopic organization of the primary infrared sensitive nucleus (LTTD) in the western diamondback rattlesnake (*Crotalus atrox*). *Journal of Comparative Neurology*, 522(18), 3943–3959.

#### Contributions of Maximilian S. Bothe (Co-author):

- Transfer of the whole-mount nerve staining technique to the rattlesnake in vitro preparation.
- Acquisition of data, except for nissl material (Figure 3)
- Analysis and interpretation of tracings
- Major part of the statistical analysis
- Preparation of Figures 1, 2, 4, 5, 6, 7
- Review and discussion of the manuscript

#### Contributions of other authors:

- Study concept and design: T.K., H.S., H.L., G.W.
- Establishment of the in vitro whole brain preparation: H.S., T.K., G.W.
- Review and discussion of data analysis and figures: T.K., H.S., H.L.
- Writing of the manuscript: T.K., H.S.
- Administrative, technical and material support: H.L., G.W., H.S., T.K.

## Chapter 2:

**Bothe, M.S.,** Luksch, H., Straka, H., Kohl, T., Physiological basis for infrared motion detection in the brainstem of the western diamondback-rattlesnake (*Crotalus atrox*); in prep.

### Contributions of Maximilian S. Bothe (First-author):

- Participated in the development of study concept and design
- Extension of the in vitro whole brain preparation to the pit organ attached state
- Setup of the IR emitter stimulus and inclusion in the in vitro recording chamber
- Acquisition of data
- Analysis of data
- Preparation of all figures
- Writing of the first draft of the manuscript
- Major part of the statistical analysis
- Review and discussion of the manuscript

### Contributions of other authors:

- Study concept and design: T.K., H.S.
- Review and discussion of data analysis and figures: T.K., H.S.
- Review and discussion of the manuscript: T.K., H.S., H.L.
- Administrative, technical and material support: H.L., H.S., T.K.

## Chapter 3:

**Bothe, M.S.,** Luksch, H., Straka, H., Kohl, T., Infrared object motion-processing in the rattlesnake hindbrain depends on rate- as well as spike time encoding mechanisms; in prep.

### Contributions of Maximilian S. Bothe (First-author):

- Participated in the development of study concept and design
- Acquisition of data
- Statistical analysis
- Preparation of all figures
- Writing of the manuscript
- Analysis of data
- Review and discussion of the manuscript

Contributions of other authors:

- Study concept and design: T.K., H.S.
- Review and discussion of data analysis and figures: T.K., H.L.
- Review and discussion of the manuscript: T.K., H.L.
- Administrative, technical and material support: H.L., H.S., T.K.

I hereby confirm the accuracy of the above declared author contributions.

Freising, 06/26/2018,

\_\_\_\_\_  
Maximilian S. Bothe

\_\_\_\_\_  
Prof. Dr. Harald Luksch